WOODEN TORNADO SAFE ROOM WALLS

MODELING AND DESIGN

By

Eric T. Heidebrecht

A thesis submitted in partial fulfillment of the requirements for the degree of

Master of Science

(Civil and Environmental Engineering)

Department of Civil and Environmental Engineering

University of Wisconsin – Madison

2015

WOODEN TORNADO SAFE ROOM WALLS

MODELING AND DESIGN

Eric T. Heidebrecht

Approved:

Steven M. Cramer 8/12/15

Signature Date

Steven M. Cramer, Professor

Table of Contents

Chapter 1 Introduction 1
1.1 Significance 1
1.2 Background 4
1.3 Hypotheses 6
1.4 Scope 9
Chapter 2 Literature Review 13
2.1 General Impact of Solids 13
2.1.1 Elastic and Inelastic Collisions 13
2.1.2 Missile Velocity 15
2.1.3 Stress Waves 16
2.1.4 Target Thickness 16
2.1.5 Failure Modes 17
2.2 Impact on Wood Structures 19
2.2.1 Load Duration 19
2.2.2 Stress Waves 21
2.3 Tornado Generated Missiles 23
2.4 Government Adoptable Documents 24
2.4.1 Federal Emergency Management Agency Guideline 24
2.4.2 Currently Adopted Wall Sections 28
2.4.3 International Code Council Standard 28
Chapter 3 Forest Products Laboratory Experimental Procedure 30
3.1 Design of Experiment 30
3.1.1 Reaction Frame 30
3.1.2 Linear Variable Differential Transformer (LVDT) Placement 32
3.1.3 Compressed Air Cannon 33
3.2 Construction of FPL Walls 35
3.3 Data Collection 37
3.3.1 Quasi-Static Load-Deflection Test 37
3.3.2 Impact Test 38
Chapter 4 Analysis and Modeling of Forest Products Laboratory Data 40
4.1 Stiffness Mechanism Method 40

4.1.1 Approximation of a Stiffness Mechanism 40
4.1.2 Analysis of Stiffness Test 43
4.1.3 Stiffness Mechanism Method Results 44
4.2 Nonlinear Regression Method 46
4.3 Verification of Nonlinear Regression Parameters 50
4.3.1 Calculation of Damping Ratio 50
4.3.2 Comparison of Parameters 51
4.4 Analysis of Midpoint/Quarter Point Stiffness Ratio 54
Chapter 5 Wall Section Design Method 56
5.1 Design Thresholds 56
5.2 Design Procedure 61
5.2.1 Determination of Stiffness Ratio 62
5.2.2 Determination of Stiffness Parameters 64
5.2.3 Determination of Effective Mass 69
5.2.4 Determination of Damping Ratio 70
5.3 Wall Designs 70
5.4 Relationship between Proposed Design and Design Thresholds 72
Chapter 6 Test Results and Analysis 75
6.1 Modification to Experimental Design 75
6.2 Impact Test Results 77
6.2.1 Midpoint Impacts 78
6.2.2 Corner Impacts 84
6.3 Analysis of Model Parameters 86
6.3.1 Analysis of the Stiffness Tests 87
6.3.2 Verification of Midpoint Displacements 87
6.3.3 Analysis of the Impact Test 91
6.4 Comparison of Results to Thresholds 93
6.4.1 Effective mass-Dynamic Stiffness Threshold 93
6.4.2 Stiffness Ratio-Dynamic Stiffness Threshold 94
6.5 Wall Construction Performance 96
6.5.1 Stacked 2x4 Construction 96
6.5.2 Perpendicular Layer Construction 97
6.6 Discussion of Predictions and Variables 98

6.6.1 Predicted and Measured Behavior of Wall A 98
6.6.2 Variation due to OSB Addition 100
6.6.3 Variation due to 2x4 Use 101
Chapter 7 Conclusion and Recommendations 102
7.1 Summary and Conclusions 102
7.2 Recommendations 104
7.2.1 Repeatability Testing 104
7.2.2 Construction with Screws 105

List of Figures

Figure 1 Occurrence of extreme tornados in the United States. 2
Figure 2 Example wall displacement measurement from the FPL safe room project 6
Figure 3 Example of an ideal damped sinusoid. 7
Figure 4 SDOF spring-mass-damper system 9
Figure 5 Effect of Strain Rate (ϵ) on material response. 15
Figure 6 Impact failures of a solid. 19
Figure 7 Working stress plotted against duration of load. 21
Figure 8 Tornado safe room design wind speed map for community safe rooms. 26
Figure 9. The load cell setup of the FPL reaction frame. 31
Figure 10 FPL wall mounted to the reaction frame. 32
Figure 11.The LVDT and Load cell layout of the FPL safe room project 33
Figure 12. The compressed air cannon used to propel the 2x4 missiles. 34
Figure 13 Typical construction of a FPL wall 36
Figure 14 Construction of FPL Wall 4 36
Figure 15 Quasi-static stiffness test setup 38
Figure 16 Cross-section and potential bending scheme from FPL safe room project 41
Figure 17 Idealized bending mechanisms for the FPL wall designs 42
Figure 18 Example load vs. displacement plot and trend line. 44
Figure 19. Midpoint displacement of model and wall for FPL Wall 8. 46
Figure 20 Plot of measured displacement and model for FPL Wall 6 49
Figure 21. Comparison of nonlinear regression model and measured data. 54
Figure 23. Dynamic stiffness and effective mass of FPL walls. 58
Figure 24. Midpoint static stiffness and stiffness ratio of FPL walls. 59
Figure 25. Dynamic stiffness and stiffness ratio of FPL walls.. 60
Figure 26. Determination of expected stiffness ratio 64
Figure 27. Dynamic/static stiffness ratio and construction of the FPL walls 69
Figure 28 Proposed minimum effective mass-stiffness threshold. 73
Figure 29. Proposed minimum dynamic stiffness-stiffness ratio threshold. 74
Figure 30. The layout and numbering of LVDTs for this project 76
Figure 31. Cannon setup modified to test wall corners. 77
Figure 32. Damage to Wall A, 1st test. 79
Figure 33. Damage to Wall A, 2nd test 80
Figure 34. Damage to Wall B, 1st test 81
Figure 35. Damage to Wall C 82
Figure 36. Damage to Wall D 84
Figure 37. Damage to Wall A, corner test. 85
Figure 38. Damage to Wall B, corner test. 86
Figure 39. Midpoint deflections of Wall A calculated with two methods. 89
Figure 40. Midpoint deflections of Wall C. 90
Figure 41. Dynamic stiffness and effective mass of tested walls. 93
Figure 42. Dynamic stiffness and stiffness ratio of tested walls 95
Figure 43. Comparison of calculation and measured parameters. 100

List of Tables

Table 1. Type of impact based on C_R 14
Table 2 Missile impact velocities for community safe rooms..... 27
Table 3 Summary of FPL wall construction..... 37
Table 4 Upper and lower stiffness bounds 43
Table 5 The midpoint and quarter point stiffness of the FPL walls 44
Table 6 Damping ratios calculated from the log decrement 51
Table 7 Comparison of nonlinear regression and measureable parameters 52
Table 8 Coefficient of determination for each FPL wall 53
Table 9 Ratios of midpoint to quarter point stiffness and elastic moduli 55
Table 10. Minimum proposed design thresholds. 60
Table 11. Description of each wall design. 71
Table 12. Summary of the 1st impact of Wall A 78
Table 13. Summary of the 2nd impact test of Wall A. 79
Table 14. Summary of the 1st impact test of Wall B. 80
Table 15. Summary of the 2nd impact test of Wall B. 81
Table 16. Summary of midpoint impact test of Wall C. 82
Table 17. Summary of midpoint impact test of Wall D. 83
Table 18. Summary of corner test of Wall A. 85
Table 19. Summary of corner test of Wall A. 86
Table 20. Summary of the stiffness test results. 87
Table 21. Coefficient of determination between midpoint displacement estimates. 89
Table 22. Mass, stiffness, and damping parameters for Walls A, B, and D. 91
Table 23. Coefficients of determination for Walls A, B, and D. 92
Table 24. Mass, stiffness, and damping parameters for Wall C. 92
Table 25. Coefficient of determination for Wall C. 92
Table 26. Predicted and measured parameters of Wall A..... 99
Table 27. Change in parameters from addition of OSB 101
Table 28. Change in parameters from use of 2x4s 101

Chapter 1 Introduction

A safe room is a room in a residence or place of business designed to provide shelter to the occupants of the building in the event of a tornado or hurricane. Currently walls for these rooms are made of cast-in-place concrete, concrete masonry units (CMU) with concrete infill, a combination of wooden studs and plywood with concrete infill, or a combination of wooden studs and plywood with steel sheet metal. Keeping costs low is important to encourage construction of safe rooms, and these Federal Emergency Management Agency (FEMA) approved wall sections may be difficult or expensive to retrofit into an existing building. Thus, a safe room design that uses only materials found at a home improvement store with a lumberyard is potentially needed.

Previous studies of safe room wall sections have relied on a trial and error, build and test, approach to design. This approach has resulted in approved wall sections, but required many tests to find a small number of designs that were suitable. The intent of this project is to establish a simple design procedure for wooden safe room walls that compares expected physical parameters of the wall to minimum thresholds that define the pass/fail behavior of the wall. Approaching design of safe room walls in this manner may decrease the number of tests required to find a passing wall design.

1.1 Significance

Between 1950 and 2013, tornadoes caused 6,073 deaths and averaged 1,500 annual injuries (FEMA P-320, 2008 and NOAA, 2015). The threat to human life from tornadic events is present in much of the United States, especially in areas to the east of the Rocky Mountains.

When compared to other regions where extreme (EF3-EF5) tornados are possible, the threat is two to three times larger in the Central United States, parts of which are called “Tornado Alley”. Figure 1 shows the areas of the United States that are susceptible to the most significant tornadic events: EF3, EF4 and EF5 tornadoes. Formation of tornadoes is unpredictable, and often people have only a few minutes notice that a tornado has formed and is moving toward their location. Given these circumstances, having a safe room in a home or place of business could mean the difference between surviving unhurt and injury or death.

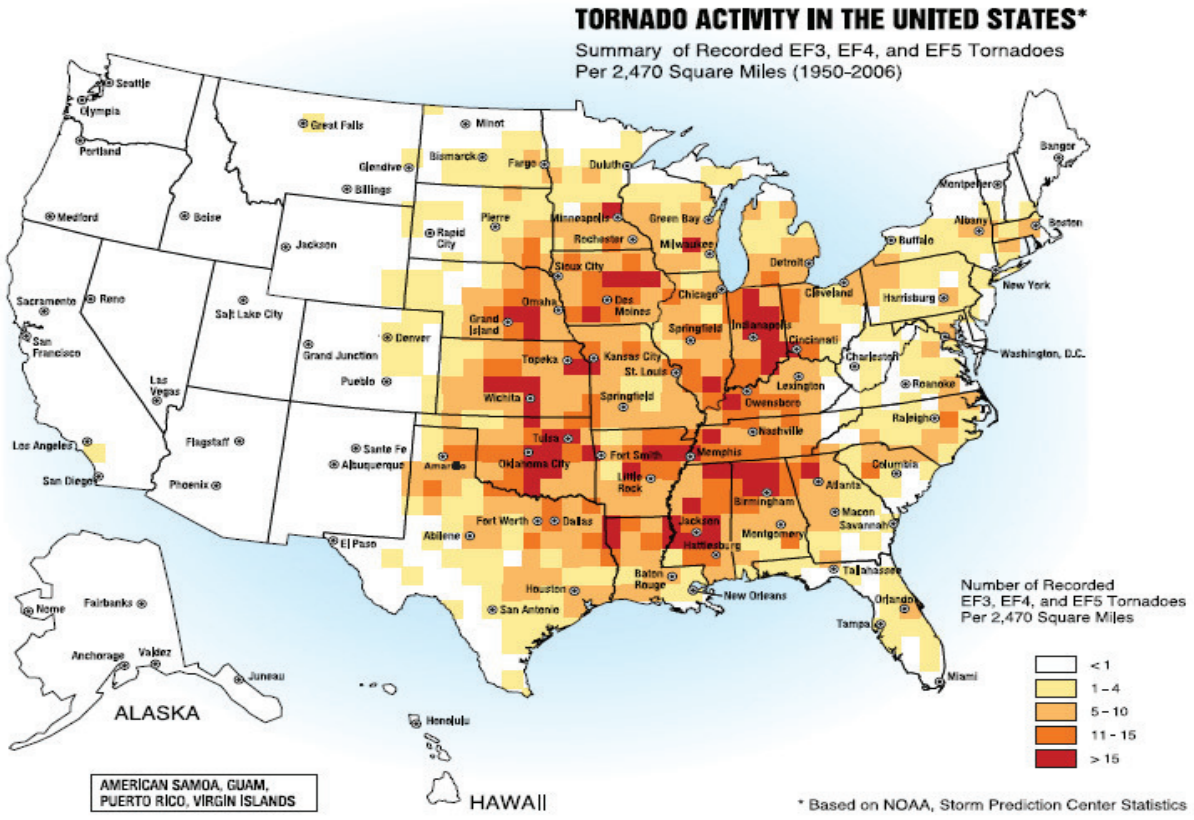


Figure 1 Occurrence of extreme tornados in the United States. (FEMA P-320, 2015)

In “Tornado Alley,” many existing homes do not have basements, which are the preferred locations to take shelter during a tornado. A lack of basements makes this area of

the country an ideal candidate for the implementation of safe rooms. Many options are available for adding a safe room to an existing home. One option is to buy a premade safe room online or from a home improvement store. These shelters are as effective as most safe rooms, but are often expensive, starting at approximately $4,000. Another safe room possibility is an underground shelter built outside the house. A potential issue with this type of shelter is that unless a very early warning is given, the trip from inside the house to the safe room can be dangerous and may undermine the purpose of the safe room. The limitations of these two types of safe rooms lead to the need for affordable, constructed, in-home safe room options.

The International Code Council (ICC) and the Federal Emergency Management Agency (FEMA) respectively maintain a standard and guidelines that regulate the testing criteria that safe rooms must pass. These documents may be adopted by state and local governments, but currently only Alabama has adopted the ICC standard, ICC-500. FEMA's guidelines, FEMA P-320 *Taking Shelter from the Storm (Residential/Small Business)* and FEMA P-361, *Design and Construction Guidance for Community Safe Rooms* provide a few design drawings and wall sections that passed the design guidelines during testing.

Most of the previously tested and approved safe room designs are made of reinforced concrete. Pouring concrete inside an existing home could be a troublesome proposition. Pumping modern concrete is possible when using admixtures, such as a superplasticizer, but existing buildings may have spatial issues, such as a lack of headroom, which make delivery of concrete difficult. Depending on the area of the country, obtaining the 12- or 14-gauge sheet metal specified in other designs may be unreasonable from a cost standpoint. FEMA P-320

(2015) provides cost estimates for the most common safe room designs. For an 8-ft by 8-ft by 8-ft safe room, the cost ranges from $6,300 to $8,300 when built during construction of the home, and costs may be approximately 20% higher when the safe room is retrofitted into an existing home (FEMA P-320, 2008).

Lumber is abundantly available across the United States and frequently used in home construction throughout the country. Beyond its abundance, another advantage to having safe room designs that use wood construction is that it allows any individual competent with measuring and nailing to perform the construction. Establishment of design criteria for wooden safe room walls may increase the number and efficiency of safe room designs in the future. Increased efficiency of the walls may lead to designs requiring less material, thus reducing the cost of building a safe room. A homeowner can build the lumber wall designs proposed in this report at a material cost of under $250 per wall and no labor cost, other than personal time. Making safe rooms inexpensive and easy to build might help increase their presence in homes and businesses across the country and save lives in the event of a tornado.

1.2 Background

From an engineering perspective, tornadoes are of interest primarily in how they load and damage structures with wind speed playing a direct role. Tornadoes also have the ability to lift and accelerate debris, such as building materials, tree limbs, and fence posts, through the air, which is also a major cause of damage and casualties (NIST/TTU, 2006). Therefore, the design of a safe room is not solely a wind pressure problem, but is also a debris impact problem.

Research projects at Texas Tech University were the first to study the impact resistance of safe room walls. Bailey (1984) developed a compressed air cannon that could propel missiles at up to 120 mph. Bailey tested 4-ft by 8-ft walls that were made of plywood, dimensional lumber, stucco, brick, and/or CMU using 2x4 lumber missiles shot from the compressed air cannon. Carter (1998) continued Bailey's work and tested an additional 60 wall designs using the same compressed air cannon. Carter (1998) used similar materials to Bailey (1984) in his walls, but with the addition of cast-in-place concrete and steel sheet metal. These studies provided the framework for the development of the first national guideline for safe room construction, FEMA P-361, in 2000. Neither thesis provided an experimental or theoretical basis for the design of these walls or for prediction of their pass/fail behavior.

A research project at the U.S. Department of Agriculture Forest Products Laboratory (FPL) studied the impact resistance of safe room walls constructed out of wood products (Falk, Hermanson, Bridwell, 2015). The project included construction and testing of eight 8-ft by 8-ft walls with multiple layers of dimensional lumber. Oriented strand board (OSB) or plywood was added to the exterior faces of the walls and construction adhesive was added between the dimensional lumber to strengthen and stiffen the walls. This project included no basis for design or prediction of pass/fail behavior of the walls. The displacements of the wall during and after impact by the 2x4 missile were recorded, but were not analyzed as part of the report. An example of the midpoint displacement of the wall measured with respect to time is plotted in Figure 2.

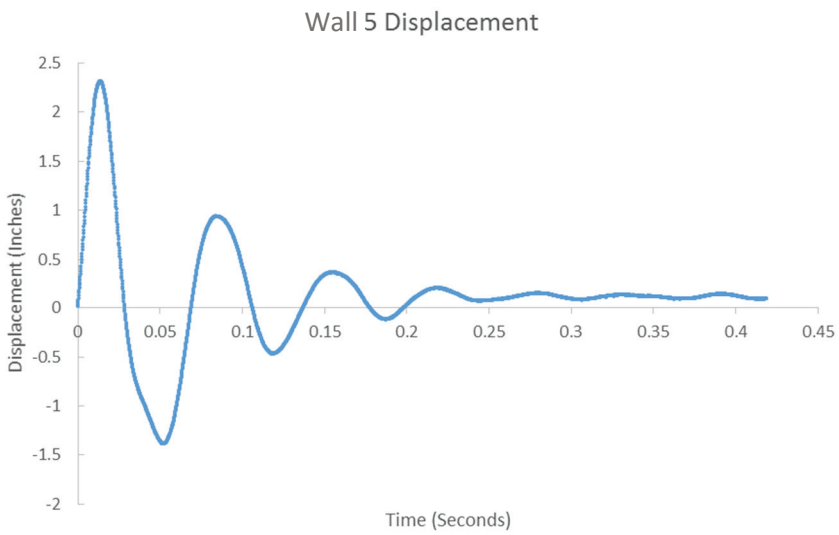


Figure 2 Example wall displacement measurement from the FPL safe room project

1.3 Hypotheses

The displacement data collected as part of the FPL safe room project formed the basis of the hypotheses of this report. The displacement of the wall in response to the impact of the missile shown in Figure 2 was typical for all walls tested in the FPL safe room project. The displacements appeared to be damped sinusoids; plotted in Figure 3 is an idealized example.

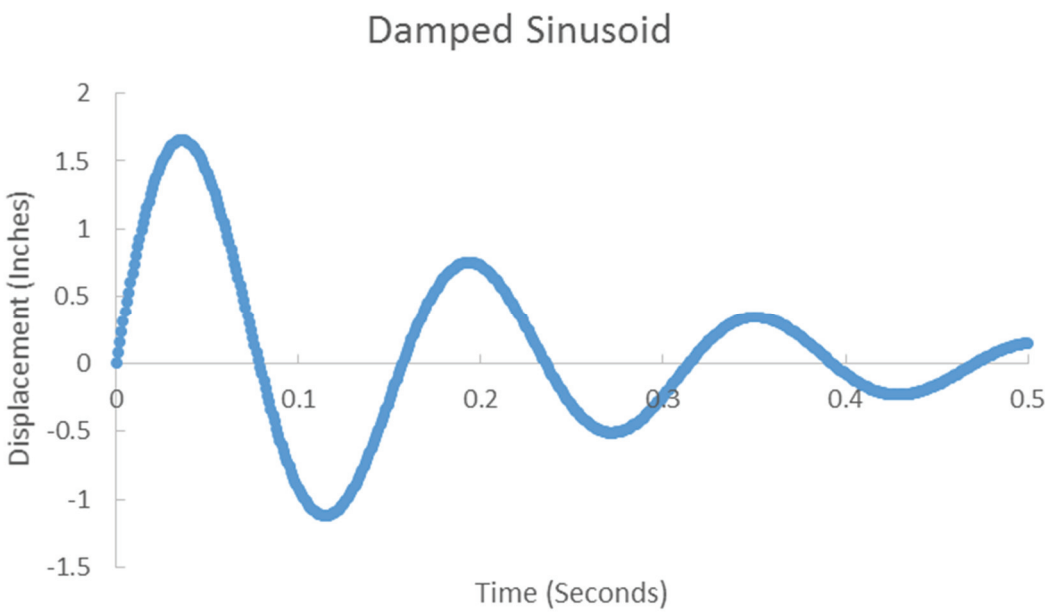


Figure 3 Example of an ideal damped sinusoid.

The displacement profile of an underdamped single degree of freedom (SDOF) spring-mass-damper system is a damped sinusoid. Therefore, the hypotheses of this project are as follows:

1. The dynamic response of wooden safe room wall sections to impact can be represented by using a SDOF spring-mass-damper system, shown in Figure 4, using Equation (1-1) (Ginsberg, 2001):

$$M\ddot{x}(t) + C\dot{x}(t) + Kx(t) = F(t) \qquad (1\text{-}1)$$

Which is presented more generally in Equation (1-2):

$$\ddot{x}(t) + 2\zeta\sqrt{\frac{K}{M}}\dot{x}(t) + \frac{K}{M}x(t) = F(t)/M \qquad (1\text{-}2)$$

Where:
ζ = Damping Ratio (Unitless)
K = Stiffness (Force/Length)
M = Mass
F = Force of excitation
t = Time
x = Displacement (Length)
$\dot{x}$ = Velocity (Length/Time)
$\ddot{x}$ = Acceleration (Length/Time^2)

2. The displacement of the wall, in response to impact of the missile, can be modeled as an impulse excitation on the spring-mass-damper system, shown in equation (1-3) (Ginsberg, 2001):

$$x(t) = \frac{F(t)}{M\sqrt{\frac{K}{M}}\sqrt{1-\zeta^2}} \exp\left(-\zeta\sqrt{\frac{K}{M}}t\right) \sin\left(\sqrt{\frac{K}{M}}\sqrt{1-\zeta^2}t\right) \quad (1\text{-}3)$$

3. Fitting Equation (1-3) with experimental data will yield a stiffness and effective mass less than, but consistent with, the stiffness and mass measured in the laboratory prior to impact testing.
4. From the estimated effective mass, stiffness and damping ratio of the wall and the performance of the walls under the impact test, a minimum passing effective mass and stiffness design threshold can be developed.

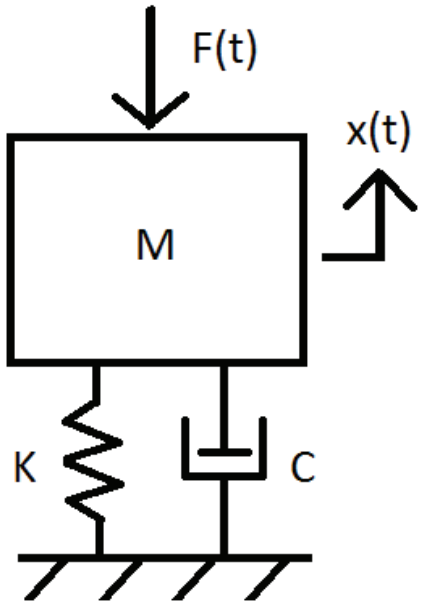


Figure 4 SDOF spring-mass-damper system

1.4 Scope

This project sought to establish design criteria and a design procedure to determine the pass/fail behavior of safe room walls subject prior to impact testing. The project proceeded in the following steps:

1. Data from the testing of seven FPL walls were examined.
2. Stiffness and effective mass parameters of the FPL walls were computed using the best fit of a SDOF spring-mass-damper model to the displacement of the wall during projectile impact testing.
3. From the parameters found, minimum design criteria (thresholds) were proposed. Walls having parameters above the minimum values were expected

to pass, and walls having parameters below the minimum values were expected to fail.

4. A design procedure to predict the parameters of a wall prior to testing was proposed.
5. Additional wall were constructed.
6. From the projectile impact testing results of the additional walls, the spring-mass damper model was validated.
7. From the testing results of the additional walls, the design criteria were verified.

The intent of this project was to establish a simple design procedure consisting of comparison of pass/fail thresholds to expected physical parameters of the wall. The presented design criteria and process should result in a wall that meets or exceeds the impact testing requirements of ICC-500-2014: *ICC/NSSA Standard for the Design and Construction of Storm Shelters*, the test standard adopted by FEMA P-361. Designers should feel confident that the wall section they have designed using these criteria would pass the impact test, without the construction of a complicated analytical model. The intent of the design criteria are not to be a replacement for the impact test. However, using the design criteria and process should move design away from a trial and error, build and test based approach and toward the use of the impact test as a verification tool. This should result in far fewer tests being necessary to identify acceptable designs.

Localized failures due to the impact test, including crush, shear, penetration, and flexural fracture, are not explicitly considered or modeled in this report. Some of these localized failures are nonlinear in nature and although some information is available to model

these, they complicate the design process. Thus, the proposed design procedure prescribes design criteria based on the behavior of the whole structure.

The modelling basis for the presented design criteria was formed by analysis of the test data from seven FPL walls (Falk, et al., 2015). The tests by Falk, et al. (2015) are referred to as the FPL safe room project throughout this report. As part of this project, four experimental wall panels were constructed and tested to validate the spring-mass damper model and the proposed design thresholds. This number of samples may provide a picture of the approximate thresholds that must be met in design, but are insufficient to confirm a finalized design envelope.

The experiments of this project and those carried out by FPL used #2 Douglas-fir 2x8s and Stud grade Spruce-Pine-Fir 2x4s, bought from a home improvement store. In addition, the walls for this project had a moisture content between 10% and 16% during construction and between 7% and 9% when tested. The criteria proposed by this project may allow designers to vary the grade and/or species of wood and determine how the change modifies the impact properties of a particular wall design. However, the moduli of wood as well as its bending and shear strength vary significantly with species, grade and moisture content. Until additional tests using different species, grades, and moisture contents are performed, the results of this project should not be assumed to apply to any other wood grades, species or moisture contents.

The connection strength between wood members is dependent both on the material properties of the wood and also the connecter size and type. Construction of the walls presented in this document was completed using 10d common nails driven with a pneumatic

nail gun for consistency with the previously constructed FPL walls. Construction of the walls presented in this document with different fasteners may change the design parameters and strength of the wall. Thus, walls constructed with different fasteners than those presented must be tested to determine their pass/fail performance and design parameters before being used. This testing may also add additional data allowing more accurate design thresholds to be established.

Chapter 2 Literature Review

2.1 General Impact of Solids

The effect impact has on a target (safe room wall) is a function of projectile velocity, stress wave propagation, material properties of the target and missile, and numerous other variables. The material properties can be difficult to classify, as the response of the target under impact loading is partially dictated by the strain rate, or missile velocity. Analysis of the fracture mechanics and localized effects of impact are outside the scope of this project. This review provides a brief overview of some of the fundamental aspects of impact and motivates a design approach that does not require an analysis of each potential local failure mechanism.

2.1.1 Elastic and Inelastic Collisions

To be considered an impact, a load must be applied over a time duration significantly smaller than the period of the structures natural frequency (Clough, 1993). The impact duration depends primarily on the type of collision, elastic or inelastic. In a perfectly elastic collision, no kinetic energy is lost and the projectile will rebound from the target. In a perfectly inelastic collision, some kinetic energy is lost. In this case, the projectile either will perforate or plug in the target. Impact tests performed on a 24 in. thick concrete wall section showed that the impact of a wind-generated missile could be idealized as an elastic collision with an impact time of 0.5 to 1.5 milliseconds (Stephenson, 1978).

A one dimensional collision may be represented by equations (2-1)and (2-2)(Plesha, Costanzo & Gray, 2009):

$$v_{af} = \frac{C_R m_b (v_{bo} - v_{ao}) + m_a v_{ao} + m_b v_{bo}}{m_a + m_b} \quad (2\text{-}1)$$

$$v_{bf} = \frac{C_R m_a (v_{ao} - v_{bo}) + m_a v_{ao} + m_b v_{bo}}{m_a + m_b} \quad (2\text{-}2)$$

Where:

v_{af} and v_{bf} = the final velocity of body a and body b (Length/Time)
v_{ao} and v_{bo} = the initial velocity of body a and body b (Length/Time)
m_a and m_b = the mass of body a and body b
C_R = the coefficient of restitution (Unitless)

The elastic or inelastic nature of a collision depends on the materials of both the target and projectile, the velocity of the projectile, and the angle of incidence between the projectile and target. These factors determine the coefficient of restitution. The effect of the coefficient of restitution on the impact is summarized in Table 1. Decreasing C_R increases the impact time, thus lessening the instantaneous stresses felt by the target and dissipating some of the energy of the collision.

Table 1. Type of impact based on C_R

Coefficient of Restitution (C_R)	Type of Impact
1	Elastic, no kinetic energy is lost, no localized damage
$0 < C_R < 1$	Inelastic, localized damage decreases as C_R increases
0	Perfectly inelastic, missile perforates or plugs in target

2.1.2 Missile Velocity

The effects that impact imposes on a target can be attributed to the impact velocity of the missile. The velocity of the projectile dictates the strain rate in the target and therefore partially determines the material response present in the target and missile. Multiple velocity ranges have been proposed to classify the velocity of a projectile. Zukas (1980), summarized projectile velocities by the strain rates and material responses they cause in targets, shown in Figure 5.

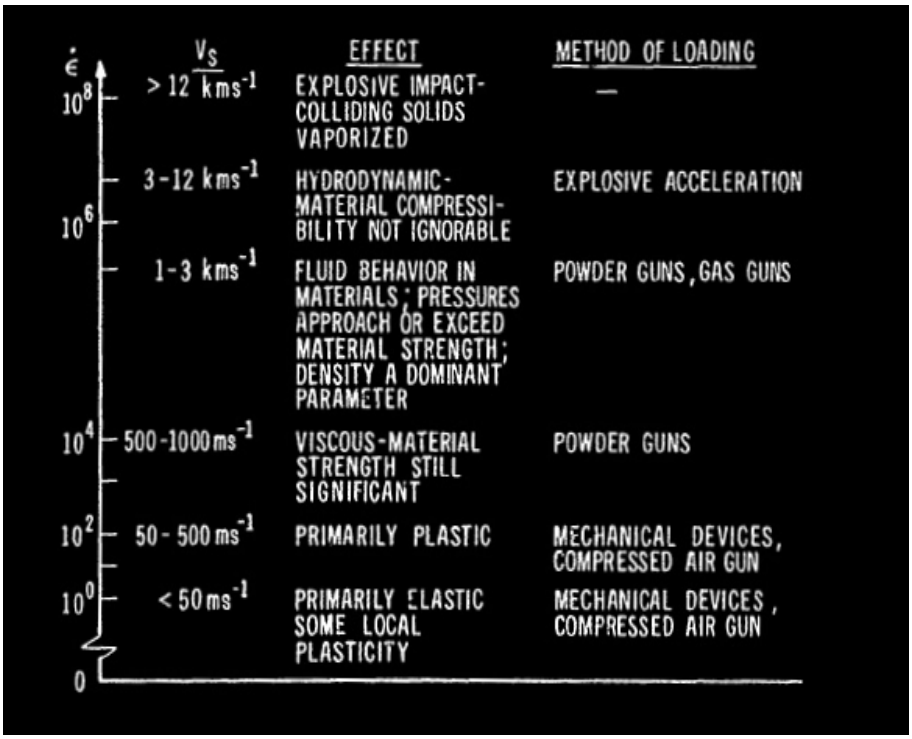


Figure 5 Effect of Strain Rate ($\dot{\epsilon}$) on material response. (Zukas, 1980)

Safe room wall sections are impacted by projectiles moving at or below 50 m/s and therefore elastic and some plastic behavior are expected. For an elastic response, the material does not yield and therefore no significant damage occurs. Stressing the material beyond its yield point results in plastic behavior, either large deformations in ductile structures, or failure

in brittle structures occurs. Many additional material responses, such as viscoelastic or hydrodynamic, occur as the projectile velocity increases, though at much higher missile velocities than safe rooms are exposed to during service. The velocity ranges given in Figure 5 should only be used as reference points because behavior of targets also depends on impact angle and geometric and material characteristics of the target and projectile (Zukas, 1980).

2.1.3 Stress Waves

To analyze the behavior of solids under impact loading, the influence of stress waves must be understood. At the moment of impact between the projectile and the target, compression waves are created in both bodies. Soon after the compression wave is generated and begins moving through the body, a tension wave forms and follows behind it. In addition, when the compression wave reaches a free boundary of the body, another tension wave is released. Each time a tension or compression wave reaches a free surface of the body it is rebounded as the opposite, compression or tension wave respectively. If the magnitude and duration of the stress waves exceed the critical values of the material, cracking, crushing, or complete penetration of the target may occur (Zukas, 1980).

2.1.4 Target Thickness

A final factor that influences the behavior of a target under impact is the thickness of the target. These thicknesses are not classified by physical thickness measured as a length, but by the characteristics they exhibit. Therefore, the use of different materials and boundary conditions may cause targets of the same physical dimensions to be classified differently. The classification of targets is as follows (Backman & Goldsmith, 1978):

1. Semi-infinite - No influence of the distal boundary on the penetration process.
2. Thick - Influence of the distal boundary on the penetration process occurs only after substantial travel into the target element.
3. Intermediate – The rear surface exerts considerable influence on the deformation process during all (or nearly all) of the penetrator motion.
4. Thin – Stress and deformation gradients do not exist throughout the target thickness.

Wooden safe room walls are flexible and therefore are classified as thin.

2.1.5 Failure Modes

Failure occurs in a target when maximum stress thresholds are reached. Potential failure modes of solid targets are shown in Figure 6. A summary of these failure modes and their characteristic conditions are: (Zukas, 1982)

1. Brittle facture – Typically called front-face spall in masonry and concrete targets. It is produced by large deformations and local inhomogeneities and anisotropies.
2. Radial fracture - The result of the initial stress wave exceeding the ultimate strength of the material. This is common in masonry structures.
3. Fragmentation - This is the result of the initial compressive stress wave reflecting off the back surface of the target as a tensile stress wave. This is common in materials that have a compressive strength greater than their tensile strength.
4. Ductile hole growth – Occurs during very high velocity impact by a malleable missile. The materials behave hydrodynamically.

5. Plugging – Occurs when the missile becomes lodged in the target and is common in plywood and other types of sheathing material. Failure occurs when the target material displaced by the missile is displaced out the backside of the target.

6. Petaling - Created by high torsional stresses after the initial stress wave has passed. Petaling involves plastic flow and permanent flexure of the target material. (Carter, 1998)

Fragmentation, plugging, radial fracture, and petaling represent the possible behaviors of wooden safe room wall sections subject to projectile impact testing.

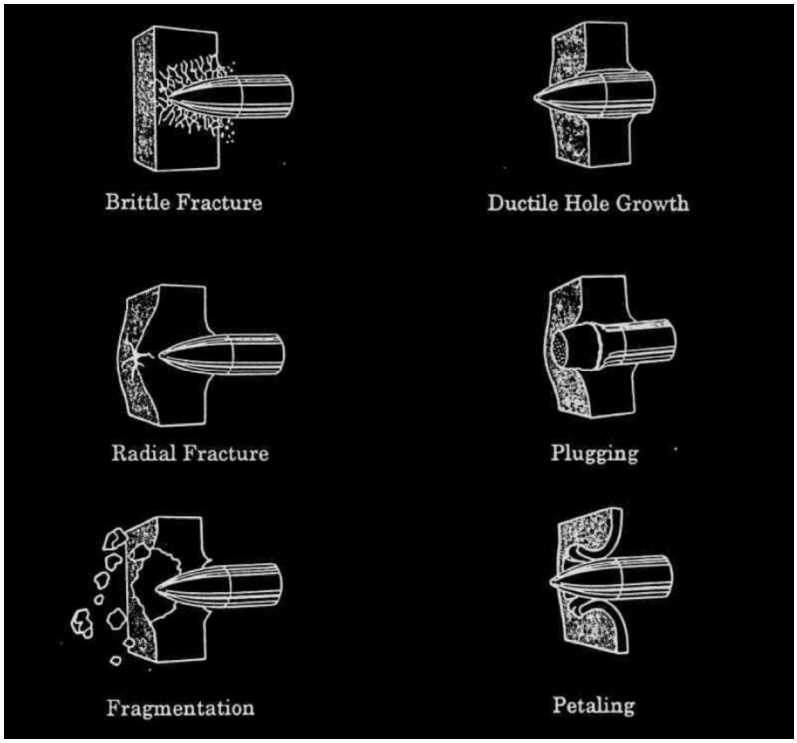


Figure 6 Impact failures of a solid. (Zukas, 1982)

2.2 Impact on Wood Structures

Impact failure is highly dependent on the material and physical properties of the two media in contact. A characteristic of wood that makes it a beneficial material for mitigating impact is its crushing ability. Ability to crush lengthens the time it takes the projectile to transfer its full energy to the wall. Crushing also dissipates some energy by making the collision more inelastic, thus reducing the energy dissipation demand on other parts of the wall section.

2.2.1 Load Duration

Load duration on wood has been studied in the past, but key studies of the effect of impact on allowable stresses were performed over 60 years ago. *The Wood Handbook* (2010) and the American Wood Council's National Design Specification (NDS) (2012) provide a load

duration factor of two that can be multiplied by the allowable bending, tension, compression and shear stresses of wood under an impact load, to adjust for the short loading duration. Studies by Wood (1951) and Gerhards (1977) are the basis of the load duration factors found in the Wood Handbook and NDS. The plot that provides the basis for the impact duration factor is shown in Figure 7 (Wood, 1951). Tabulated allowable stress values from the NDS and *The Wood Handbook* are based on normal loading conditions, which are defined with a ten-year load duration. Normal loading conditions were shown to provide 110% of the long-term loading strength while impact loading yielded about 220% of long-term loading strength. The relationship between these percentages is the basis for the load duration factor of two, which assumes a one-second impact duration.

The experiments performed by Wood (1951) consisted of loading 126 1-in. by 1 in. clear[1] Douglas fir beams. A previous experiment determined the amount of sustained load that caused a similar beam to fail after five minutes. The 126 beams were then loaded with 60%-90% of the five-minute failure load and the time to failure was recorded. In addition to the long-term tests, Wood used previous impact tests from Elmendorf (1916) to fit a curve that extended from long term and short term loading to impact loading. The data for impact loading on this curve came from dropping a 50-lbf weight, 4 feet onto a beam spanning approximately 4 feet. (Elmendorf, 1916). The kinetic energy possessed by this projectile is an order of magnitude less than the kinetic energy possessed by the projectile in the safe room problem

[1] A clear specimen is considered to be homogeneous, free from knots, and has grain oriented parallel to the longitudinal direction of the specimen

(200 ft-lbf to 5014 ft-lbf respectively). The limitations of the previous wood testing, including low energy and only using small, clear specimens, casts some doubt on the validity of using a load duration factor in safe room design.

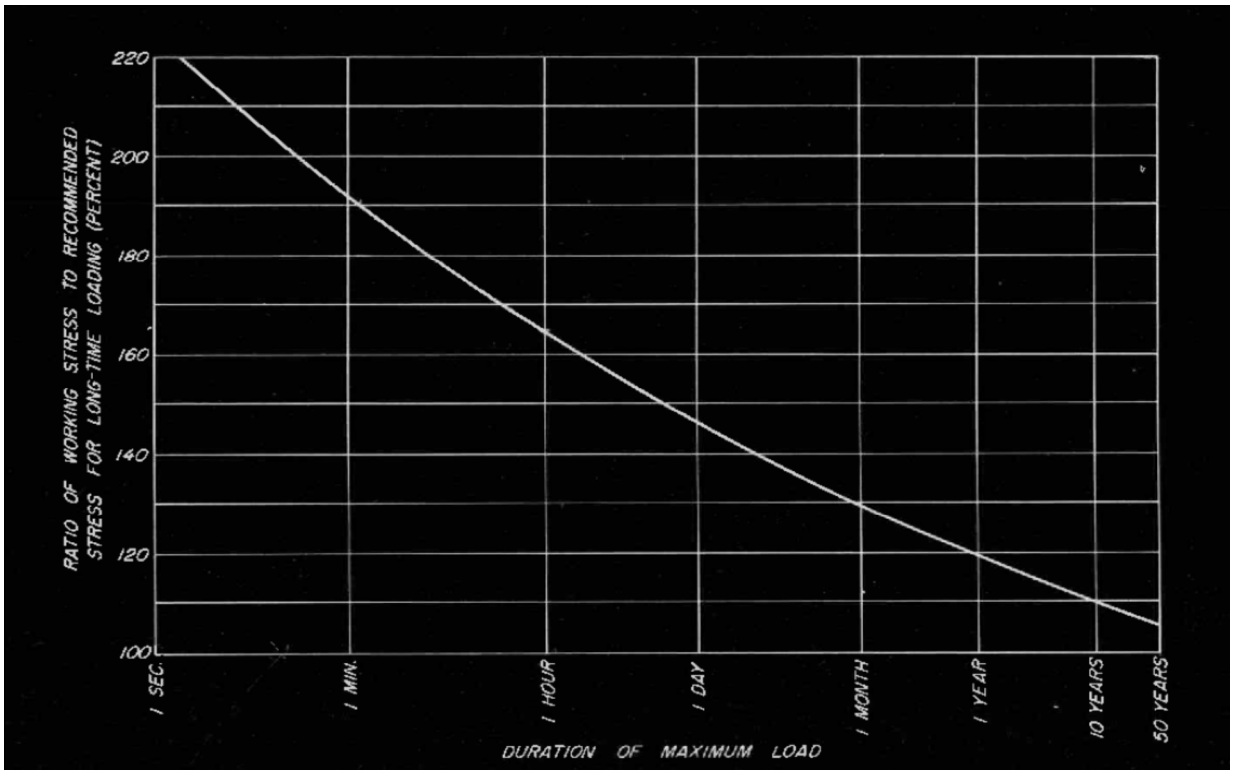


Figure 7 Working stress plotted against duration of load. (Wood, 1951)

2.2.2 Stress Waves

In wood, the grain and any defects in the specimen dictate the propagation of stress waves. As was previously mentioned, under impact loading a compression wave is generated, followed by a tension wave. When these waves intercept free boundaries of the wood they generate an opposite reaction wave, switching between tension and compression. The highest stresses and therefore potential for failure occurs when two tension, or two compression waves intersect.

To determine strength properties of wood, individual boards are graded to account for any defects such as knots, warping, unusual grain patterns, etc., that may lower its strength. Traditionally, trained individuals visually inspected lumber and assigned it a grade. In the 1960s, mechanical systems were developed to evaluate lumber strength and were especially good at differentiating high strength lumbers (Gerhards, 1980). Gerhards (1980) attempted to enhance the testing of mechanically graded lumber by timing how stress waves move through both clear wood and wood defects. These analyses led to most of the data currently available on stress wave propagation in wood.

A characteristic of lumber that may cause abnormalities in the movement of stress waves is cross grain. Cross grain consists of a grain pattern that does not run parallel to the longitudinal direction of the lumber. Cross grain can be created by the growth pattern of the tree, where the board was cut from the log, or the manner in which the board was cut from the log. Gerhards (1980) conducted a study of boards that had cross grain between three and nine degrees from parallel to the longitudinal axis. The study was conducted by impacting the boards at one end and using a series of accelerometers to measure how fast the waves travelled. The study found that stress waves travel the quickest parallel to the grain. This study also examined the static and dynamic modulus of elasticity of the boards. In general, the dynamic modulus was 0% to 20% greater than the static modulus.

Knots are formed at what was formerly the base of a branch on the trunk of a tree. The change in grain direction and the limited connectivity between the knot and the surrounding wood causes lumber with large knots to be downgraded in terms of strength. Gerhards (1980) examined boards that had a knot approximately in the middle of the specimen and a board that

had two knots approximately in the middle. This study revealed that stress waves move through the clear, or knot free, section of the lumber significantly faster than through the knot, causing part of the wave to lag.

2.3 Tornado Generated Missiles

Research of wind and tornado generated missiles did not begin until the 1970s (Bailey, 1984). Prior research of missile impact phenomena was limited to military and spacecraft applications, such as the mechanics of missile penetrations with a projectile velocity of greater than 500 m/s, and the development of armor to stop them (Bailey, 1984). Throughout the 1970s, experiments were undertaken to test the low velocity (Less than 50 m/s) impact resistance of concrete, glass, steel, and some plywood products. These tests were performed in various laboratory settings and before any specific test standards were developed (Bailey, 1984).

Minor, McDonald, and Mehta (1978) found that after a tornado in residential areas the most common type of debris present was 2x4s or other dimensional lumber used in stick framing construction. This study, led to the implementation of a 2x4 as a representative tornado generated missile for impact protection analysis. Researchers at Texas Tech University's Institute for Disaster Research devised a compressed air system that was able to propel a 2x4 missile at up to 120 mph (Bailey, 1984). The development of the compressed air cannon allowed a standardized testing procedure to be used by Bailey (1984) and in future tests. This research led to the adoption of a design missile, consisting of a 15 lbf 2x4 travelling at 100 mph (FEMA P-361, 2008).

Carter (1998) conducted further research into safe room walls at the Institute for Disaster Research. Carter constructed 60 unique composite wall sections made up of combinations of concrete, concrete masonry units, steel, lumber, and plywood. A goal of Carter's project was to cause walls to behave as one of the classes of targets (i.e., semi-infinite, thick, intermediate, and thin) organized by Backman & Goldsmith (1978) and fail in one of the modes outlined by Zukas (1980). Another goal of this research was to determine whether the composite wall sections were able to withstand an impact from the design 2x4 missile. The pass/fail criterion used by Carter (1998) was missile perforation: if the missile perforated the wall, it was deemed a failure, if it did not; the wall was deemed a pass.

2.4 Government Adoptable Documents

The first government guideline for construction of safe rooms was adopted in 1998 when FEMA published the first edition of FEMA P-320. This document published previously tested room designs, but did not provide general testing requirements for design of wall sections. In 2000, FEMA published the first edition of FEMA P-361 providing the first nationally adoptable design criteria for community and residential safe rooms. In 2008, the ICC published ICC-500, which provided other adoptable design criteria. ICC-500 and FEMA P-361 largely outline similar design criteria. This project focuses on FEMA P-361 due to the slightly more restrictive nature of these criteria (FEMA-P361, 2015).

2.4.1 Federal Emergency Management Agency Guideline

The FEMA guidelines have two main criteria that must be met in regards to occupant safety during a tornado. The first requirement is that the safe room must be able to withstand

the wind pressure generated by the design wind speed, as outlined in FEMA P-361. These design wind speeds differ from those present in ASCE 7-10, which are adopted by most United States codes and specifications. FEMA P-361 adjusts the load factors in both Load and Resistance Factor Design (LRFD) and Allowable Stress Design (ASD). This adjustment is done because the LRFD and ASD load factors are intended to be used with the wind speeds from ASCE 7-10, which are calculated with a different method. The design wind speed map for community safe rooms is shown in Figure 8 (FEMA P-361, 2015). Residential safe rooms are required to be designed with a 250 mph wind speed no matter the location of the home to ensure “near absolute protection” of the occupants (FEMA-P320, 2015).

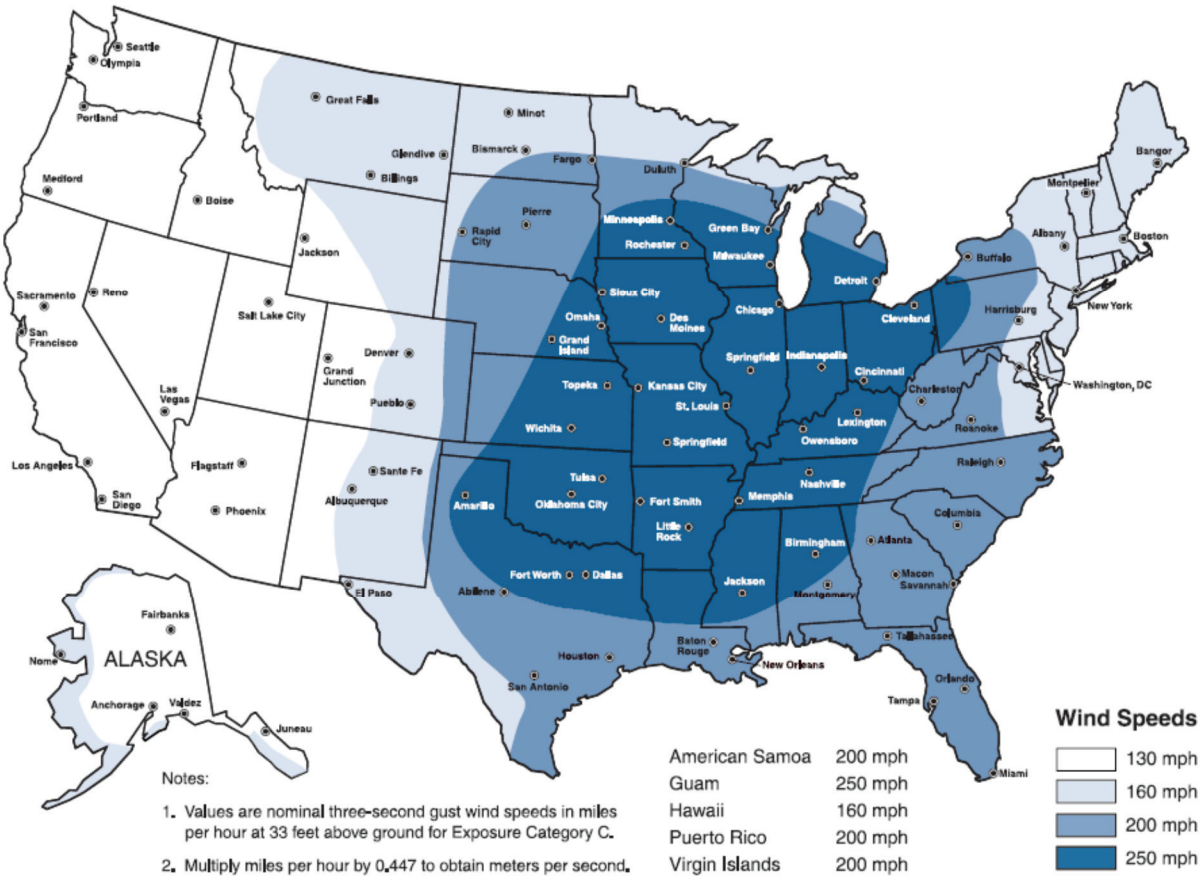


Figure 8 Tornado safe room design wind speed map for community safe rooms. (FEMA P-361, 2015)

Using the design wind speed, the wall section can be designed to resist wind loading with standard structural design procedures. An example calculation of a wall design that meets the wind pressure requirement is provided in Appendix A. The example calculation used the lumber layout from the walls of the previous FPL safe room project and considered no composite action between the members. This conservative example demonstrates that the FPL safe room project wall designs, which are the basis of the initial analysis of this report, meet the wind pressure criterion. The designs presented later in this report all exceeded this design check and therefore this check was not performed on each individual wall.

The second aspect of FEMA's design criteria is the ability of the safe room to resist impact from an airborne tornadic missile. FEMA adopted the previous design missile of a 15 lbf 2x4, but provided multiple velocities based on the design wind speed at a particular location. Varying missile velocities are adopted for the design of community safe rooms, but residential safe rooms are required to be designed for the worst case, no matter the location. The missile impact velocities for community safe rooms are presented in Table 2. Residential safe rooms must resist a 2x4 impact of 100 mph (FEMA P-361, 2015).

Table 2 Missile impact velocities for design wind speeds for community safe rooms. (FEMA P-361, 2015)

Safe Room Design Wind Speed	Missile Speed (of 15 lb 2x4 board member) and Safe Room Impact Surface
250 mph	Vertical Surfaces: 100 mph Horizontal Surfaces: 67 mph
200 mph	Vertical Surfaces: 90 mph Horizontal Surfaces: 60 mph
160 mph	Vertical Surfaces: 84 mph Horizontal Surfaces: 56 mph
130 mph	Vertical Surfaces: 80 mph Horizontal Surfaces: 53 mph

The procedure for testing the ability of a wall to resist tornadic missile impact is provided in ICC-500. The procedure requires the wall be impacted with a projectile in multiple areas, based on the type of construction of the wall. For a solid panel, the category that most closely resembles the wall sections built by the FPL safe room project and this study, the impact locations are the center of the wall and within 6 in. of the corner of the wall. ICC-500 and FEMA P-361 have three criteria that result in failure if they occur:

- Any amount of penetration of the missile through the entire wall section results in failure.
- No fastener or any other part of the wall section may become dislodged from the overall wall. This is tested by placing a taut sheet of kraft paper 5" behind the interior surface

of the wall section. The wall is deemed a failure if the kraft paper is perforated during the test.

- The maximum permanent deformation of the wall must be less than or equal to three inches when measured to the nearest 1/8".

2.4.2 Currently Adopted Wall Sections

Thompson (1973), Bailey (1984), and Carter (1998) conducted research at Texas Tech University on constructing safe rooms. These studies used a trial and error approach to designing a wall. Combinations of plywood, studs, sheet metal, CMU, and cast in place concrete were used to construct the walls of these projects. Walls that passed the tests performed by Carter (1998) were published in Appendix E of FEMA P-361 as walls that met the testing requirements. These walls are the only FEMA approved wall sections, as of the third edition of FEMA P-361 from 2015, and provide a starting point for engineers designing safe rooms.

2.4.3 International Code Council Standard

ICC published the first nationally adoptable safe room design standard, ICC-500, around the time of the release of the second edition of FEMA P-361 in 2008. ICC-500 relied heavily on the first printing of FEMA P-361, and the design requirements of both documents are similar. Because of the similarities of these two documents, the requirements of ICC-500 are only discussed when they differ from FEMA P-361.

2.4.3.1 Residential Safe Room Design Criteria

FEMA P-361 has a set of design criteria specific to residential safe rooms that are not included in ICC-500. FEMA P-361 requires that all residential safe rooms be constructed to the most restrictive wind speed, 250 mph, and the most restrictive missile speed, 100 mph for

horizontal surfaces. In contrast, ICC-500 allows all safe rooms, community and residential, to be designed to the same set of conditions as the FEMA guideline for community safe rooms, see Figure 8 and Table 2.

2.4.3.2 Fire Safety

Fire safety is another difference between the two documents. For community safe rooms ICC-500 requires two-hour fire barriers between the safe room and the surrounding building construction. FEMA P-361 does mention the hazards of fire, but relies on the local building code to establish fire protection guidelines rather than defining their own. Neither document requires any special fire rated construction for residential safe rooms.

2.4.3.3 Design Review Process

The final notable difference in the standards is that FEMA P-361 requires the plans of community safe rooms with an occupant load of greater than 50 people be peer reviewed by an independent design professional. ICC-500 requires peer review, but only when the design occupancy exceeds 300.

Chapter 3 Forest Products Laboratory Experimental Procedure

The data collected as part of the FPL safe room project was not analyzed or used as part of the published report (Falk, et al., 2015). This unused data provided a starting point for this project.

3.1 Design of Experiment

The testing of the walls constructed in the FPL safe room project consisted of two steps. First, a scissor jack was used to measure the quasi-static stiffness of the wall section, by applying a steadily increasing displacement to the midpoint of the wall and recording the load this caused. Second, a 2x4 missile was fired at the midpoint of the wall to determine the impact performance of the wall section. The setup and testing procedure used during the impact test conformed to ASTM Standard E1886 (2013).

3.1.1 Reaction Frame

The testing setup at FPL used a four sided reaction frame constructed of W shape steel sections. These sections attached directly to the floor slab and to a concrete structure behind the frame. The concrete structure acted as a shear wall transferring the load from the frame to the floor. In addition, a 1 ft. deep, glulam beam was mounted vertically on either side of the reaction frame. The glulam beams were attached to the steel frame through a load cell, mounted at each corner of the wall, allowing the load applied by the missile to be measured. The load cell setup is depicted in Figure 9.



Figure 9. The load cell setup of the FPL reaction frame (Falk, et al, 2015).

The walls were mounted to the reaction frame and aligned so the outer edges of the wall were approximately 1 in. inside the outer edges of the glulam beams. The walls were attached to the glulam beams by 11 in. by 15/64 in. screws at approximately 14 in. on center. The screws were driven through the walls and into the centerline of the glulam beams. The single column of bolts on each side of the wall created what was idealized as a simply supported connection. A wall mounted to the reaction frame is shown in Figure 10.

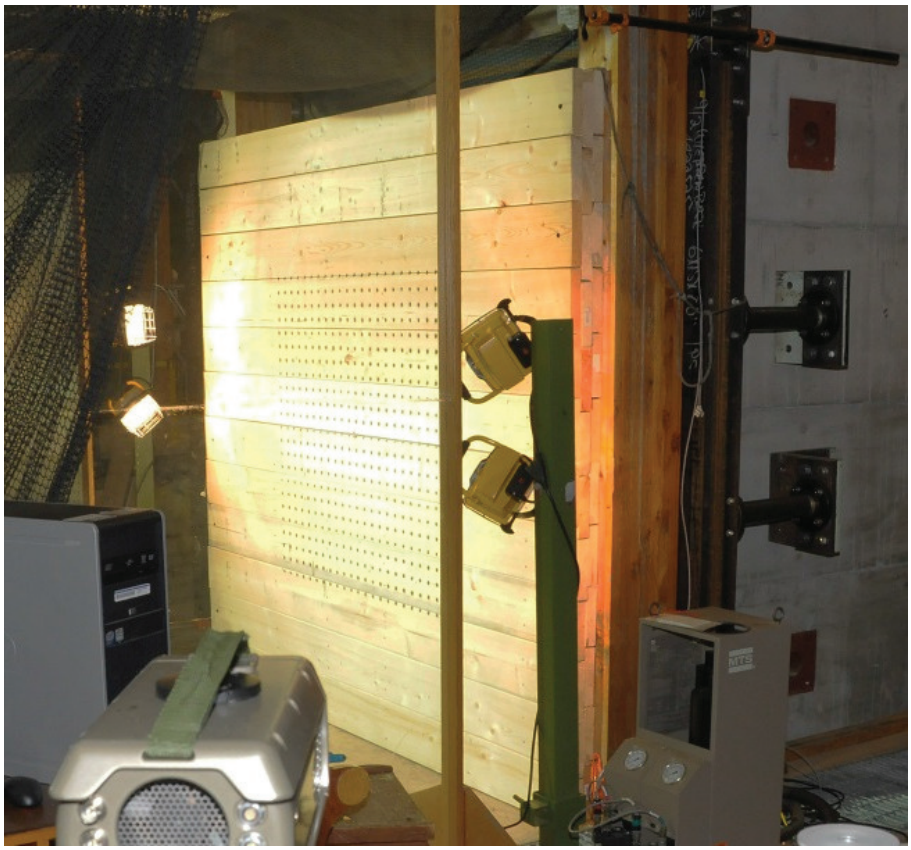


Figure 10 FPL wall mounted to the reaction frame (Falk, et al, 2015).

3.1.2 Linear Variable Differential Transformer (LVDT) Placement

The FPL safe room project used linear variable differential transformers (LVDTs) to determine the displacement of the wall. Four sensors were installed on each wall, and were located at the corners of a 44 in. square, centered in the wall. The intent of these sensors was to record the quarter point displacement of the wall during the quasi-static load-deflection test (Stiffness test) and the impact test. The location of the LVDTs and load cells used by the FPL safe room project are shown in Figure 11.

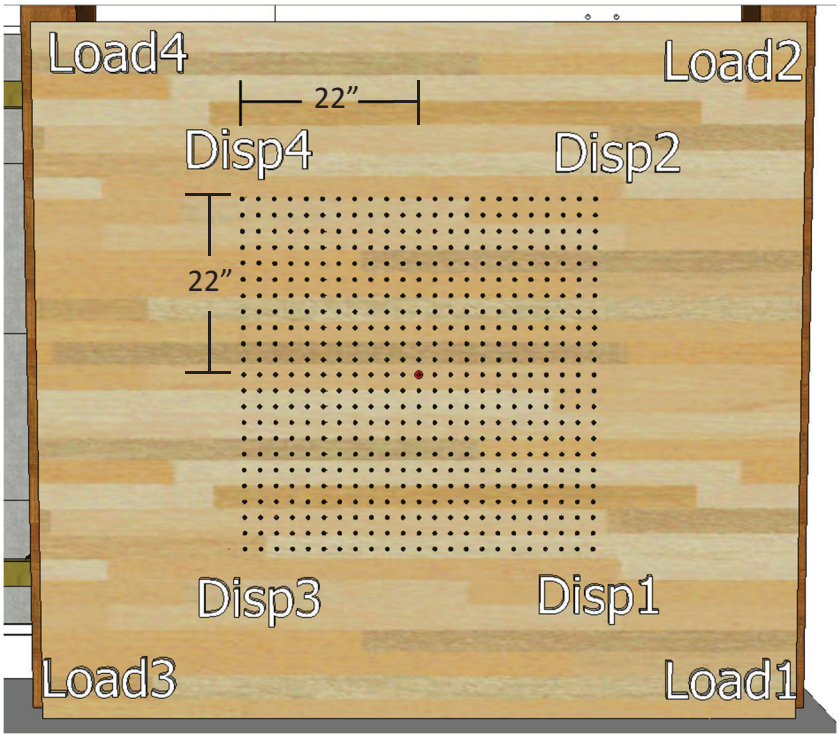


Figure 11.The LVDT (Disp) and Load cell (Load) layout of the FPL safe room project

3.1.3 Compressed Air Cannon

A compressed air cannon was used to generate a 2x4 missile at the velocity required by the FEMA guideline and ICC standard. The air cannon used at FPL is depicted in Figure 12. The user input for the cannon is air pressure (psi). Firing of the cannon prior to the testing determined that 70-psi air pressure was required to generate a missile velocity of 100 mph. The cannon was positioned so that the missile traveled a very short distance between leaving the cannon and impacting the wall. This ensured that the missile did not decelerate below the 100 mph threshold prior to impacting the wall.

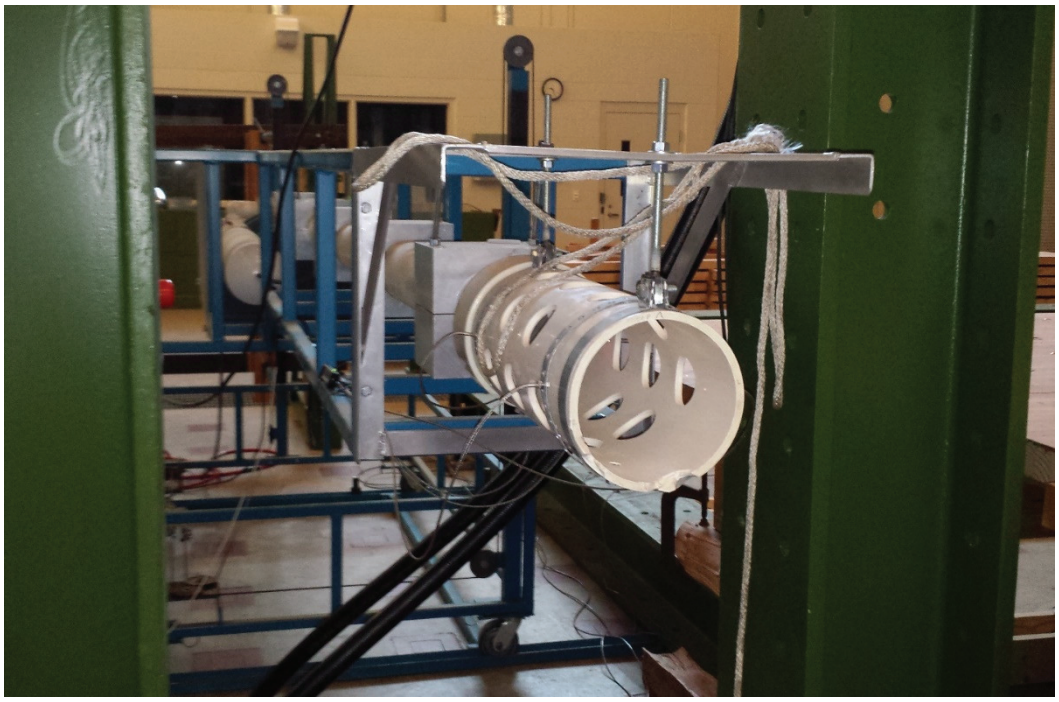


Figure 12. The compressed air cannon used to propel the 2x4 missiles.

During each test, a timing system determined the velocity of the missile upon leaving the cannon to ensure velocity requirements were being met. The muzzle of the cannon had two electro-optical sensors. When the missile was expelled from the cannon, the light from the first and then second sensor was interrupted. The interruption of each sensor sent an electrical signal to a conditioner in the instrument panel. The conditioner then calculated the time between signals. Finally, using the measured travel time and the distance between sensors, the velocity of the missile was calculated.

To generate consistent testing results and avoid damaging the sensors on the backside of the wall, the cannon had to be properly aimed. The cannon was aimed using both a laser pointer and a string. The aim of the cannon was adjusted prior to each test; making sure the missile impacted the desired area of the wall. For each test, the missile's impact location was within 2" of the target location.

3.2 Construction of FPL Walls

The FPL safe room project included the construction and testing of eight wall sections. Seven of the walls were constructed using three layers of 2x8s with addition of OSB or plywood on the front and back faces. 10d nails were used in all FPL walls to connect the layers of wood. FPL Walls 6-8 also used Liquid Nails Heavy Duty Construction Adhesive (LN-901) to connect wood layers. A picture of the basic construction of FPL Walls 1-3 and 5-8, is displayed in Figure 13. FPL Wall 4 was constructed in a different manner, using 2x4s stacked vertically with their wide face in the horizontal plane and OSB on both faces. A picture of the construction of FPL Wall 4 is displayed in Figure 14. The construction of the FPL walls is summarized in Table 3. More detailed construction drawings of the FPL walls are located in Appendix B.



Figure 13 Typical construction of a FPL wall



Figure 14 Construction of FPL Wall 4

Table 3 Summary of FPL wall construction

FPL Wall	Construction
1	Interlocking sections of 2x8s. Nailed
2	Interlocking sections of 2x8s. Nailed, with 1/2" OSB nailed to back.
3	Interlocking sections of 2x8s. Nailed, with 1/2" OSB nailed to back.
4	Stacked 2x4s oriented in strong direct. Nailed, with 1/2" OSB nailed to both faces
5	Interlocking sections of 2x8s. Nailed at an angle, with 3/4" CD grade Plywood nailed to back
6	Interlocking sections of 2x8s. Nailed with 3/4" CD grade Plywood nailed to both sides. Adhesive between 2x8s and Plywood, between adjacent 2x8s and between 2x8 layers.
7	Interlocking sections of 2x8s. Nailed with 3/4" CD grade Plywood nailed to both sides. Adhesive between 2x8s and Plywood and between adjacent 2x8s
8	Interlocking sections of 2x8s. Nailed with 3/4" CD grade Plywood nailed to both sides. Adhesive between 2x8s and Plywood.

3.3 Data Collection

The previously described LVDT and load cell setup was used for both the stiffness and impact test. During the stiffness test, a fifth LVDT was installed behind the midpoint of the wall to provide a midpoint displacement reading. This LVDT was removed during the impact test to avoid damaging the sensor due to missile perforation.

3.3.1 Quasi-Static Load-Deflection Test

The stiffness test was performed to provide stiffness values of the wall, under quasi-static loading, prior to being damaged by impact testing. A scissor jack was gradually elongated to force the wall to deflect. A load cell was located between the jack and the wall and contacted the wall using a 2x4 load head. The load cell and scissor jack setup was attached to a triangular frame of three steel members that was bolted directly to the floor. A depiction of the setup used for the stiffness test is shown in Figure 15.

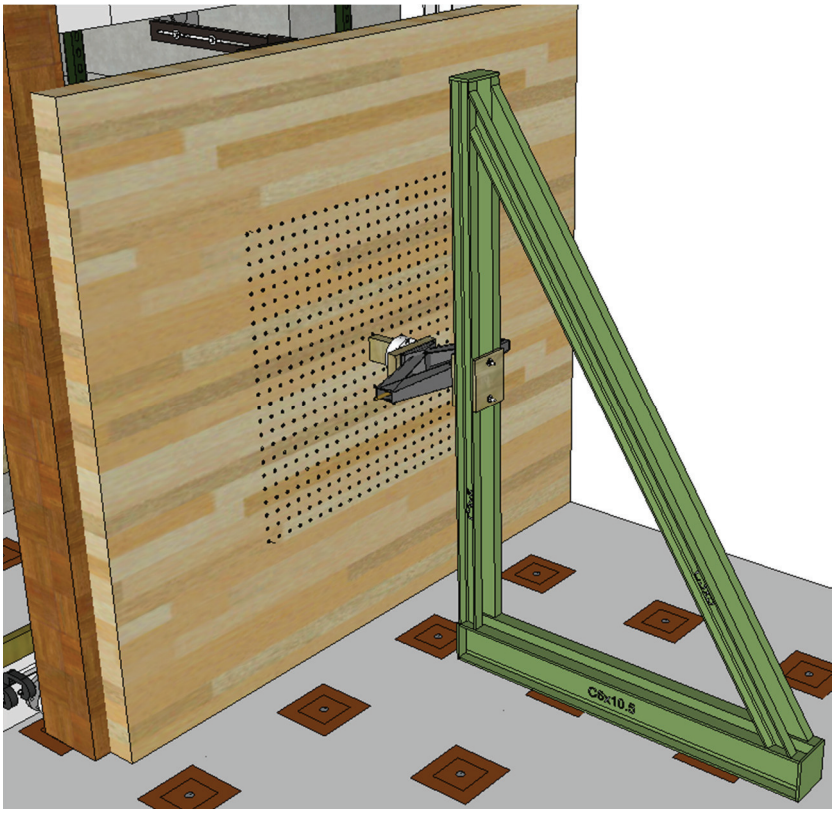


Figure 15 Quasi-static stiffness test setup

The FPL safe room project used the following procedure during the stiffness test:

- Start the data collection program to gather the displacement of the midpoint and quarter points of the wall.
- Gradually extend the jack to apply load to the wall through the load cell and 2x4 load head.
- At each increment of approximately 125 lbf the displacement reading of each LVDT was taken. The last displacement readings were taken when the load cell read approximately 1000 lbf.

3.3.2 Impact Test

The impact test used the previously described compressed air cannon to launch a 2x4 missile at the wall mounted on the reaction frame. The missile was kept at the required weight of 15 lbf by storing it in a climate-controlled room prior to the test. Shortly before the test took place, the missile was brought out of the climate-controlled room and loaded into the cannon.

The air in the cannon was then compressed to 70 psi. When the cannon fired, the speed of the 2x4 missile was recorded and the LVDTs recorded the displacement of the wall at a rate of 7000 samples per second. The LVDTs recorded displacements for two seconds after the cannon fired, after that time the displacements were deemed negligible. After the test was completed, measurements of penetration and permanent deflection were made. The results of the impact test and the pass/fail performance of each wall are summarized in Table 4.

Table 4 Summary of FPL Wall Impact Test Performance. (Falk, et al. 2015)

Panel	Missile Speed (mph)	Impact Location	Front Penetration (in.)	Permanent Rear Def. (in.)	Perforation	Pass/Fail (Criteria)
1	99.4	2" right, 1" below center.	1.6	3.0	No	Fail (Rear Def.)
2	100.5	1" left, 0" below center	2.8	4.1	No	Fail (Rear Def.)
3	102.6	0" right, 1" below center.	1.8	8.9	No	Fail (Rear Def.)
4	97.8	0" right, 3" below center	4.5	40.0	Yes	Fail (Rear Def., Pen.)
5	97.7	3" left, 3" below center	2.8	2.9	No	Pass
6	101.0	1" right, 2" below center	2.1	0.6	No	Pass
7	102.0	1" left, 0.5" below center	2.4	1.4	No	Pass
8	104.5	2" left, 1" above center	2.0	0.5	No	Pass

Chapter 4 Analysis and Modeling of Forest Products Laboratory Data

Under impact loading the displacements measured by the quarter point LVDTs appeared to take the form of a damped sinusoid, see Figure 2. Thus, a SDOF spring-mass-damper system was hypothesized to be good model of the dynamic response of the wall. Review of the high-speed video taken during the FPL tests revealed that contact between the 2x4 missile and the walls took place over less than a tenth of a second. Thus, the response of a spring-mass-damper system, subject to an impulse excitation, was deemed appropriate. To use the impulse equation (see Equation (1-3)) four pieces of information needed to be determined: K-the stiffness of the wall, M-the effective mass of the section, ζ-the damping ratio and F(t)-the forcing function.

4.1 Stiffness Mechanism Method

The first attempt to fit a spring-mass-damper model to the displacement profile of the walls used the construction of the wall to estimate its dynamic stiffness and effective mass. The static stiffness of the wall was used to help determine the effective mass and dynamic stiffness parameters. To create a model of the wall displacement, the damping ratio and the forcing function were also determined. The results of this method were then compared to the measured displacements of the FPL walls.

4.1.1 Approximation of a Stiffness Mechanism

To determine the dynamic stiffness and effective mass of the wall using its quasi-static stiffness, an approximation of the flexural mechanism of the wall was developed. The tests performed by FPL, with the exception of FPL Wall 4, used cross-sections of three layers of 2x8s

that ran parallel to each other. The boards of the middle layer were offset and crossed the gap between boards in the inner and outer layers. Each wall consisted of 2x8s, OSB and/or plywood that were held together using either nails or adhesive and nails. Figure 16 presents an idealization of the cross-section used.

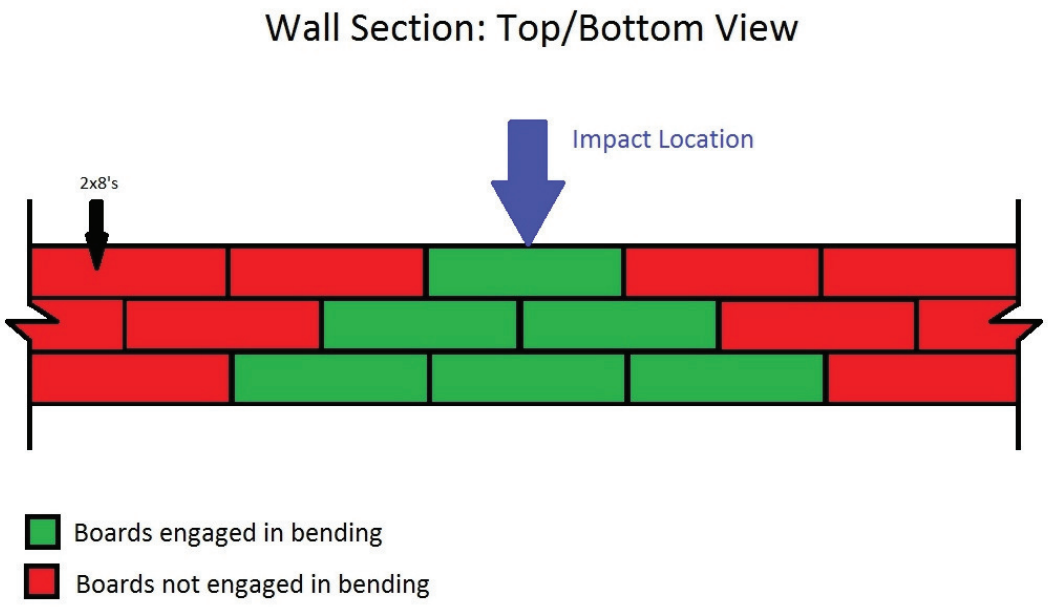


Figure 16 Cross-section and a potential bending scheme from the FPL safe room project

The construction scheme dictated that the wall engaged the boards in bending through a pyramidal scheme shown in Figure 16. When more fasteners, adhesive, and/or thicker outer layers of OSB or plywood were added, the wall had a greater stiffness and behaved with a pyramid of bending that was wider, had greater partial composite action between the layers of wood, or both. To determine the stiffness mechanism for a particular wall, an upper and lower bound consisting of a pyramidal cross-section with full composite and non-composite action

was developed. The non-composite lower bound was determined by adding the moments of inertia of each individual board in the pyramid.

Using the moments of inertia of the fully composite and non-composite sections, the upper and lower bound stiffnesses were determined using equation (4-1), assuming that all displacement was associated with flexure. The walls were not significantly deeper than they were wide so shear deformation was deemed negligible. In addition, a calculation of energy dissipated by combined crushing and shearing of the exterior layer accounted for less than 5% of the missile's energy, which was also deemed negligible. The pyramidal mechanisms used to determine the bounds are shown in Figure 17 and the upper and lower bounds are shown in Table 5.

$$k = \frac{48EI}{L^3} \qquad (4\text{-}1)$$

Where:

I = Dynamic moment of inertia (Length^4)
E = Modulus of elasticity of the wood (Force/Length^2)
L = Length of wood member (Length)

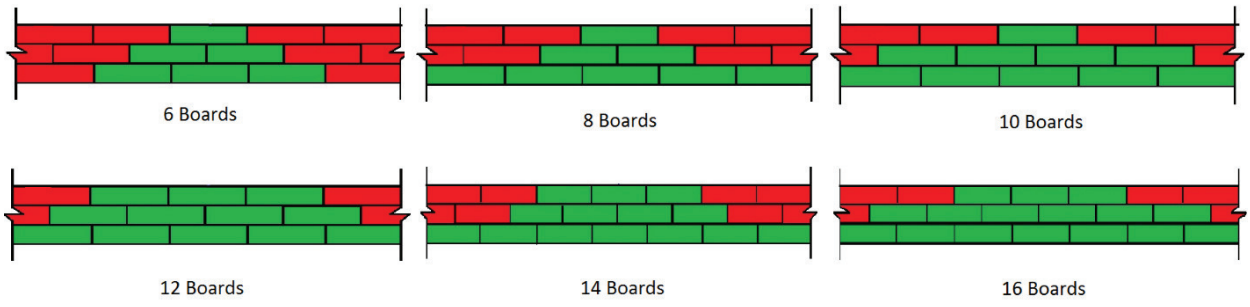


Figure 17 Idealized bending mechanisms for the FPL wall designs

Table 5 Upper and lower stiffness bounds

# Boards	Lower Bound (lbf/in.)	Upper Bound (lbf/in.)
6	929	7124
8	1239	8673
10	1549	9726
12	1859	16020
14	2168	18630
16	2478	19210
18	2788	24680

4.1.2 Analysis of Stiffness Test

To estimate the partial composite action and thus the dynamic stiffness, the static stiffness was first analyzed and bound by the upper and lower bounds of the previous section. The measured data for load, plotted with respect to midpoint displacement, were fit with a line and the resulting slope was the stiffness of the wall section. Wood is typically modeled as linear before the proportional limit, thus a line was used to determine the relationship between load and displacement. From the displacements recorded by the quarter point LVDTs a quarter point stiffness was also determined using the same method. An example of the load-displacement data fit and stiffness calculation is shown inin Figure 18. A stiffness summary of the FPL walls is displayed in Table 6. Once the midpoint stiffness was known, the difference between the upper bound and the static stiffness was divided by the difference between the upper and lower bound to determine an estimate of partial composite action.

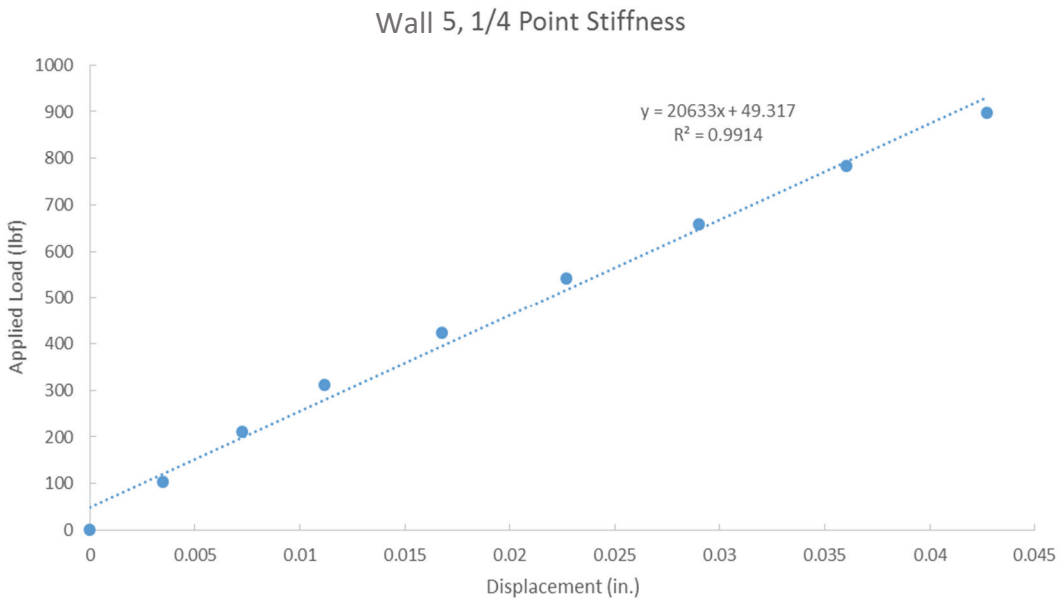


Figure 18 Example load vs. displacement plot and trend line.

Table 6 The midpoint and quarter point stiffness of the FPL walls

Stiffness (lbf/in.)		
FPL Wall	Midpoint	1/4 Point
1	3486	39694
2	3500	35673
3	4292	21405
4	8885	24021
5	5169	20633
6	6928	13849
7	9439	18870
8	5123	10238

4.1.3 Stiffness Mechanism Method Results

Analysis of the stiffness test for the midpoint of each wall yielded a stiffness below 7000 lbf/in. for six of the eight FPL walls. Using just this information and the upper and lower bounds found in Table 5, six of the FPL walls may have had between 6 and 18 boards engaged in flexure during the stiffness test. Therefore, use of this method involved a significant amount of

engineering judgement and guesswork to determine values of partial composite action, dynamic stiffness, and effective mass. Thus, the results of this method were arbitrary and were not used for further modelling, so the derivations of values of effective mass, stiffness, and damping ratio are omitted from this report.

Use of the stiffness mechanism method to determine values of dynamic mass and stiffness returned unreliable fits to the measured displacement of the wall. The comparison for FPL Wall 8 between the SDOF model and the measured displacement as shown in Figure 19 was typical for all wall specimens The agreement of the amplitude for the first two cycles was almost exact, but the model failed to match the frequency of the tested wall. Accurately finding the peak deflection is important, since it relates to maximum stress, but frequency matching is also important. The frequency is defined by both the effective mass and stiffness of the system; therefore, either the wrong effective mass and/or stiffness were input into the model. The disagreement of the frequency predicted by the stiffness mechanism method and the measured frequency of the wall response was deemed unsatisfactory and led to the development of another method to fit the model parameters to the data.

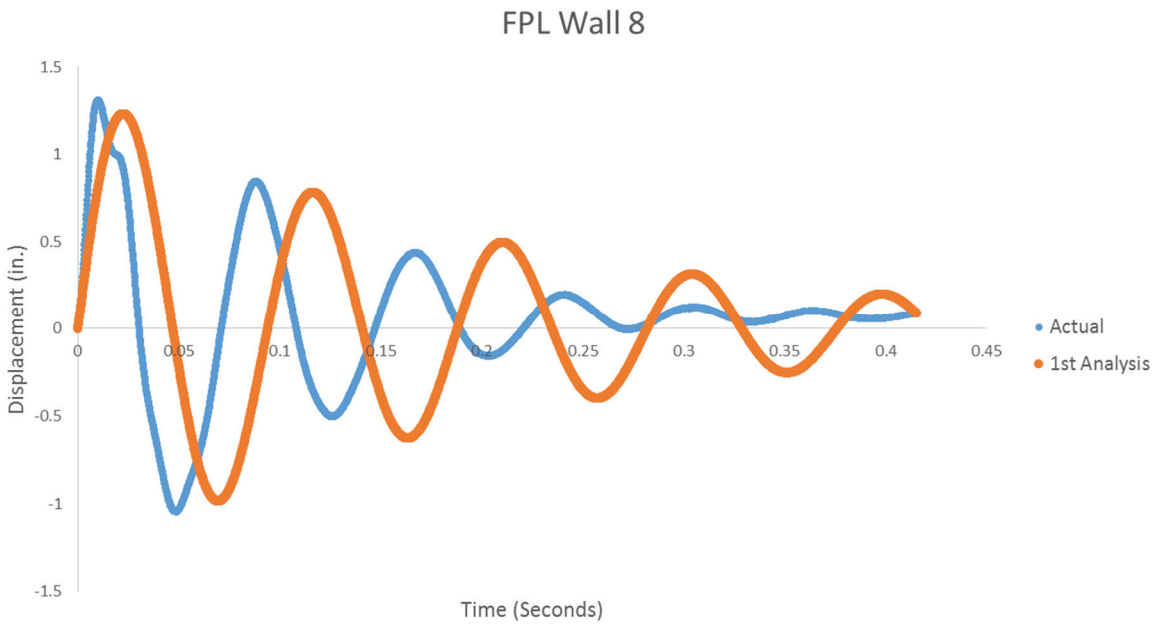


Figure 19. Midpoint displacement of model (Orange) and wall (Blue) for FPL Wall 8.

4.2 Nonlinear Regression Method

Results from initial modeling showed that experimental data fit the impulse excitation closely enough to justify more investigation. The stiffness mechanism method used static stiffness to approximate dynamic stiffness and effective mass. The results of this method were then compared to the measured displacement response. For the second attempt, the problem was reversed. Using a nonlinear regression program, written in the R programming language, the dynamic stiffness, effective mass, and damping ratio that best fit the measured data were determined. The displacement profiles were then compared to determine how well the new spring-mass-damper model approximated the measured behavior of the wall. Refer to Appendix C for the nonlinear regression program.

Data from the FPL tests provided displacement data for the quarter points of the walls, but the midpoint dynamic mass, stiffness, and damping ratio were sought. The quarter point

displacement was multiplied by the ratio between the midpoint and quarter point stiffness to determine the midpoint displacement. The assumption that this ratio of stiffness is valid for both quasi-static and dynamic loading is verified later in this report.

To use nonlinear regression, the forcing function of the spring-mass-damper response had to be provided. The two excitations of a spring-mass-damper system that are most applicable to this particular scenario are the impulse excitation and the step excitation. An impulse excitation uses a change of momentum (Force*Time) to excite the system. A step excitation applies a force to the system for a length of time determined by the user. Impact has a very short duration, thus, it was determined that the impulse excitation fit the loading scenario most closely. Equation (4-2) was used to determine the change of momentum in the wall due to impact of the 2x4 missile.

$$F(t) = m * v = \frac{15\ lbf}{32.2\frac{ft}{s^2}} * 100\ mph * 5280\frac{ft}{mile} * \frac{1\ hr}{3600\ sec} = 0.068\ kip * s \qquad (4\text{-}2)$$

Equation (1-3) represents the hypothesized behavior of a wall subject to impact loading of a safe room. Stiffness does not appear as an isolated term in this equation, but appears as a ratio with effective mass in each instance. Nonlinear regression programs cannot find variables that do not appear as isolated terms. Therefore, the generalized exponential decay equation was solved. Then effective mass, stiffness, and damping ratio were sought from those results. The general exponential decay equation is shown in Equation (4-3). After the program found values for the variables in Equation (4-3) that provided the best fit to the measured displacement data, a comparison between Equations (1-3) and (4-3) yielded Equations (4-4),

(4-5), and (4-6) which were used to determine damping ratio, effective mass, and stiffness respectively.

$$y = Ae^{-\lambda t}\sin(\omega t + \phi) + Offset \quad (4\text{-}3)$$

$$\zeta = \frac{1}{\sqrt{\frac{\omega^2}{\lambda^2} + 1}} \quad (4\text{-}4)$$

$$M = \sqrt{\frac{mv^2}{A^2\omega^2 + A^2\lambda^2 - 1}} \quad (4\text{-}5)$$

$$k = \lambda^2 \frac{M}{\zeta^2} \quad (4\text{-}6)$$

Where:

mv = Momentum of missile (Force*Time)
ζ = Damping ratio (Unitless)
M = Mass ({Force*Time}/Length)
k = Stiffness (Force/Length)

Once the stiffness, effective mass, and damping ratio were determined, they were substituted into the spring-mass-damper equation for an impulse excitation and compared with the displacement data. As an example of this output, the displacement and impulse equation with fitted mass, stiffness, and damping ratio of FPL Wall 6 are plotted in Figure 20.

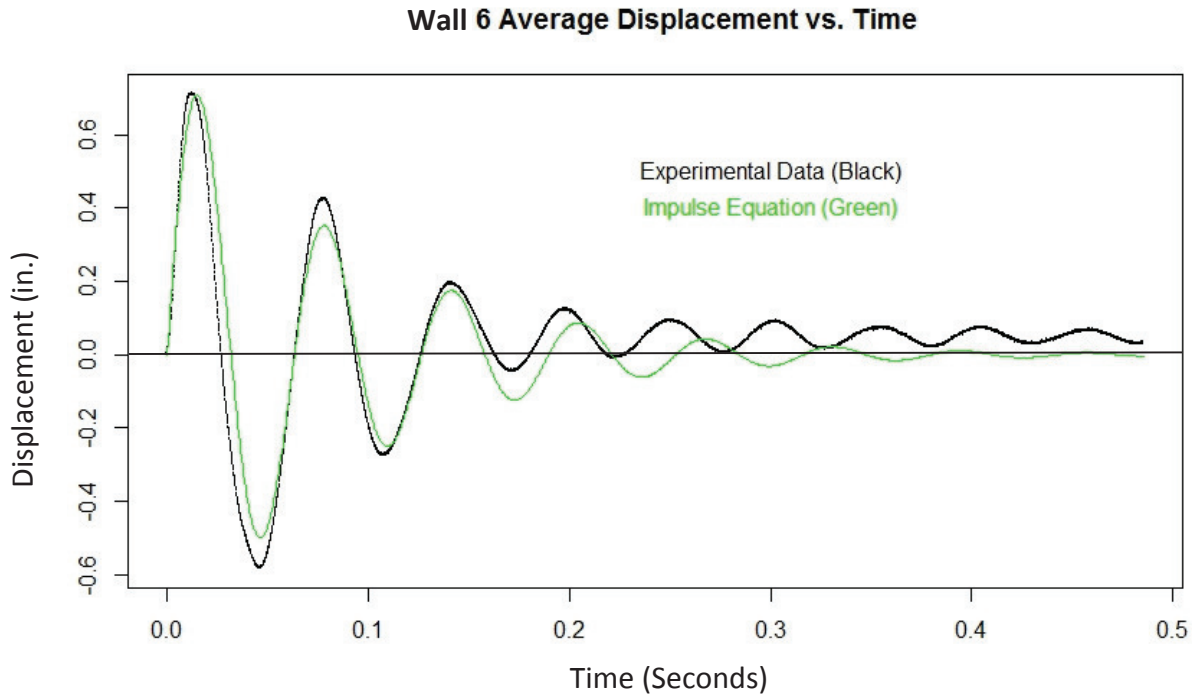


Figure 20 Plot of measured displacement (Black) and model (Green) for FPL Wall 6.

The frequency began to deviate between the model and the measured displacements after the third peak. This was due to a shift in the frequency of the displacement data. For the purposes of this project, the shift was deemed not to be in conflict with the objective of matching the behavior of the first few cycles. Thus, the nonlinear regression program was focused on fitting the first few cycles and ignored the shift. The shift suggested that the effective mass or the stiffness of the wall is changing at this point, either the effective mass is decreasing, or the stiffness is increasing. A slight increase in stiffness may make sense. Reexamination of Figure 18 shows that although the stiffness can reasonably be approximated as linear, the stiffness of the wall appears to be higher at low levels of load. A decrease in effective mass may also have occurred due to damage of the wall from the impact of the missile.

4.3 Verification of Nonlinear Regression Parameters

Nonlinear regression may provide unrealistic values for mass, stiffness and damping ratio. In this case, no limitations were imposed in the nonlinear regression program with regard to ranges of mass, stiffness or damping ratio. This meant that the program could output parameters that did not make physical sense, such as an effective mass higher than the mass of the entire wall. Therefore, the computed parameters of effective mass, stiffness, and damping ratio were compared to the static stiffness, total mass of the system and the damping ratio calculated using the log decrement to ensure they were reasonable.

4.3.1 Calculation of Damping Ratio

The static stiffness and total mass of the walls was known, so only the damping ratio had to be calculated. An analysis of the displacement of the quarter points in response to the impact of the 2x4 was used to determine the damping ratio of wall section. An example of the displacement of the quarter points measured in the FPL impact test was shown in Figure 2. The exponential decay of the displacement indicates that the system is underdamped. The damping ratio (ζ) was determined using the log decrement method in Equations (4-7) and (4-8) (Ginsberg, 2001).

$$\delta = \ln\left(\frac{x_j}{x_{j+1}}\right) \qquad (4\text{-}7)$$

$$\zeta = \frac{\delta}{\sqrt{4 * \pi^2 + \delta^2}} \qquad (4\text{-}8)$$

Where:

x_j = Peak value of displacement (Length)

x_{j+1} = Subsequent peak value of displacement (Length)

Using the plots of displacement and the above equations damping ratios were computed for FPL Walls 2-8. FPL Wall 1 was the first tornadic safe room wall section constructed at FPL and was therefore used as a trial wall. Because this was the first test specimen, calibration issues had not been fully debugged when it was tested. For this reason, no reliable displacement data was collected to determine the damping ratio. The damping ratios calculated using the first two peak values of displacement are shown in Table 7.

Table 7 Damping ratios calculated from the log decrement

Wall	Damping Ratio (Unitless)
2	0.152
3	0.111
4	0.158
5	0.142
6	0.083
7	0.070
8	0.072

4.3.2 Comparison of Parameters

The effective mass, stiffness, and damping ratio of each wall as derived from the models are tabulated in Table 8. The nonlinear regression and measurable parameters from Table 8 were in general agreement, in that they do not differ by orders of magnitude. As expected the dynamic mass and stiffness of the walls were found to be less than the total mass of the wall and the static stiffness of the wall respectively. The only exception to this was FPL Wall 4, which had a higher dynamic stiffness and effective mass than its measured static stiffness and total mass.

Table 8 Comparison of nonlinear regression and measureable parameters

	Comparison Parameters			Nonlinear Regression Parameters		
FPL Wall	Total Mass (slugs)	Static Stiffness (lbf/in.)	Damping Ratio (Unitless)	Effective mass (slugs)	Stiffness (lbf/in.)	Damping Ratio (Unitless)
2	19.2	3500	0.152	1.5	572	0.180
3	19.2	4292	0.111	3	1860	0.121
4	13.4	8885	0.158	15.74	13700	0.085
5	19.2	5169	0.142	3	2560	0.160
6	19.2	6928	0.083	9.3	8160	0.104
7	19.2	9439	0.070	8.4	5960	0.103
8	19.2	5123	0.072	6.9	4040	0.080

Unlike the other walls, FPL Wall 4 was constructed using a series of 2x4s stacked vertically with their wide dimension oriented horizontally, shown in Figure 14. In addition, there was no exterior layer, other than OSB, to reduce the impact force and distribute the load through crushing. When FPL Wall 4 was tested, the 2x4 missile perforated through the wall by over a foot. This localized failure was attributed to a lack of a sacrificial layer to distribute the load to the other members of the wall. Therefore, due to the localized failure of FPL Wall 4 the sensors were displaced very little. This caused an analysis of the displacement data to suggest that the wall performed with an abnormally high stiffness and effective mass.

The fit of the nonlinear regression model to the measured displacement data was quantified by using the coefficient of determination (R^2). The R^2 values for each FPL wall are shown in Table 9. The R^2 values were significantly closer to one for walls 5, 6, 7, and 8, indicating that as the stiffness of the wall increased, a perfect spring-mass-damper system more accurately modeled the behavior. As an example, the spring-mass-damper model using parameters from nonlinear regression and the measured displacement of FPL Wall 5 are

plotted in Figure 21. Discounting the issues with FPL Walls 1 and 4, output parameters from nonlinear regression were shown to fit displacement data from the impact tests in an accurate and precise manner.

Table 9 Coefficient of determination for each FPL wall

Nonlinear Regression	
FPL Wall	R^2
2	0.74
3	0.88
4	0.62
5	0.90
6	0.93
7	0.91
8	0.92

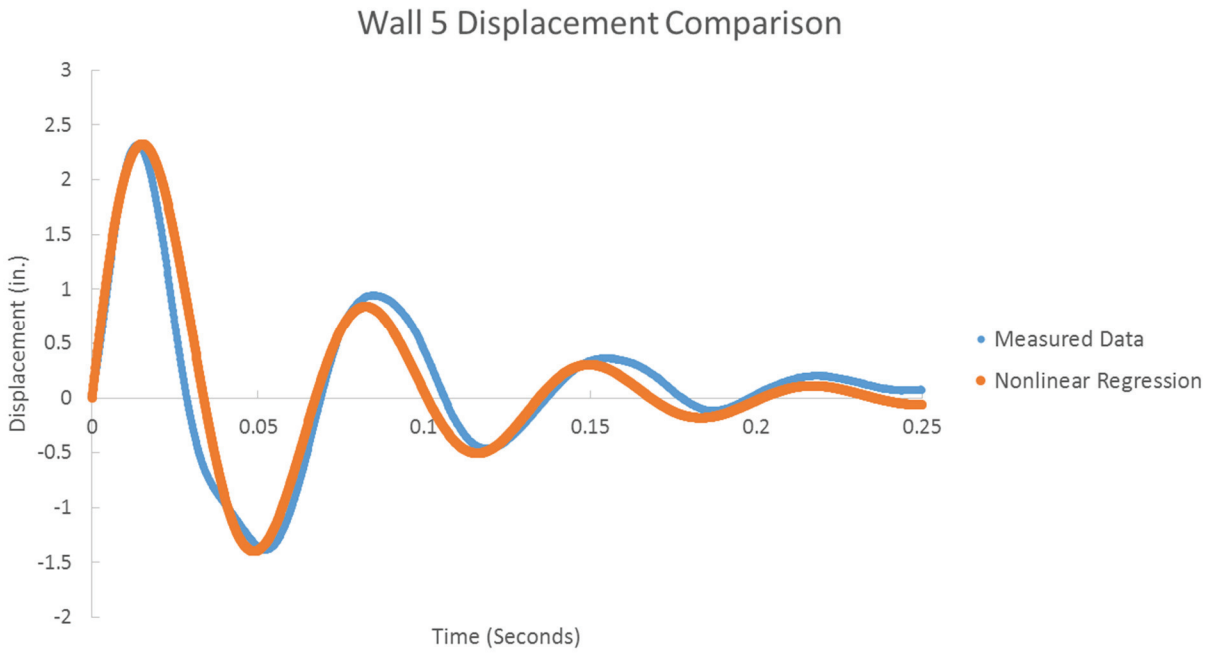


Figure 21. Comparison of nonlinear regression model and measured data.

4.4 Analysis of Midpoint/Quarter Point Stiffness Ratio

The FPL tests recorded the stiffness of the wall at its midpoint and quarter point under quasi-static loading. The ratio between these stiffness values was compared to the same ratio from a finite element model of an orthotropic plate. This comparison was used to analyze how close the behavior of the walls matched that of theoretical plate theory. A finite element model of eight node solid elements with orthotropic material properties was built using the ADINA finite element analysis package, creating a model of an orthotropic plate. Under a unit load at the midpoint of the plate, a Python script was used to iterate the material properties to best match the measured behavior of the walls. The iterations reduced the elastic modulus of the plate in the tangential direction of the boards, leaving the elastic modulus in the longitudinal direction constant. The initial values of these moduli were estimates of wood

moduli taken from *The Wood Handbook* (2010). The moduli were reduced from their initial values until the midpoint deflection to quarter point deflection ratio in the finite element model matched the same ratio from the stiffness test of the wall.

The tangential modulus that matched the behavior of the wall was divided by the initial modulus value to determine the modulus ratio. A ratio of one meant that the wall behaved like an orthotropic plate, while a ratio of zero meant that the wall behaved like a narrow beam that did not affect the quarter point. Analysis of further walls in this manner may lead to the development of relationships between the various connections and the effect they have on the average material properties on the section. In addition, it may be found that walls with a modulus ratio and dynamic stiffness above some threshold always pass the impact test. The ratios found by this analysis are tabulated in Table 10.

Table 10 Ratios of midpoint to quarter point stiffness (K) and elastic moduli (E).

FPL Wall	K Ratio	E Ratio
1	0.088	0.014
2	0.098	0.014
3	0.201	0.014
4	0.370	0.162
5	0.251	0.027
6	0.423	0.846
7	0.462	1
8	0.394	0.268

Chapter 5 Wall Section Design Method

Based on the modeling and analysis of the FPL tests presented in Chapter 4, a design procedure was developed. The procedure presented here was then evaluated against a set of new wall test results.

The key steps in this procedure are as follows:

1. Determine the stiffness ratio (midpoint vs. quarter point)
2. Estimate a lower bound midpoint stiffness
3. Estimate an upper bound midpoint stiffness
4. Estimate the static stiffness from the bounds and a partial composite action calculation
5. Estimate the dynamic stiffness from the static stiffness estimate
6. Estimate the effective mass of the system
7. Compare the stiffness ratio, stiffness, and effective mass from the design to the proposed design thresholds
8. If the effective mass and stiffness parameters of the wall are above the threshold, build and test the wall, if not modify the design and start over

5.1 Design Thresholds

In Chapter 4 the nonlinear regression parameters were shown to provide agreement with the physics of the wall under impact loading. Therefore, these parameters were used in the design procedure to design additional walls. The parameters provided insight into how the wall sections performed when tested in impact and the physical properties of wall. From these

parameters, relationships that appeared to relate the physical properties of the wall to its pass/fail performance were found. These relationships formed the basis of the minimum design thresholds proposed by this project. The walls designed in this section were subsequently tested to determine the viability of the proposed design procedure and thresholds.

The effective mass and stiffness calculated from the displacement data of the FPL walls using nonlinear regression are plotted in Figure 22. The data suggested that the effective mass and stiffness of a wall section subject to impact are related in a roughly linear fashion. A linear relationship might be logical for the FPL walls because the construction method created a partial composite beam that linked the stiffness and effective mass. The stiffness of this beam varied based on the connections used between boards. In this case, each individual board that contributed to the stiffness was bending in approximately the same manner. Thus, the amount of mass engaged in bending was directly related to the stiffness of the wall section. The imperfect fit of a line to these data demonstrates that where the additional boards are added to the cross section also mattered. A board engaged in the inner or outer layer, away from the neutral axis, added more stiffness than a board engaged in the middle layer.

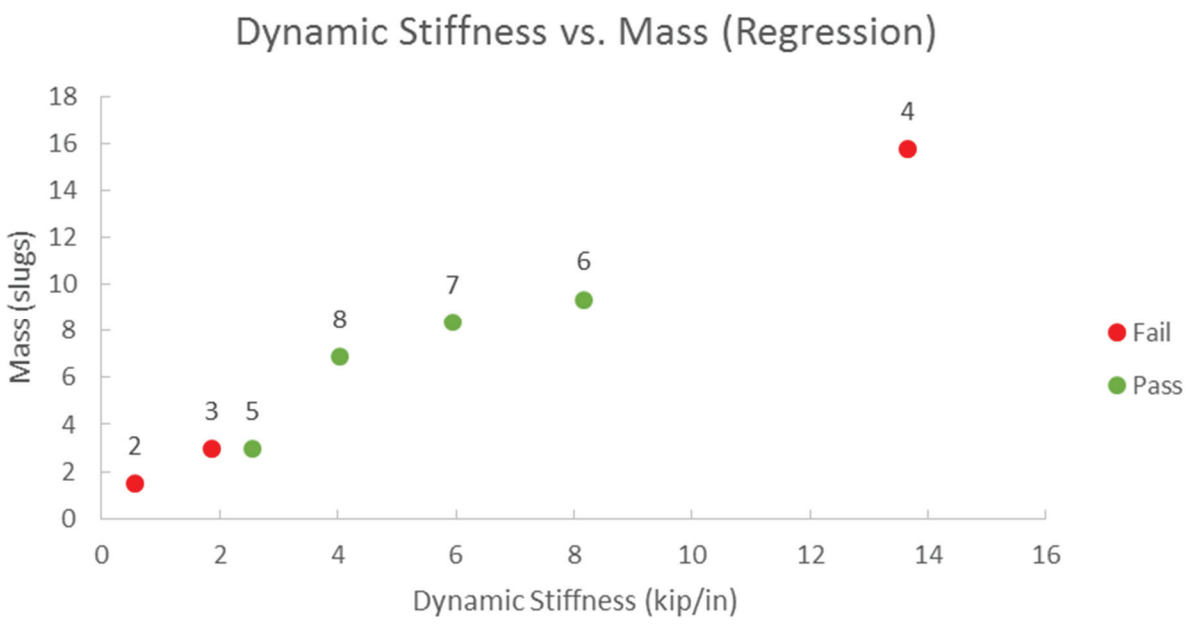


Figure 22. Dynamic stiffness and effective mass of FPL walls (Wall number). Pass (Green). Fail (Red).

The midpoint stiffness and the ratio between the midpoint stiffness and quarter point stiffness (stiffness ratio) of the wall sections constructed by FPL are plotted in Figure 23. The curve implied by this relationship appears to asymptotically approach a value between 0.45 and 0.5 as the overall stiffness of the section increased. From plate theory, for an isotropic plate, the ratio between the deflection of the quarter point and the midpoint under a unit load at the midpoint is 0.47. The data from Figure 23 suggested that as the stiffness of the wall sections was increased, by adding plywood and/or adhesive, the walls acted more like a plate. The total stiffness provided by a wall directly related to stiffness ratio, therefore stiffness ratio was hypothesized to be an important factor in the pass/fail behavior of the walls.

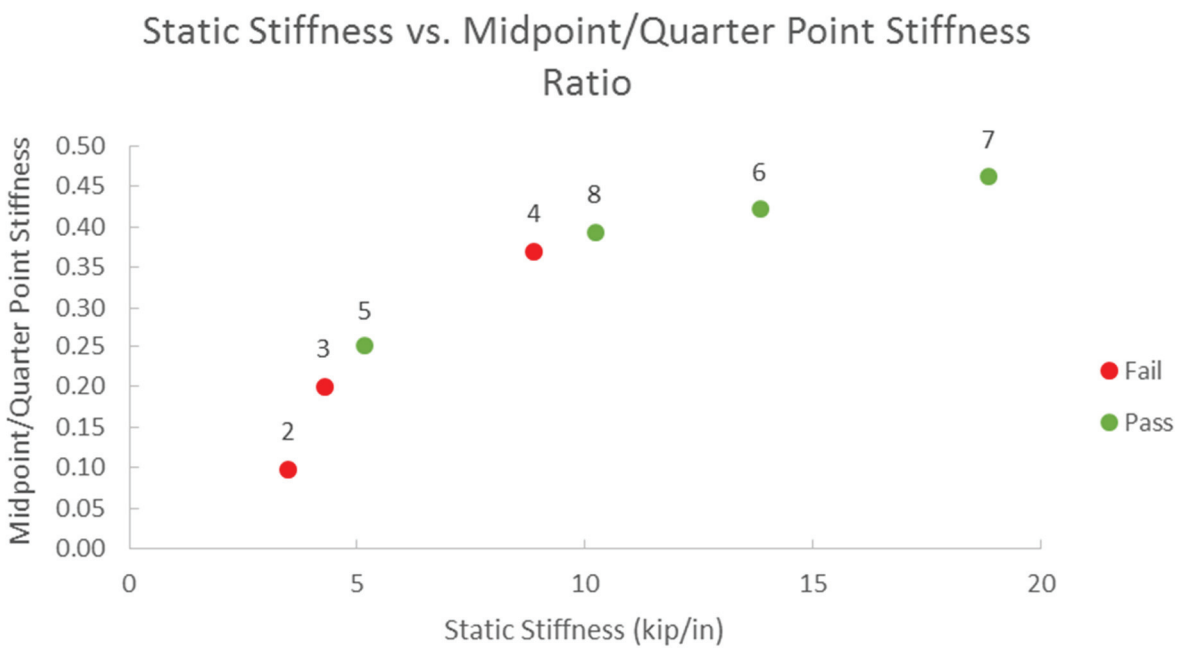


Figure 23. Midpoint static stiffness and stiffness ratio of FPL walls (Wall number). Pass (Green). Fail (Red).

Static stiffness is only a preliminary indicator of the dynamic stiffness of the system, thus it was not used in a design threshold. Instead, the relationship between dynamic stiffness and the stiffness ratio was considered for design. The dynamic stiffness and stiffness ratio of the FPL walls are plotted in Figure 24.

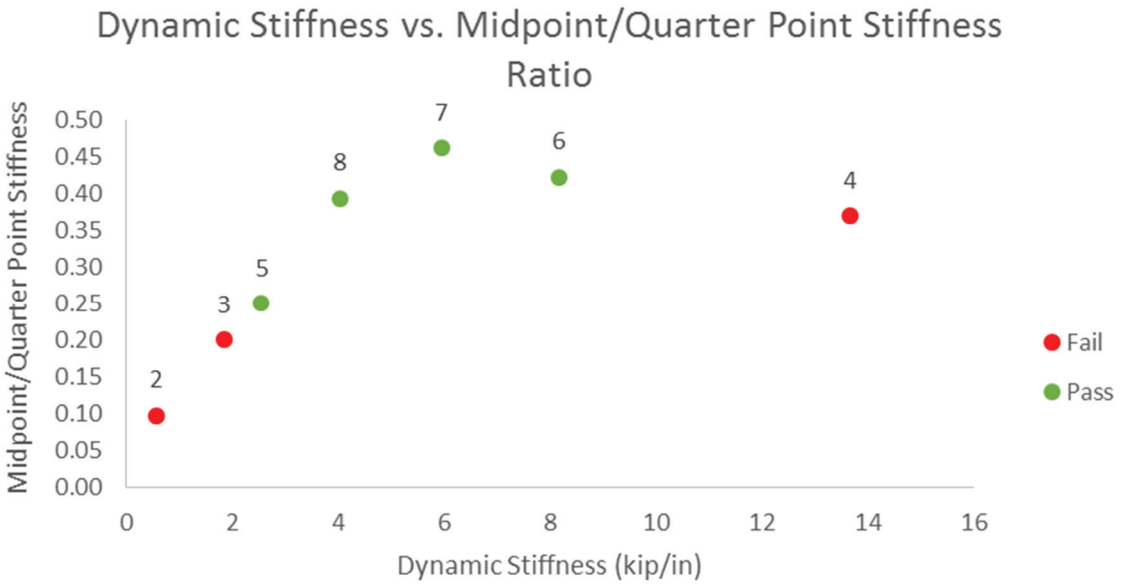


Figure 24. Dynamic stiffness and stiffness ratio of FPL walls (Wall number). Pass (Green). Fail (Red).

The minimum proposed design thresholds are presented in Table 11. These thresholds were selected based on the pass/fail performance and parameters of the FPL walls shown in Figure 22 and Figure 24. FPL Wall 5 had the lowest dynamic stiffness, effective mass, and stiffness ratio of the walls from the FPL safe room project that passed the impact test, therefore its values provide the minimum thresholds in Table 11. Not enough data exists to determine if both thresholds are valid or need to be met; therefore, the current design procedure assumes they are both valid.

Table 11. Minimum proposed design thresholds.

Proposed Threshold	Dynamic Stiffness (lbf/in.)	Effective mass (slugs)	Stiffness Ratio
Dynamic Effective mass-Stiffness	2500	3	N/A
Dynamic Stiffness-Stiffness Ratio	2500	N/A	0.25

To provide more evidence to the validity of pass/fail thresholds the walls of this project were constructed in a slightly different manner than the FPL walls. The middle layer of 2x8s were rotated 90^{o} to run in the vertical direction, while the orientation of the outer and inner layers remained the same. If pass/fail thresholds are shown to be valid for safe room wall design, future research and development can focus on methods to more exactly determine the effective mass, stiffness, and stiffness ratio.

The data points of FPL Wall 4 contradict the minimum design threshold hypothesis. The tests performed by FPL suggested that during impact of the wall section, the missile penetrated 1.5" to 2", before stopping and forcing the wall into flexure. FPL Wall 4 had no outer layer of wood that could be used sacrificially to dissipate and distribute the energy of the missile. Therefore, it was hypothesized that a large amount of the wood required to carry the flexural load was lost due to crushing. Thus, one of the designs carried out in this project was the same 2x4 wall with an added layer of 2x4s, oriented with their wide face perpendicular to the direction of impact. If this wall were found to pass the impact test, a caveat would be added to the design procedure for wooden walls. The caveat would be that a sacrificial outer layer of wood or some other energy absorbing material must be present in addition to the inner layer(s), which provide the flexural stiffness.

5.2 Design Procedure

The main wall design of this report took the three layers of 2x8s that the FPL design used and rotated the middle layer 90^{o}. The purpose of the proposed design change was to allow biaxial bending to occur in the wall section. Thus, by having two layers of wood oriented in the horizontal direction and one layer oriented in the vertical direction, the wall had a

stronger effective modulus of elasticity in the vertical direction. This would allow the wall to behave in a manner similar to a plate, but do so without resorting to the use of adhesives or the thick plywood used by the FPL walls. Elimination of plywood and adhesives lead to a savings of at least $100 per wall.

Currently no procedure exists for the design of a partially composite wood structure built in this manner. Therefore, one of the goals of this project was to determine a preliminary design procedure that could be used to design wooden safe room walls. The design of these walls is unique to the construction type, meaning some of the presented equations and assumptions for design, will not directly translate to walls with wood oriented differently. However, the same procedural steps, thought processes, and general equations should be followed for all types of wooden safe room wall designs. Refer to Appendix D for detailed calculations using the proposed procedure.

5.2.1 Determination of Stiffness Ratio

Data collected from the FPL safe room project and engineering judgment suggested that the stiffness ratio might be important for the pass/fail behavior of a wall section subject to impact. The stiffness ratio is an indication of two-way bending capability, and when the capability increases the wall becomes stiffer, and its load distribution ability increases.

The elastic modulus ratio relationships developed in Section 4.4 were used to estimate the stiffness ratio. If a wall had the same elastic modulus in all directions, its elastic modulus ratio would be one. To determine an estimate of the ratio between the elastic moduli for a particular section, an average of the elastic moduli in the weak direction was normalized to an average of the elastic moduli in the strong direction. In this context, the strong direction is the

direction with more boards oriented in it, and the weak direction is the direction with fewer boards oriented in it. The narrow faces of the lumber had no connectivity between them, so the tangential modulus of the wood was discontinuous across the section and was set to zero in this calculation. The elastic modulus ratio was then found using Equation (5-1), which takes the form of Equation (5-2) for this particular design.

$$E_{ratio} = \frac{(Et)_{weak}}{(Et)_{strong}} \quad (5\text{-}1)$$

Where:

E_{ratio} = Elastic modulus ratio (Unitless)
E_{weak} = Modulus of elasticity in weak direction (lbf/in.^{2})
E_{strong} = Modulus of elasticity in strong direction (lbf/in.^{2})
t = Thickness of the wall (in.)

$$E_{ratio} = \frac{E_L h + E_T 2h}{E_L 2h + E_T h} = \frac{E_L h + 0}{E_L 2h + 0} = 0.5 \quad (5\text{-}2)$$

Where:

E_L = Longitudinal modulus of elasticity of wood species (lbf/in.^{2})
E_T = Tangential modulus of elasticity of wood species (lbf/in^2)
h = Depth of each layer of wood (in.)

The ratio found using Equation (5-2) was traced onto the plot of elastic modulus ratio versus stiffness ratio. From this trace, the stiffness ratio was determined to be 0.405, which is greater than the stiffness ratio of the FPL walls that did not use adhesives. The plot of elastic modulus ratio and stiffness ratio with the trace drawn on it is shown in Figure 25.

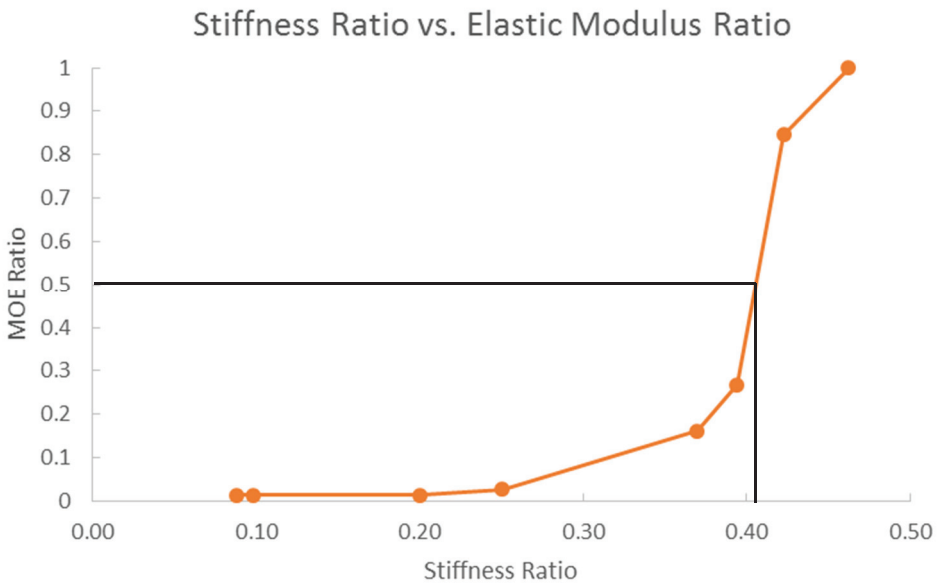


Figure 25. Determination of expected stiffness ratio

5.2.2 Determination of Stiffness Parameters

Expected static stiffness of the wall was found by using an estimate of partial composite action and relation to an upper bound and lower bound. The lower bound was a non-composite section and the upper bound was a plate with a thickness determined using the transformed section method.

5.2.2.1 Lower Stiffness Bound

The lower bound solution idealized each layer of 2x8s as wide beams, which were non-composite and simply supported. Because the layers were assumed non-composite, the full width of each layer would not be fully engaged in bending. Thus, a method to approximate an effective width of the idealized beams was sought. The deflected shape of a simply supported beam was integrated and compared to the area of a rectangle defined by the length and maximum deflection of the beam. The integral of the deflected shape made up approximately 60% of the area of the rectangle. Thus, if another wide beam was oriented perpendicular to

the first beam, and was required to have compatible deflections, approximately 60% of the second beam would be fully engaged in flexure.

Once the approximate beam width subject to bending was determined, calculation of the beam stiffness was straightforward. The effective width of one beam was determined by multiplying the width of the wall (94 in.) by 60%, yielding 56 in. Then, the moment of inertia of the beam (15.8 in.^{4}) was calculated using the effective width (56 in.) and the layer thickness (1.5 in.). Next, the midspan stiffness of the beam (1.6 kip/in.) was calculated using Equation (4-1). For this design, under quasi-static loading, the wall was approximated as three wide beams. Thus, the lower bound quasi-static stiffness of the wall was three times the midspan stiffness of the wide beam, or 4.8 kip/in.

The lower bound solution presented in this section is unique to wall designs that use layers of wood in alternating directions. For other wall designs, a suitable lower bound must be determined from the expected bending mechanisms of the wall. For example, a non-composite lower bound solution for the FPL walls may use the six-board bending stiffness mechanism displayed in Section 4.1.1.

5.2.2.2 Upper Stiffness Bound

To determine an upper bound of the stiffness of the wall section, an idealization of the wall as an isotropic plate was used. The effective thickness of the isotropic plate was determined by finding the flexural depth in the horizontal and vertical directions of the wall and averaging them. The effective depth of the plate, 2.36”, was found using Equation (5-3). If the wall was isotropic, Equation (5-3) would yield an effective depth equal to the total depth of the wall, thus this method should yield a reasonable upper bound for all wooden wall designs.

For this wall design, Equation (5-3) is rewritten as Equation (5-4) . The upper bound solution considers a fully composite wall, thus the tangential modulus of the wood is set to a reasonable value from *The Wood Handbook* (2010).

$$h_{eff} = \frac{\frac{E_{weak}t}{E_L} + \frac{E_{strong}t}{E_L}}{2} \quad (5\text{-}3)$$

Where:

E_{weak} = Modulus of elasticity in weak direction (lbf/in.^{2})
E_{strong} = Modulus of elasticity in strong direction (lbf/in.^{2})
E_L = Longitudinal modulus of elasticity of wood species (lbf/in.^{2})
t = Thickness of the wall (in.)

$$h_{eff} = \frac{\frac{E_L 2h + E_T h}{E_L} + \frac{E_L h + E_T 2h}{E_L}}{2} = 2.36" \quad (5\text{-}4)$$

Where:

E_L = Longitudinal modulus of elasticity of wood species (lbf/in.^{2})
E_T = Tangential modulus of elasticity of wood species (lbf/in.^{2})
h = Depth of each layer of wood (in.)

To solve for the upper bound, the plate equation with a unit load at the midpoint was solved and midpoint displacement was found. Inverting this result provided an upper bound solution, 21.2 kip/in., for the stiffness of the wall section.

5.2.2.3 Partial Composite Action Estimate

McCutcheon (1977) proposed a method for determining the deflection of a partially composite wooden floor system consisting of wood joists and sheathing. This method was modified slightly, by changing the sheathing to dimensional lumber, to determine the amount of partial composite action present in the wall. The modification only affected the load/slip parameter of the nails. The use of a 1.5 in. thick 2x8, instead of sheathing, yielded a load/slip

per nail of 13,640 lbf/in. For the same size nail with 1.125 in. thick sheathing, the largest thickness tabulated by McCutcheon (1977), the load/slip per nail was 12,600 lbf/in. Thus, changing the sheathing to dimensional lumber was deemed valid, as it did not significantly change the parameters of the calculation. The detailed calculation of partial composite action is located in Appendix E.

For the design wall, during the stiffness test the inner layer would be under tension, while the outer layer was under compression. When a layer is under compression the boards tend to compress between each other, creating what was idealized as a continuous flange. In contrast, when a layer is under tension the boards have no connectivity between them and the flange is not continuous. Therefore, the calculation of partial composite action was completed twice, once for the tension layer and once for the compression layer. The partial composite action estimates were then averaged to determine a partial composite action estimate for the entire wall of 16%.

5.2.2.4 Static Stiffness Estimate

Estimation of the static stiffness proceeded using the lower and upper bounds of stiffness, the partial composite action estimate and linear interpolation. The difference between the upper bound and lower bound stiffness was multiplied by the estimation of partial composite action. This number was then added to the lower bound stiffness to determine the expected static stiffness of the wall. For the design wall this was 7.3 kip/in.

5.2.2.5 Dynamic Stiffness Estimate

In general, the dynamic modulus of a material is higher than its static modulus, but analysis of the data collected by the FPL safe room project showed a higher static modulus. In

this case, the modulus was found for the entire wall rather than an individual member. Thus, the smaller dynamic modulus was attributed to the loss of connectivity between lumber members due to the higher strain rate and loading of the dynamic loading case.

Calculation of percent reduction from static stiffness to dynamic stiffness was based on empirical relationships with few data points. This data, plotted in Figure 26, suggested that the ratio of dynamic stiffness to static stiffness ranged from 0.16-1.54. FPL Wall 2 was constructed in the same manner as FPL Wall 3, but had a significantly larger reduction in dynamic stiffness; the exact cause of this was unknown. In addition, FPL Wall 4 had a ratio of dynamic to static stiffness that was greater than one, which conflicted with the results of the other FPL walls, and was thought to be due to issues measuring the behavior of the wall. Thus, engineering judgment was used to rule out the lowest and highest values. From the remaining range of 0.32-0.58, a simple average of 0.45 was used to estimate the dynamic stiffness to static stiffness ratio. An estimate of dynamic stiffness was then found by multiplying this value by the expected static stiffness of 7.3 kip/in. For the design wall this calculation yielded an expected dynamic stiffness of 3.3 kip/in.

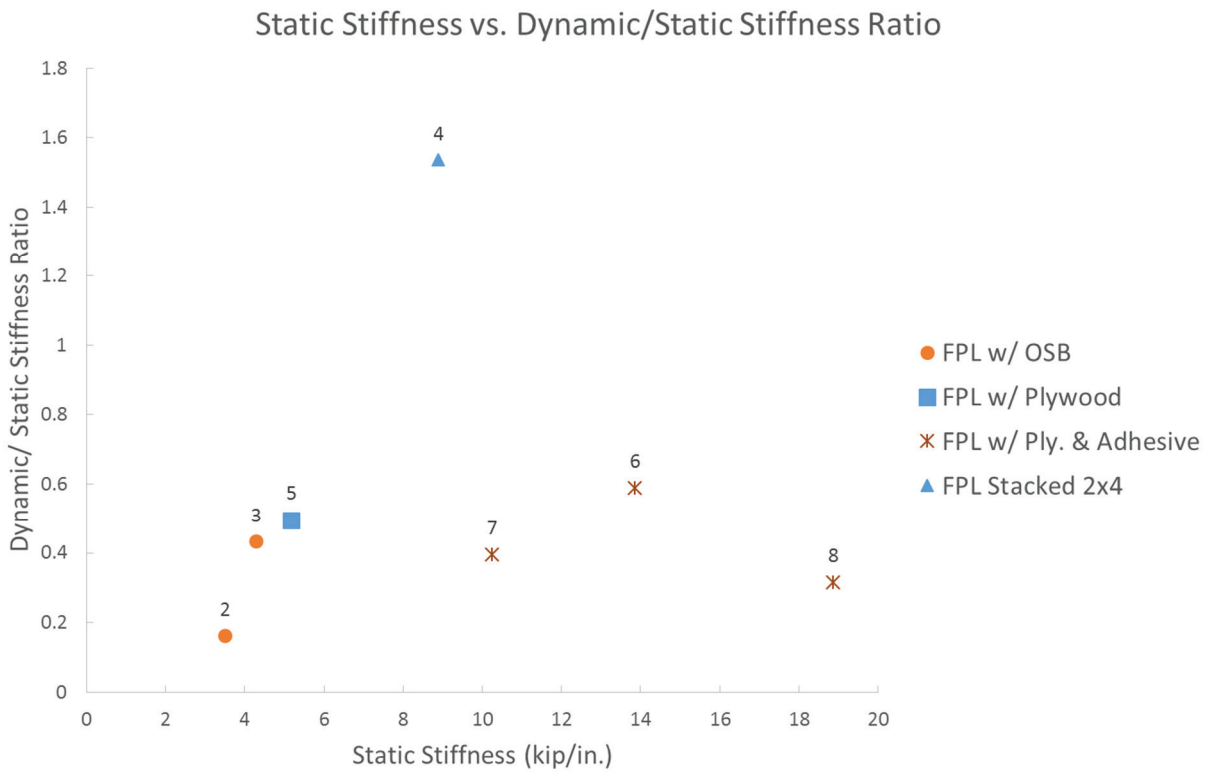


Figure 26. Dynamic/static stiffness ratio and construction of the FPL walls

5.2.3 Determination of Effective Mass

The orientation of one layer in the opposite direction was done with the intent of helping distribute the load throughout the entire wall more fully. The effects of having the second layer of wood in the opposite direction were not fully known until the wall sections were built and tested. Under this assumption, compared to the sections constructed for the FPL safe room project using the same type of fastening, the proposed walls were expected to be stiffer. The greater effect was hypothesized to be on the effective mass of the system. If the wood oriented in the opposite direction did distribute the load more fully, more of the section would engage in bending, causing the effective mass of the system to increase significantly.

The determination of the expected dynamic mass consisted of using educated estimation and engineering judgment. In the estimation of the stiffness of the section, a lower

bound estimate of three beams in flexure was used. Under this assumption, each beam had a width of approximately half the total wall width. Thus, it was deemed reasonable to assume that the effective mass of the system would be the mass of half the boards of the wall, or 9.8 slugs. This determination of effective mass placed the expected value of effective mass of the example wall above the effective mass exhibited by every FPL wall.

5.2.4 Determination of Damping Ratio

The hypotheses of this project do not include anything concerning the damping ratio. Therefore an in depth examination of the damping ratio is outside the scope of this project, and its discussion will be brief. However, in order to determine the displacement and rate of energy dissipation of a spring-mass-damper system the damping ratio must be known. Additionally, if a future design method included a deflection limit at which the wood in the wall fails, the damping ratio would need to be known.

For the design method of this project, the damping ratio was estimated using the damping ratios found from the FPL safe room project. In general, the damping ratio was found to be higher when no adhesive was used in the wall. An average value for walls that did not include any adhesive was determined to be 0.13, which is the damping ratio assumed for this design.

5.3 Wall Designs

The numbers provided in the previous section apply to Wall A of this study. Wall A was estimated to have a dynamic stiffness that was only marginally larger that the proposed stiffness threshold. Wall A was designed to test the theory that a minimum effective mass and

stiffness determines whether a wall will pass the impact test or not. Walls B and D follow the same initial design of Wall A, but were chosen to provide additional information regarding how slight changes to the wall construction may change its behavior. The wall designs of this study are summarized in Table 12.

Table 12. Description of each wall design.

Wall	Wall Description	Lumber Species and Grade	Moisture Content (Average)
A	Front layer – 2x8s horizontal, Middle layer – 2x8s vertical, Back layer – 2x8s horizontal	2x8s – #2 Douglas-fir	Construction – 15% Testing – 9%
B	Front layer – 2x8s horizontal, Middle layer – 2x8s vertical, Back layer – 2x8s horizontal, with 15/32 in. OSB nailed to front and back faces	2x8s – #2 Douglas-fir	Construction – 16% Testing – 9%
C	Front layer – 2x4s vertical, Back layer – 2x4s horizontal, narrow face in impact direction, with 23/32 in. OSB nailed to front and back faces	2x4s – Stud Grade Spruce-pine-fir	Construction – 12% Testing – 8%
D	Front layer – 2x4s horizontal, Middle layer – 2x8s vertical, Back layer – 2x8s horizontal	2x4s – Stud Grade Spruce-pine-fir 2x8s – #2 Douglas-fir	Construction – 10% Testing – 7%

Comparison of Walls A and B provided an estimate of how much the effective mass and stiffness of the wall increased when OSB was added. The presence of OSB may help to hold the boards together in addition to adding its own effective mass and stiffness to the wall. Thus, the stiffness and effective mass of the wall may increase in an indirect manner. The understanding of the effect OSB and plywood have on the wall system may be a useful tool for future wall designs.

A comparison of the behavior between Walls A and D provided insight into how the behavior of the wall changed when the exterior layer was constructed with cheaper and more abundant lumber, such as 2x4s. To encourage the construction of more safe rooms in tornado prone regions, costs must be kept low. This document previously discussed a theory that the exterior layer of lumber primarily provides energy dissipation and distribution and is a sacrificial layer. If it is shown that using smaller, lower grade, and cheaper lumber as the exterior layer of the wall has a minimal effect on the performance of the wall, costs may be reduced.

The design drawings of each wall are located in Appendix F. Included in the design of each wall is the orientation of members and the nailing scheme used to fasten individual members together. In addition to the drawings, a summary of the materials used to construct each wall is included.

5.4 Relationship between Proposed Design and Design Thresholds

The design parameters of Wall A were plotted with respect to the proposed design thresholds and were labelled as “Proposed”. Walls B and D were initially assumed to have similar design parameters to Wall A, and the assumption was checked after testing. The design parameters of Wall C were assumed to be similar to those of FPL Wall 4, which had a similar design.

The first proposed requirement of this study is that wall designs must have an effective mass and stiffness higher than the threshold. The thresholds were set equal to the lowest passing values from the FPL tests. Thus, the effective mass and stiffness of the proposed wall design are plotted versus the results of the FPL tests in Figure 27.

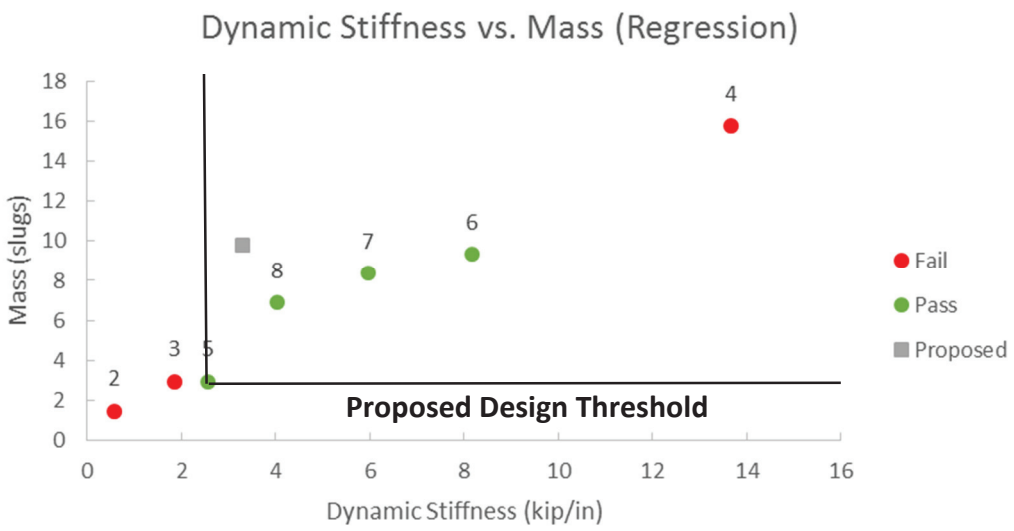


Figure 27 Proposed minimum effective mass-stiffness threshold. Pass (Green). Fail (Red).

The second proposed threshold was based on a hypothesis that the ratio between midpoint and quarter point stiffness is important for pass/fail prediction. A plate has a higher stiffness ratio than a beam and is able to distribute load throughout the section more effectively than a beam. Therefore, a plate would be expected to perform better than a beam if the midpoint stiffness and strength of the plate and beam are equal. This proposed threshold is plotted in Figure 28

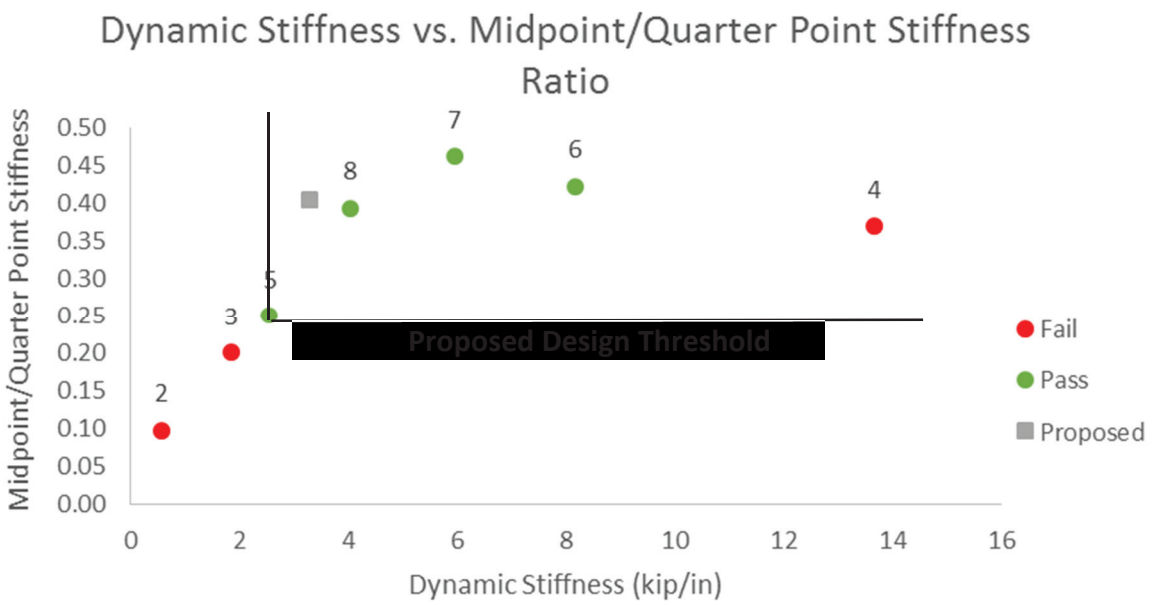


Figure 28. Proposed minimum dynamic stiffness-stiffness ratio threshold. Pass (Green). Fail (Red).

Chapter 6 Test Results and Analysis

6.1 Modification to Experimental Design

This project used the same testing setup and equipment as the previous FPL tests except for the LVDT placement. The only modification to the procedure was that an additional impact test was also performed at the corner of the walls. The changes to the equipment and procedure did not change the results of the tests, but provided additional information on the behavior of the wall.

The FPL safe room project used four LVDTs to record the displacement of the quarter points of the wall. This number of LVDTs provided the minimum required information to model the behavior of the wall. For this project, the number of LVDTs was increased to fourteen, allowing the midpoint displacement to be calculated using cubic spline interpolation. Calculation of the midpoint displacement using cubic spline interpolation allowed the assumption relating quarter point and midpoint displacement to be checked. The layout of the LVDTs for the testing of this project is shown in Figure 29.

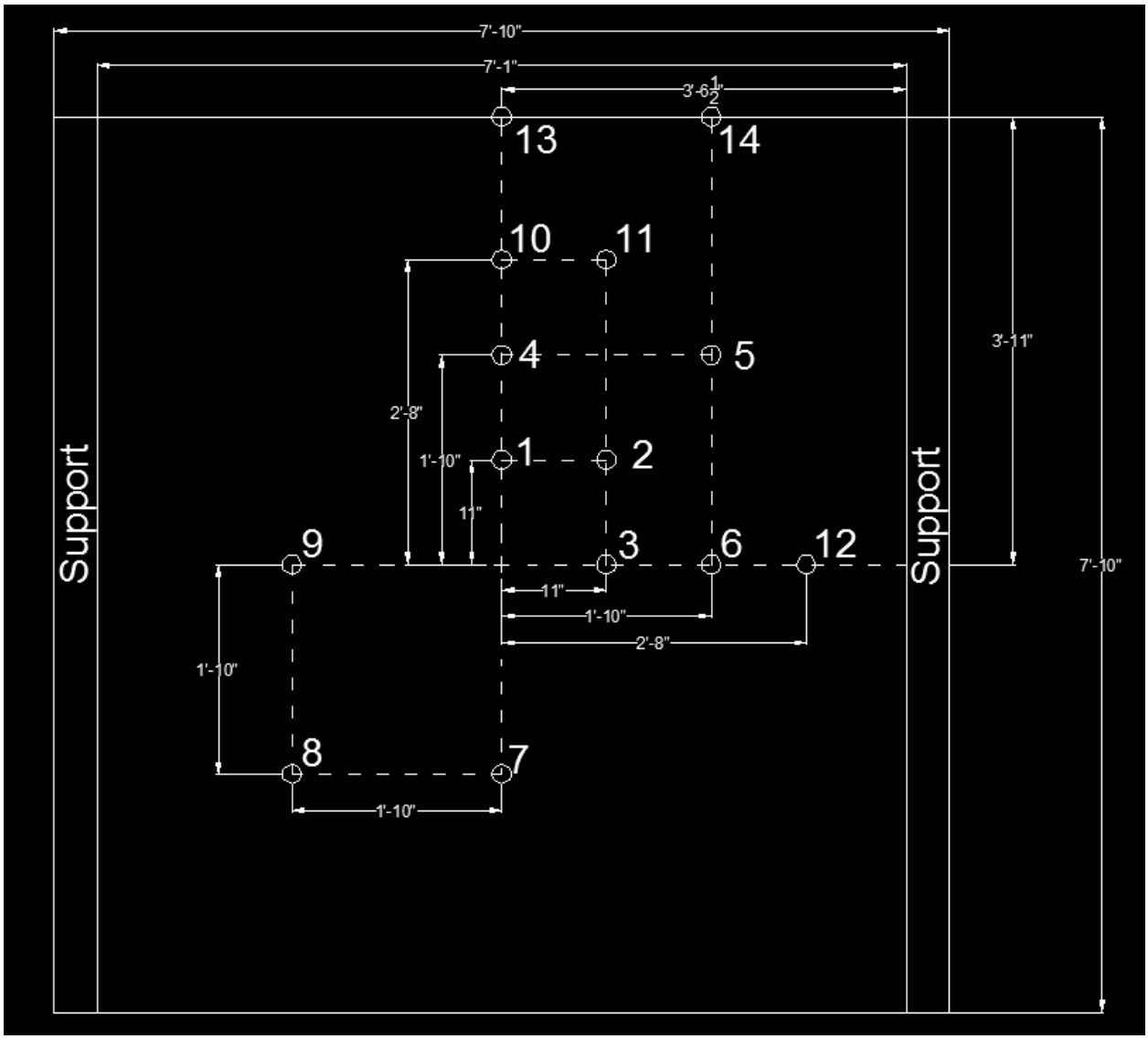


Figure 29. The layout and numbering of LVDTs for this project.

To meet the requirements of FEMA P-361 and ICC-500 the walls had to be impacted approximately 6 in. from one of its corners. This test was only performed on the walls that passed the initial midpoint test. The angle of incidence between the missile and the wall had to remain near zero, so the muzzle of the cannon needed to be positioned at the height of a corner. Placing the muzzle of the cannon on the floor was not feasible, so a top corner of the wall was tested. This was accomplished by mounting the existing cannon setup on top of two

concrete barriers. After this was completed the cannon was operated in the same manner. The modified cannon setup is shown in Figure 30.



Figure 30. Cannon setup modified to test wall corners.

6.2 Impact Test Results

The impact tests proceeded in the same manner as the FPL safe room project for the midpoint and corner point tests of this project. The pass/fail behavior of a wall after each test was noted along with parameters such as missile velocity. The performance of each wall is summarized in the following sections.

6.2.1 Midpoint Impacts

6.2.1.1 Wall A

Wall A passed the midpoint impact test. The missile impacted the center of wall, leaving a gouge in the wall, before rebounding and landing on the floor. The board on the backside of the wall, at the height the missile impacted, obtained a small amount of damage. The damage to the backside consisted of a crack formed at the impact location, in the direction of the grain. This board also had a noticeable permanent deflection with a maximum value of 0.8” near the location of impact. The parameters of the test are summarized in Table 13, and the appearance of the wall after testing is shown in Figure 31.

Table 13. Summary of the 1st impact of Wall A

Wall	Test	Missile Speed (mph)	Impact Location	Front Penetration (in.)	Permanent Rear Def. (in.)	Pass/Fail
A	1	103.6	0.5" left, 1" below center	1.8	0.8	Pass



Figure 31. Damage to Wall A, 1st test. Backside crack (Left). Front penetration (Right)

Wall A performed well, and a decision was made to test it again. The wall passed the second test, but sustained a significant amount of additional damage. In this test, the missile impacted the wall approximately 1 ft. from the center point and plugged in the wall. Compared to the first test, much larger cracks propagated in the boards near the impact location. The largest crack was parallel to the grain, but cracks also formed perpendicular to grain. The board on the backside, at the height of the impact location, had a permanent deflection of 1.5 in. The nails in the impact region appeared to have lost most of their connectivity due to withdrawal. The parameters of the test are summarized in Table 14, and the appearance of the wall after testing is shown in Figure 32.

Table 14. Summary of the 2nd impact test of Wall A.

Wall	Test	Speed (mph)	Impact Location	Front Penetration (in.)	Permanent Rear Def. (in.)	Pass/Fail
A	2	103.3	12" right, 8" above center	3.9	1.5	Pass





Figure 32. Damage to Wall A, 2nd test. Backside cracking (Left). Missile plugging (Right)

6.2.1.2 Wall B

Wall B also passed the midpoint impact test. The missile impacted a seam between the two OSB sheets, which may be the weakest point of the wall. After punching a short distance into the wall the missile was ejected, landing on the floor. The OSB on the backside of the wall showed no sign of damage. No permanent deflection was visible, but the LVDT data suggested that a permanent deflection of approximately 0.5" occurred. The parameters of this test are summarized in Table 15, and the appearance of the wall after testing is shown in Figure 33.

Table 15. Summary of the 1st impact test of Wall B.

Wall	Test	Speed (mph)	Impact Location	Front Penetration (in.)	Permanent Rear Def. (in.)	Pass/Fail
B	1	105.1	1" left, 1.5" below center	2.5	0.5	Pass



Figure 33. Damage to Wall B, 1st test. Backside, no damage (Left). Front penetration (Right)

Wall B performed well, and a decision was made to test it again. The impact from the second test was located approximately 1 ft. away from the center point. The appearance of the wall after the 2nd test did not change meaningfully therefore pictures are omitted. The parameters of this test are summarized in Table 16.

Table 16. Summary of the 2nd impact test of Wall B.

Wall	Test	Speed (mph)	Impact Location	Front Penetration (in.)	Permanent Rear Def. (in.)	Pass/Fail
B	2	102.6	11" right, 10" above center	1.875	0.75	Pass

6.2.1.3 Wall C

Wall C failed the midpoint impact test. The missile plugged in the wall after impacting the midpoint of the wall, near the seam of the OSB sheets. Only one 2x4 appeared to have been significantly engaged in bending, therefore the load was poorly distributed. This 2x4 appeared to have fractured almost completely through the section. The loss of strength caused a large amount of permanent deflection, in addition to delamination of the OSB in the impact

area. The permanent deflection was greater than the allowable limit of 3”, causing the wall to be deemed a failure. Additionally, a nail was pulled through the member directly above the board that failed, and was ejected from the wall, causing failure of a second FEMA P-361 criterion. The parameters of this test are summarized in Table 17, and the appearance of the wall after testing is shown in Figure 34.

Table 17. Summary of midpoint impact test of Wall C.

Wall	Test	Speed (mph)	Impact Location	Front Penetration (in.)	Permanent Rear Def. (in.)	Pass/Fail
C	1	104.0	1" left, 1" below center	4.0	> 3	Fail

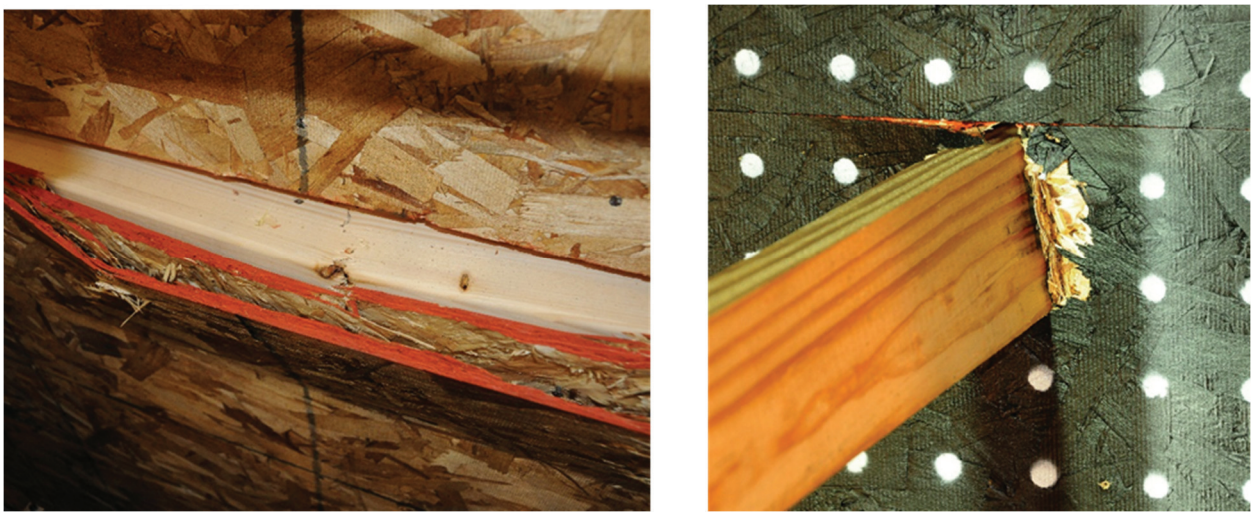


Figure 34. Damage to Wall C. Fracture of 2x4 member from backside (Left). Front penetration (Right)

6.2.1.4 Wall D

Wall D failed the impact test due to a large permanent rear deflection. The missile impacted the wall along a seam between two 2x4s, near the midpoint of the wall. The missile penetrated into the wood and plugged in the wall. The missile punched almost entirely through the exterior layer of 2x4s and middle layer of 2x8s. The backside 2x8 at the height of impact

cracked perpendicular to the grain through the thickness of the board. All the nails in the board at the height of impact, except those very near to the supports, failed in withdrawal. Nails in the boards above and below the impacted backside 2x8 experienced noticeable pullout as well. A knot with a 1” diameter was located very near the impact point, and significant edge grain slope was present in the impact region. The parameters of this test are summarized in Table 18, and the appearance of the wall after testing is shown in Figure 35.

Table 18. Summary of midpoint impact test of Wall D.

Wall	Test	Speed (mph)	Impact Location	Front Penetration (in.)	Permanent Rear Def. (in.)	Pass/Fail
D	1	104.9	0" left, 1" below center	3.5	> 3	Fail



Figure 35. Damage to Wall D, Failure of 2x8 member from backside (Left). View of wall interior (Right).

6.2.2 Corner Impacts

Walls A and B passed the midpoint impact test, so to ensure they met FEMA requirements they were both tested under a corner impact. Walls C and D failed the midpoint impact test and therefore were not tested with a corner impact.

6.2.2.1 Wall A

Wall A passed the corner impact test. After impacting near the corner, the missile rebounded at a high velocity, due a high stiffness near the corner, into the netting that surrounded the test setup. The missile impacted the seam between the top two 2x8s of the wall, causing significant cracking near the impact region. The top two backside 2x8s also appeared to have a number of nails that had withdrawn from the middle layer. The parameters of this test are summarized in Table 19 and the appearance of the wall after testing is shown in Figure 36.

Table 19. Summary of corner test of Wall A.

Wall	Test	Speed (mph)	Impact Location	Front Penetration (in.)	Permanent Rear Def. (in.)	Pass/Fail
A	3	102.6	6" right, 7.5" below corner	2.1	1.8	Pass



Figure 36. Damage to Wall A, corner test. Backside cracking (Left), Front impact location (Right).

6.2.2.2 Wall B

Wall B also passed the corner impact test. The missile again rebounded from the wall at a high velocity. Very little visible damage was present near the location of impact on the backside of the wall. The only noticeable damage occurred near the top middle of the wall, where the OSB withdrew slightly from the rest of the wall. The top line of nails also withdrew from both the outer layer of 2x8s and the OSB. The withdrawal of the nails became more significant near the vertical centerline of the wall. The parameters of this test are summarized in Table 21, and the appearance of the wall after testing is shown in Figure 37.

Table 20. Summary of corner test of Wall A.

Wall	Test	Speed (mph)	Impact Location	Front Penetration (in.)	Permanent Rear Def. (in.)	Pass/Fail
B	3	102.2	3" right, 9.5" below corner	1.4	0.5	Pass





Figure 37. Damage to Wall B, corner test. Backside nail and OSB withdrawal (Left). Front impact location (Right).

6.3 Analysis of Model Parameters

The analysis of the displacement data from the stiffness and impact tests proceeded in the same manner as the FPL tests. The only difference in the analysis procedure was that the use of the midpoint to quarter point stiffness ratio to convert the quarter point displacements to midpoint displacements was evaluated. Nonlinear regression was again used to determine the effective mass, stiffness, and damping ratio that the wall section exhibited during the impact test. The analysis is summarized in the following sections.

6.3.1 Analysis of the Stiffness Tests

The stiffness of the midpoint and quarter points was calculated from the outputs of the quasi-static load displacement test. The slope of the line connecting the points of load and displacement was the tabulated stiffness value. See Section 4.1.2 for details on calculating the static stiffness. The results of the stiffness test are summarized in Table 21.

Table 21. Summary of the stiffness test results.

Stiffness (lbf/in.)		
Wall	Center Point	1/4 Point
A	7553	18193
B	9396	20806
C	10768	27323
D	6525	15287

6.3.2 Verification of Midpoint Displacements

Analysis of the FPL impact tests was performed by using the quarter point stiffness and deflection to determine the deflection of the midpoint. To check this assumption, the midpoint deflections of Walls A, B, C, and D were calculated by two methods. The first method multiplied the quarter point displacement by the ratio of the quarter point stiffness to the midpoint stiffness. The second method used a cubic interpolation program to determine the midpoint displacement.

The cubic interpolation program used was an add-in for MS Excel. The program operated by fitting a cubic spline to a set of data. First, the locations of the LVDTs were entered as constant values, for example, the locations of LVDTs 9, 3, 6, and 12 were used. Then, the displacement of those LVDTs was entered for a given time step. Next, the location of the

midpoint was entered and held constant. Finally, the program calculated the midpoint displacement from the cubic spline fitted to the known displacement data. This formula was then copied for each time step, generating the midpoint displacement time history.

The agreement between the two midpoint displacement models for Walls A, B, and D was good qualitatively. The two methods of calculating the midpoint displacement of Wall A, as a representative example, are plotted in Figure 38. A quantitative analysis of these walls was also done by using the coefficient of determination. These R^2 values show that some correlation exists between the two data sets, but that the fit is imperfect. The R^2 values are summarized in Table 22.

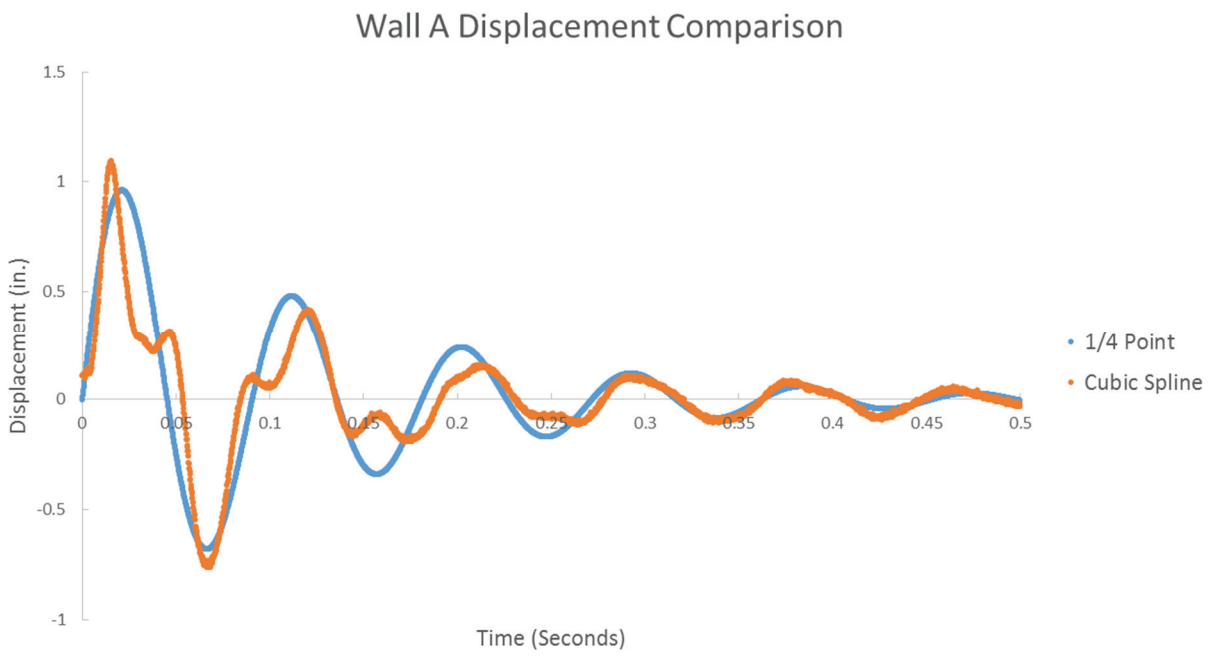


Figure 38. Midpoint deflections of Wall A calculated with two methods.

Table 22. Coefficient of determination between midpoint displacement estimations.

R^2	
Wall	Displacement
A	0.76
B	0.74
C	0.42
D	0.73

Cubic spline interpolation and the quarter point displacement method are both approximate ways of determining the midpoint displacement. Inspection of these plots shows that the frequency of the data sets is approximately the same, but there are issues with the agreement of the amplitudes. Disagreement of the amplitudes occurring after the first cycle suggests a slight difference in the damping ratio exhibited by each model. The frequency and the first peak amplitude of the oscillation are primarily defined by the effective mass and stiffness of the system. The hypotheses of this report are centered on the effective mass and

stiffness of the system, thus reasonable agreement between the frequencies of the methods added credence to the validity of the results of the FPL wall analyses.

The two midpoint displacement models for Wall C did not agree nearly as well as those of Walls A, B, and D. Plots of the two different methods of calculating midpoint displacement of Wall C are presented in Figure 39. The inconsistency between these two methods is apparent when examining the plots qualitatively. For consistency, the R^2 value for the displacement estimates of Wall C was calculated and is tabulated in Table 22.

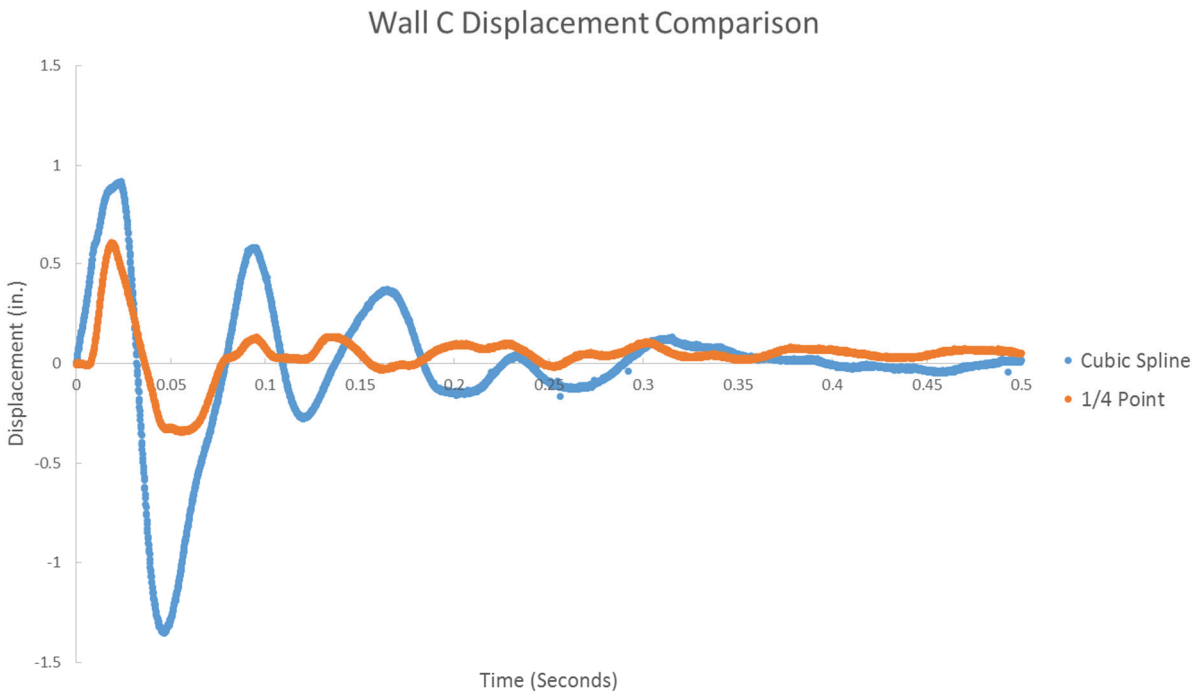


Figure 39. Midpoint deflections of Wall C.

The disagreement between the two approximate methods of calculating midpoint displacement values for Wall C may be logical. The cubic interpolation method was heavily influenced by LVDTs that were relatively near to the location of impact. These sensors were therefore subject to displacements similar in frequency, but with smaller amplitude than what

was expected of the midpoint. The load transfer between the boards near the midpoint and those near the quarter points was poor, which was likely a factor in the failure of the wall. The poor load transfer also meant that the displacement of the quarter point was isolated in phase and amplitude from that of the midpoint. The comparatively smaller amplitudes, determined using the quarter point displacement and stiffness ratio, were likely part of the reason for abnormally high effective mass and stiffness results of FPL Wall 4.

6.3.3 Analysis of the Impact Test

The midpoint displacements, estimated using the quarter point displacements, were used to determine the stiffness, effective mass, and damping ratio of Walls A, B, and D. Because analysis using each method yielded approximately the same parameters, for consistency with the analysis of the FPL data, the quarter point method was used. The parameters of Walls A, B, and D found using nonlinear regression are summarized in Table 23. The R^2 values between the model displacements and the measured wall midpoint displacements are tabulated in Table 24.

Table 23. Effective mass, stiffness, and damping parameters for Walls A, B, and D.

Wall	Effective mass (slugs)	Stiffness (lbf/in.)	Damping Ratio (Unitless)
A	10.3	4070	0.11
B	11.8	4240	0.15
D	6.9	2500	0.15

Table 24. Coefficients of determination for Walls A, B, and D.

Wall	R^2
A	0.91
B	0.87
D	0.80

The midpoint displacements estimated using quarter point displacements and cubic spline interpolation were significantly different for Wall C. The difference caused a large variance between the effective mass, stiffness, and damping ratio of each method. Because of this difference, parameters found using nonlinear regression on both midpoint displacement estimates are tabulated in Table 25. Additionally the coefficients of determination of the two methods are summarized in Table 26.

Table 25. Effective mass, stiffness, and damping parameters for Wall C.

	1/4 Point Displacement			Cubic Interpolation Displacement		
	Effective mass	Stiffness	Damping Ratio	Effective mass	Stiffness	Damping Ratio
Wall	(slugs)	(lbf./in.)	(Unitless)	(slugs)	(lbf./in.)	(Unitless)
C	12.3	7010	0.2	6.9	4350	0.11

Table 26. Coefficient of determination for Wall C.

R^2	
1/4 Point	Cubic Spline
0.74	0.75

6.4 Comparison of Results to Thresholds

6.4.1 Effective mass-Dynamic Stiffness Threshold

The first proposed threshold was a minimum effective mass and stiffness that the wall must provide during the impact test. The initial plot was based on data from the FPL walls, which were indicated as pass/fail. The dynamic stiffness and effective mass of Walls A-D are plotted in Figure 40 alongside data from the FPL tests and the proposed minimum threshold.

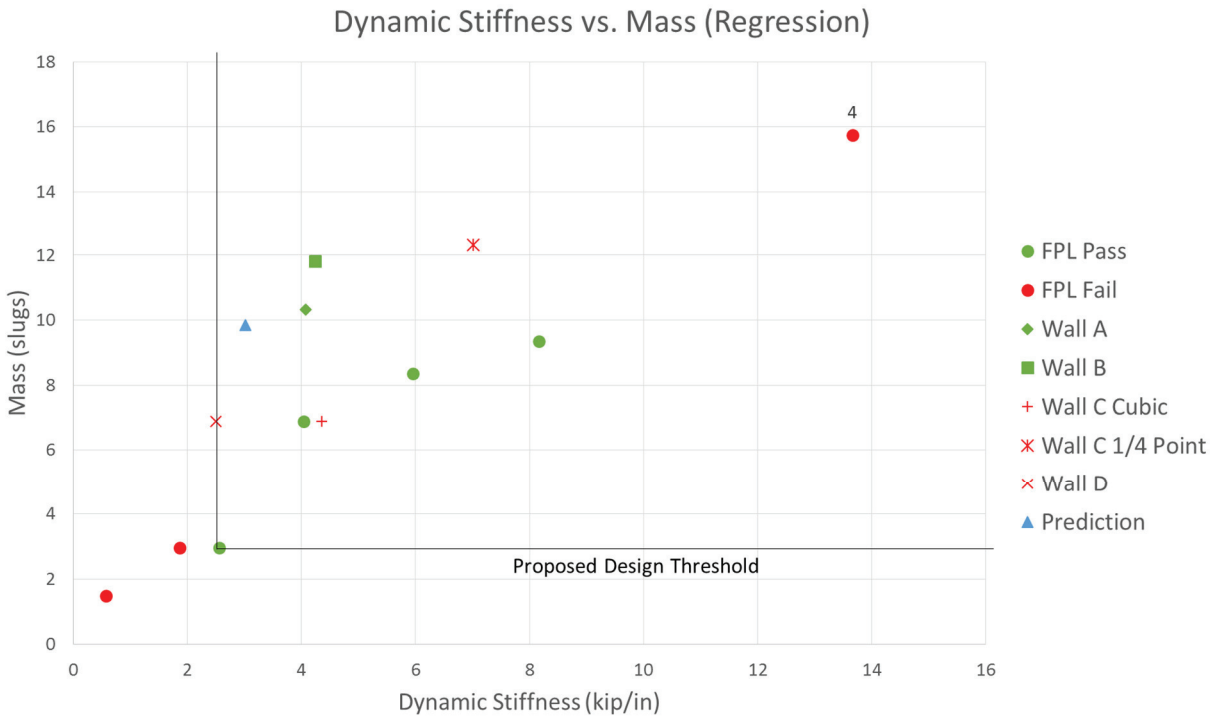


Figure 40. Dynamic stiffness and effective mass of tested walls. Pass (Green). Fail (Red).

The proposed minimum effective mass-stiffness design threshold was evaluated using the additional data gathered from Walls A-D. Walls A and B passed the impact test and had values of effective mass and stiffness above the design threshold. Wall D failed the impact test and had a stiffness value of 2500 lbf/in, which was below the minimum design threshold of

2560 lbf/in. from FPL Wall 5. The results from Walls A, B, and D, the three walls constructed with boards subject to flatwise bending, added evidence to support the theorized minimum effective mass-stiffness threshold.

Wall C failed the impact test, but the dynamic mass and stiffness parameters it exhibited suggested that it should pass. Thus, similar to FPL Wall 4 the stacked 2x4 design again provided results that did not match expectations. Even if a sacrificial layer requirement was added to the design requirements, results from the stacked 2x4 designs of Wall C and FPL Wall 4 cast doubt on this threshold.

6.4.2 Stiffness Ratio-Dynamic Stiffness Threshold

The second proposed threshold was the wall must provide a minimum dynamic stiffness and midpoint to quarter point stiffness ratio (Stiffness ratio) to pass the impact test. The initial plot was based on data from the FPL walls, which were indicated as pass/fail. Dynamic stiffness and stiffness ratio parameters from Walls A-D are plotted in Figure 41 alongside previous test data and the proposed threshold.

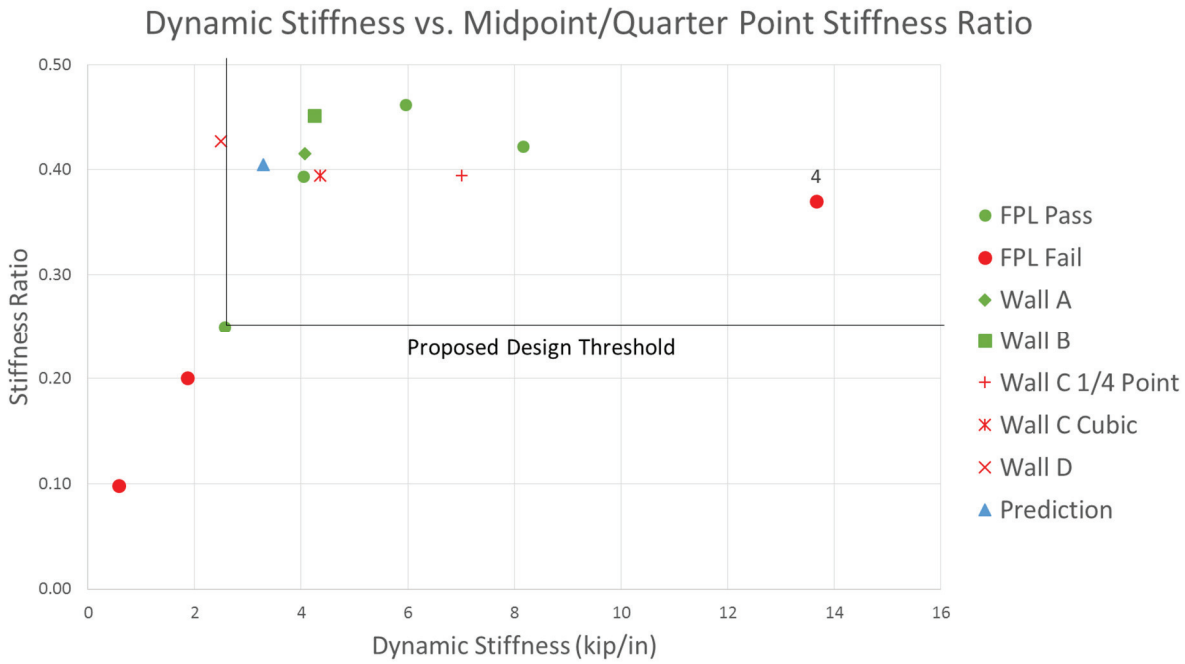


Figure 41. Dynamic stiffness and stiffness ratio of tested walls. Pass (Green). Fail (Red).

Evaluation of the minimum dynamic stiffness-stiffness ratio threshold using the additional data from Walls A-D yielded similar results to the effective mass-stiffness threshold. Walls A and B passed the impact test and had parameters of dynamic stiffness and stiffness ratio that were above the threshold minimums. Wall D failed the impact test with a dynamic stiffness less than the minimum prescribed by the design threshold. Finally, Wall C had a stiffness ratio and dynamic stiffness that were significantly higher than the proposed threshold and failed the impact test. The performance of Walls A, B, and D again provided evidence to support the validity of a minimum threshold and the performance of Wall C cast doubt upon it.

6.5 Wall Construction Performance

6.5.1 Stacked 2x4 Construction

The failure both Wall C and FPL Wall 4 underwent when subject to the impact test was dramatic. Both these walls used the stacked 2x4 design (Wall C had an additional layer of 2x4s added to its impact face), and estimates of their midpoint deflections provided parameters that suggested they would pass the impact test. FPL Wall 4 was perforated by over a foot, and one of the flexural 2x4s of Wall C fractured, causing a large permanent deflection. The failure of both these walls was highly localized, for example, the 2x4 directly above the impacted 2x4 of Wall C appeared undamaged.

Wall C and FPL Wall 4 relied primarily on nails to transfer the load from the flexural 2x4 that was loaded, to the other flexural 2x4s in the wall. The importance of the nails to the stiffness of these walls can be demonstrated by a calculation of the stiffness of one 2x4. E = 1400 ksi, I = 5.4 $in.^4$, and L = 7 ft. were used as reasonable estimates for the elastic modulus, strong axis moment of inertia, and span length of a 2x4 in these walls Using Equation (4-1) the stiffness of a 2x4 was found to be approximately 600 lbf/in. Thus, disregarding composite action between the 2x4s and the OSB, FPL Wall 4 required the equivalent of 15 2x4s to achieve a midpoint stiffness of 8885 lbf/in. The ability of FPL Wall 4 to achieve this stiffness demonstrated that the nails were capable of transferring load under the relatively light and slow loading of the stiffness test.

The nails did not appear to transfer the load well in Wall C and FPL Wall 4 when subject to impact loading. The behavior of Wall C and FPL Wall 4 under impact loading showed a failure of the nails to hold the impacted members in position, relative to the rest of the wall. The

inability of the nails to distribute the load caused the members near the impact zone to resist most of the impact force, causing the wood and wall to fail in a localized manner.

The localized failures of Wall C and FPL Wall 4 caused issues with the use of the spring-mass-damper model. The use of LVDTs to determine the midpoint displacement using either cubic interpolation or the quarter point method assumed that the wall system deformed in a uniform manner. Neither method was capable of calculating the large localized deflections near the midpoint of Wall C and FPL Wall 4.

The inability of the nails to transfer the load to other members of the wall created what might be idealized as two spring-mass-damper systems. The first system was made up of the boards near the midpoint that were being loaded to failure by the impact. The second system was the system of boards above and below those boards, experiencing only a secondary excitation from the impact. The location of the LVDTs meant the displacements found for Wall C and FPL Wall 4 were of the second system. Therefore, the output nonlinear regression parameters were not representative of the system as a whole, but likely modeled a smaller, secondary excitation of the undamaged portions of the wall. Inability to accurately capture the displacements of the midpoint spring-mass-damper system may be the reason that Wall C and FPL Wall 4 did not match the expected pass/fail behavior outlined by the proposed thresholds.

6.5.2 Perpendicular Layer Construction

Walls A, B, and D had pass/fail performance consistent with the proposed design thresholds. These walls were constructed using three layers of wood with each layer running in alternating directions and were nailed together. The displacement behavior of these walls

under impact loading suggested that the load was well distributed throughout the cross-section.

The results of the impact tests suggested that using multiple layers of wood to add strength and stiffness to the wall, corresponded to less localized failure, compared to the stacked 2x4 design. Walls A, B, and D transferred load via contact between members, rather than relying directly on nails to transfer load. In addition to load transfer through member contact, the nails between the layers of wood added partial composite action to the strength and stiffness of the walls. Building walls in this manner appeared to increase load distribution, and allowed the walls to deform like plates. Thus, the behavior of these walls appeared to be better approximated by a single spring-mass-damper model, when compared to the stacked 2x4 walls.

6.6 Discussion of Predictions and Variables

After the nonlinear regression analysis was completed on Walls A-D, the output parameters were compared to the predictions of the design procedure. The response of Wall A was compared to the response predicted by the design procedure. Walls B and D were also analyzed to determine the effects of ½" OSB and 2x4s used on the impact face respectively.

6.6.1 Predicted and Measured Behavior of Wall A

The stiffness ratio, dynamic stiffness, mass, and damping ratio of Wall A were predicted using the proposed design procedure. To evaluate the performance of the procedure these parameters were compared to the model values. The predicted and model values, along with the percent error of the prediction are summarized in Table 27.

Table 27. Predicted and measured parameters of Wall A.

Wall A Parameters			
Parameter	Calculated	Measured	Percent Error
Stiffness Ratio	0.41	0.42	2
Dynamic Stiffness (kip/in.)	3.29	4.07	19
Effective mass (slug)	9.8	10.3	5
Damping Ratio	0.13	0.11	18

The two parameters that appear to be the most difficult to predict are dynamic stiffness and damping ratio. The dynamic stiffness was estimated based on a predicted static stiffness and an empirical estimate of reduction between static and dynamic stiffness. The percent error between the predicted and measured static stiffness was 3%, therefore the main issue with the calculation of dynamic stiffness lies in calculating the reduction from static to dynamic stiffness. Similar to the reduction from static to dynamic stiffness the estimate of damping ratio was taken based off empirical data from the FPL walls. The relatively large error in both these estimates demonstrates the issues with using a small empirical data set. Thus, more test data is needed to increase the accuracy of the design procedure.

The calculated design wall response and the nonlinear regression model response are plotted in Figure 42. These data sets appear to have good agreement, especially over the first two cycles, after which the difference in the natural frequency begins to become clear. The data sets show that the proposed design procedure may be used to reasonably predict the response of a wall to the impact test.

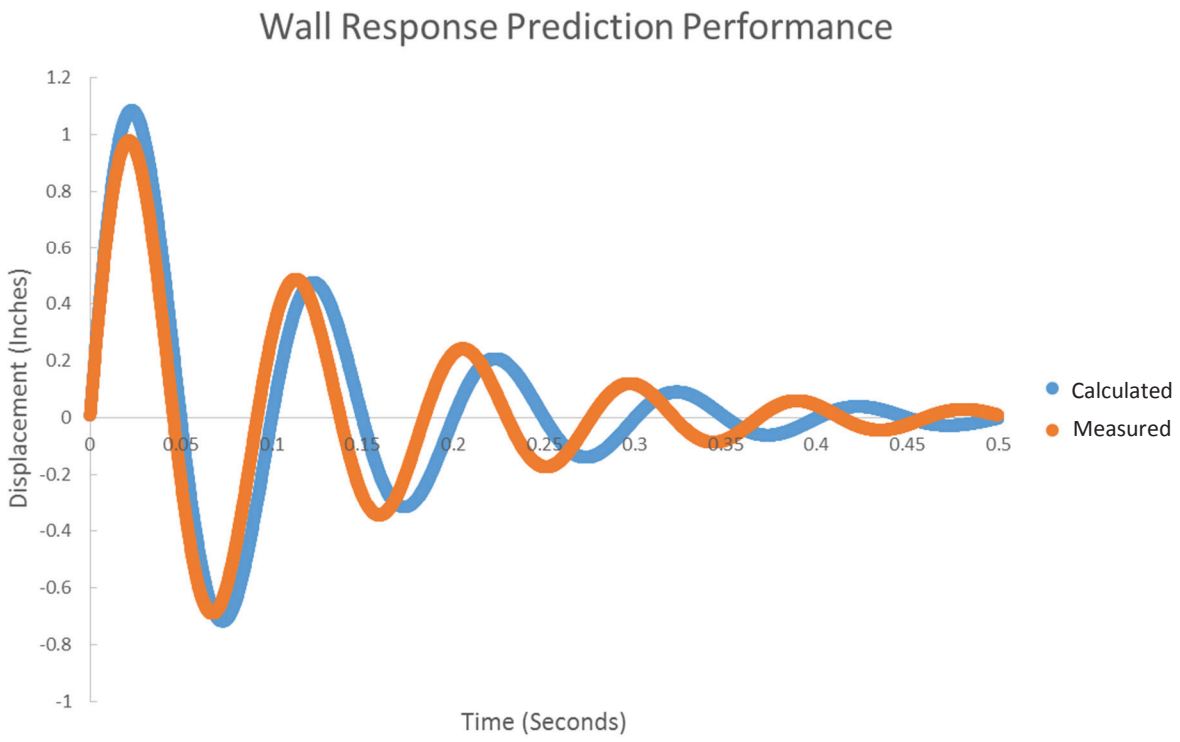


Figure 42. Comparison of predicted and measured nonlinear regression parameters.

6.6.2 Variation due to OSB Addition

Addition of a layer of OSB on both the front and back faces of the wall increased the measurable parameters of the wall. The percent difference between parameters of Wall A, which had no OSB and Wall B, which had ½" OSB on its faces, are tabulated in Table 28. The OSB appeared to help hold the boards of the wall together and thus increased the stiffness ratio, stiffness, and effective mass. In addition, the added connections and frictional surfaces provided by the use of OSB may have contributed to the increase in damping ratio.

Table 28. Change in parameters from addition of OSB

Addition of OSB			
Parameter	Wall A	Wall B	Percent Difference
Stiffness Ratio	0.42	0.45	8
Dynamic Stiffness	4.07	4.24	4
Effective mass	10.3	11.8	13
Damping Ratio	0.11	0.15	31

6.6.3 Variation due to 2x4 Use

Replacement of the #2 Douglas-fir 2x8s on the impact face with stud grade Spruce-pine-fir 2x4s decreased the dynamic stiffness, effective mass and damping ratio of the wall. The only parameter that remained relatively unchanged was the stiffness ratio. The purpose of using 2x4s to replace the 2x8s was to reduce the cost of the wall. The hypothesis that using cheaper lumber in the sacrificial layer will have little impact on the performance of the wall was not supported by this result. The percent difference between the parameters of Wall A, which was constructed of all 2x8s and Wall D, which had a layer of 2x4s are summarized in Table 29.

Table 29. Change in parameters from use of 2x4s

2x4s on Impact Face			
Parameter	Wall A	Wall D	Percent Difference
Stiffness Ratio	0.42	0.43	3
Dynamic Stiffness	4.07	2.5	-48
Effective mass	10.3	6.9	-40
Damping Ratio	0.11	0.15	31

Chapter 7 Conclusion and Recommendations

7.1 Summary and Conclusions

The behavior of a wooden tornado safe room wall resisting an impact load consists of many localized material failures, such as crushing, shear, and flexure, occurring simultaneously. An exact understanding of how these phenomena interact with each other is unknown. Thus, development of a model that considers these failures would consist of a significant amount of time constructing and validating a finite element model. This process would have to be modified and repeated for each different wall layout and connection scheme. Taking into account that at this time these walls must all be built and tested under impact loading anyway, a simple, less time consuming, design procedure was sought.

Data from a previous research project carried out at FPL indicated that displacements of walls under impact loading approximated exponentially decaying sinusoids. Thus, a spring-mass-damper model was used to match the physics of the wall to definable parameters such as stiffness, effective mass, and damping ratio. Parameters that fit the measured displacements well were found using nonlinear regression. Thus, it was demonstrated that a simple model could represent global behavior of wooden safe room walls.

Once a model that resulted in good prediction of the physics of the problem was settled upon, a design basis was developed. Numerous plots were generated with parameters found from the spring-mass-damper model and the quasi-static load-displacement test. Two of the plots generated appeared to have minimum parameters above which the walls passed and below which they failed. Plots of dynamic stiffness versus mass and dynamic stiffness versus

the ratio between the midpoint and quarter point stiffness were used to propose design thresholds.

A procedure to design wooden safe room walls was developed using minimum design thresholds. From this procedure, an example calculation was performed to determine how well the performance of a wall could be predicted. Finally, a series of four walls were constructed to compare with this calculation and either add credibility to the proposed design thresholds, or disprove them. These walls were tested and analyzed in the same manner as the data from the previous FPL tests.

Data from all the tests were compiled to reevaluate the proposed design thresholds. The walls that were constructed using three layers of boards oriented with their wide face perpendicular to the direction of impact agreed with the proposed thresholds. The walls that had parameters above the thresholds passed and those with parameters below failed. In contrast, the walls constructed using 2x4s oriented with their narrow face perpendicular to the direction of impact failed and contradicted the thresholds. Thus, due to the disagreement of the 2x4 walls, the findings of this research project were divided by construction method.

The walls constructed of three layers of boards with their wide face perpendicular to the direction of impact fit the spring-mass-damper model well. In addition, the parameters fit to the spring-mass-damper model showed good agreement with the measureable stiffness and effective mass of the wall. Finally, from the limited sample size of this project, the proposed design thresholds appeared to hold for walls constructed in this manner, although more testing is need to confirm this. Therefore, it is recommended to design and construct future wooden safe room walls with boards oriented in flatwise bending. The findings of this project indicate

that the pass/fail behavior of walls built in this manner may be predicted with the design procedure outlined in Section 5.2.

The walls constructed using 2x4s oriented with their narrow face perpendicular to the direction of impact had relatively poor correlation to the spring-mass-damper model. A hypothesized reason for this lack of correlation was poor connectivity between members. In addition, the spring-mass-damper parameters found for these walls indicated the walls should pass the impact test; instead, they failed. Inability of the spring-mass-damper equation and LVDTs to accurately model the highly localized failure of these walls was hypothesized as the reason for this disagreement. Due to their poor testing performance and issues with modeling their behavior, design and use of stacked 2x4 walls is not recommended in the future. The behavior of these walls means that the proposed minimum design thresholds of this report are not universal for all construction methods of wood safe room walls.

7.2 Recommendations

7.2.1 Repeatability Testing

Walls A and D were constructed in an identical manner, with the exception of the impact face. The impact face of Wall A used #2 Douglas-fir 2x8s and Wall D used stud grade Fir 2x4s. Wall A performed well during impact testing and passed three consecutive impact tests. In contrast, Wall D failed the initial impact test. Thus, the failure of Wall D might be attributed to the 2x4s on the impact face failing to distribute the load as thoroughly as the 2x8s did.

The failure of Wall D also may be attributed to localized imperfections in the wood used in the wall. There appeared to be knots in the two nonimpact layers of Wall D near the location

of impact. Additionally, the edge grain of the backside 2x8, near the location of impact, had a significant amount of cross grain. Concentration of these imperfections near the impact point may have been a major contributor to Wall D failing the impact test.

Due to the variability of strength and stiffness parameters between pieces of lumber of the same grade and species, a single impact test of a wall design may not be satisfactory to ensure occupant safety during a tornado. The grade assigned to a piece of dimensional lumber is intended to provide an indication of the quality and therefore lack of defects that the board has. However, using Wall D as an example, construction may concentrate imperfections at locations near where the missile impacts. Concentration of imperfections cannot necessarily be predicted in design. Therefore, carrying out several impact tests on a wall design, in particular Walls A and B of this project, is recommended. If any of a series of walls fails the impact test, the grade of lumber may need to be increased to reduce the presence of knots and cross grain and increase the safety of the safe room. An increase of lumber grade would result in added material cost.

7.2.2 Construction with Screws

This project demonstrated that a safe room wall could pass the impact test using only nails for fasteners. The walls in this project used nails as the connections between wood members in part because four of the FPL walls were held together using only nails. Thus, only one major variable, the orientations of the wood members, changed between the two testing series. In addition, using a nail gun, the large number of nails needed to hold the wall together and provide good connectivity between each layer could be driven quickly. However, screws, while taking longer to drive, may prove to be a more efficient connector.

The superiority of screws, when subject to withdrawal loading, is demonstrated using two equations from *The Wood Handbook* (2010). The withdrawal strength for common nails is calculated using Equation (7-1), and withdrawal strength for screws is calculated using Equation (7-2). The specific gravity for wood species commonly used in construction varies between approximately 0.3 and 0.6. Thus, with the diameter and penetration length of the fasteners held constant, the withdrawal strength for screws is 2.5 to 3.5 times higher.

$$p_n = 7850G^{5/2}DL \qquad (7\text{-}1)$$

$$p_s = 15700G^{2}DL \qquad (7\text{-}2)$$

Where:

P_n = Withdrawal strength of nails (lbf)
P_s = Withdrawal strength of screws (lbf)
G = Specific gravity of wood (Unitless)
D = Diameter of nail/screw (in.)
L = Penetration length of nail/screw threads (in.)

Walls A and D experienced nails withdrawing from the middle layer during the impact test. The inability of the nails to hold the impacted 2x8 on the backside of the wall may have caused the failure of Wall D. Had there been better connectivity between the backside and middle layers, the impacted backside 2x8 may have not fractured, or the load may have been better distributed to other members. Equations (7-1) and (7-2) suggest that if nails were replaced with screws, even half the number of screws would provide a stronger resistance to withdrawal. Thus, using half the number of screws to attach each layer may have increased the withdrawal strength sufficiently to allow Wall D to pass the impact test

In future testing, construction of walls with identical member layouts using both screws and nails may be beneficial. Carrying out tests in this manner might improve efficiency of the

design. One possible scenario is the screws hold the wood in place during the impact test, but the missile causes a punching shear failure instead of a withdrawal failure. In that case, the screws may not add significant value. However, the use of screws as fasteners in safe room walls may help avoid withdrawal failure and lead to stronger, stiffer and more efficient walls. Therefore, further investigation of using screws as fasteners for safe room walls is recommended.

References

Federal Emergency Management Agency. (2015). *Taking Shelter from the Storm: Building a Safe Room for Your Home or Small Business* (FEMA P-320 Third Edition)

National Oceanic and Atmospheric Administration (NOAA). (2015). *Annual Fatal Tornado Summary*. Retrieved from http://www.spc.noaa.gov/climo/torn/fatalmap.php#tmap

Federal Emergency Management Agency. (2015). *Design and Construction Guidance for Community Safe Rooms* (FEMA P-361 Third Edition)

ICC 500, (2008). *Standard for the Design and Construction of Storm Shelters*, International Code Council, Washington DC, ISBN: 978-1-58001-746-6

NIST/TTU. (2006). *Debris impact resistance of building assemblies*. A compilation of testing performed by the Wind Science and Engineering Research Center Texas Tech University and Florida A&M University, Florida State University , and University of Florida. Summary report submitted to National Institute of Science and technology (N.I.S.T.). August 2006.

Bailey, J. (1984). *Wall Barrier Resistance to the Impact of Tornado Missiles*, Master's Thesis, Department of Civil Engineering, Texas Tech University, Lubbock, TX.

Carter, R. (1998). *Wind-Generated Missile Impact on Composite Wall Systems*, Master's Thesis, Department of Civil Engineering, Texas Tech University, Lubbock, TX.

Falk, B., Hermanson, J., Bridwell, J. (2015). *Tornado Safe Rooms from Commodity Wood Products: Wall Development and Impact Testing*, Currently under review.

Ginsberg, J. H. (2001). *Mechanical and Structural Vibrations: Theory and Applications*. New York, NY: John Wiley & Sons, Inc.

Clough, R. and Penzien, J. (1993) *Dynamics of Structures*. New York, NY: McGraw-Hill, Inc.

Stephenson, A., Sliter, G., Burdette, E. (1978). *Full-scale tornado-missile impact tests*, Nuclear Engineering and Design, Volume 46 pp. 123-143

Plesha, M., Costanzo, F., Gray, G. L. (2009). *Engineering Mechanics: Dynamics*. New York, NY: McGraw-Hill

Zukas, J.A., (1980). *Impact Dynamics: Theory and Experiment*, (US Army Armament Research and Development Command Ballistic Research Laboratory Technical Report ARBRL-TR-02271) Aberdeen Proving Ground, Maryland

Backman, M.E., Goldsmith, W. (1978). The Mechanics of Penetration of Projectiles into Targets. *International Journal of Engineering Science*, *16,* 1-99

Zukas, J. A., Nicholas, T., Swift, H. F., Greszczuk, L. B., Curran, D. R., (1982). *Impact Dynamics*. John Wiley & Sons, Inc., New York, NY.

Ross, R. J. (Ed.) (2010). *Wood Handbook: Wood as an Engineering Material.* (General Technical Report FPL-GTR-190). Madison, WI. Forest Products Laboratory

AWC Standard, 2012. *ASD/LRFD NDS: National Design Specification for Wood Construction,* American Wood Council, Leesburg, VA, ISBN: 978-0-9827380-2-3

Wood, L. (1951). *Relation of Strength of Wood to Duration of Load*. USDA Forest Service Research Paper, FPL 1916, Forest Products Laboratory. Madison, WI.

Gerhards, C. C. (1977). *Effect of Duration and Rate of Loading on Strength of Wood and Wood-Based Materials.* USDA Forest Service Research Paper, FPL-RP-283, Forest Products Laboratory. Madison, WI.

Elmendorf, A. (1915). *Stresses in Impact*. Journal of the Franklin Institute, Volume 182, Issue 6.

Gerhards, C. C., (1980). *Effects of Knots on Stress Waves.* USDA Forest Service Research Paper, FPL 384, Forest Products Laboratory. Madison, WI.

Gerhards, C. C. (1980). *Effect of Cross Grain on Stress Waves in Lumber.* USDA Forest Service Research Paper, FPL 368, Forest Products Laboratory. Madison, WI.

Minor, J., McDonald, J., Mehta, K. (1978). *The tornado: an engineering-oriented prespective.* (NOAA Technical Memorandum ERL NSSL-82) Boulder, CO. National Oceanic and Atmospheric Administration, Environmental Research Laboratories.

Thompson, R. (1973). *A Preliminary Study in Missile Penetration of Residential Walls*, Master's Thesis, Department of Civil Engineering, Texas Tech University, Lubbock, TX.

ASTM Standard E1886, 1997 (2013a). *Standard Test Method for Performance of Exterior Windows, Curtain Walls, Doors, and Impact Protective Systems Impacted by Missile(s) and Exposed to Cyclic Pressure Differentials*, ASTM International, West Conshohocken, PA, 2013, DOI: 10.1520/E1886-13A, www.astm.org

Safe Room Wall Dimensions:

$W := 8\ ft \qquad H := 8\ ft$

Design Wind Pressure:

$p_w := 113\ psf$ (From procedure outlined in ASCE 7-10)

Thickness of Individual Boards:

$t := 1.5\ in$

Bending Stress Calculation, per foot of width:

$I := 3 \cdot \frac{1\ ft \cdot t^3}{12}$ $I = 10.125\ in^4$ (Moment of Inertia of 3 layers of boards)

$w_w := p_w$ $w_w = 113\ \frac{plf}{ft}$ (Distributed Load)

$M_w := \frac{w_w \cdot H^2}{8}$ $M_w = 904\ \frac{lbf \cdot ft}{ft}$ (Bending Moment)

$V_w := \frac{w_w \cdot H}{2}$ $V_w = 452\ \frac{lbf}{ft}$ (Maximum Shear)

$F_b := \frac{M_w \cdot t}{I}$ $F_b = 1607\ \frac{psi}{ft}$ (Design Bending Stress)

$F_v := \frac{3 \cdot V_w}{2 \cdot 1\ ft \cdot t}$ $F_v = 37.667\ \frac{psi}{ft}$ (Design Shear Stress)

LRFD Stress Check

Adjustment Factors:

$C_M := 0.85$ It's possible that the wood is wet (Conservative)

$C_r := 1$ The construction dictates each member relies on others (Conservative)

$C_t := 1$ Unlikely to have wood >100 degrees F

$C_L := 1$ No lateral torsional buckling possible

$C_F := 1.2$ For 2x8's

$C_{fu} := 1.15$ 2x8's bent in weak direction

$C_i := 1$ No incising present

$K_F := 2.54$ Bending

$\phi_b := 0.85$

Resistance factors

$\phi_v := 0.75$

$\lambda := 1$ For wind loading

NDS Stress and Adjustment:

$f_b := 1000\ psi$

Mid-level value

$f_v := 800\ psi$

$f_b' := f_b \cdot C_M \cdot C_r \cdot C_t \cdot C_L \cdot C_F \cdot C_{fu} \cdot C_i \cdot K_F \cdot \phi_b \cdot \lambda$

$f_v' := f_v \cdot C_M \cdot C_t \cdot C_i \cdot K_F \cdot \phi_v \cdot \lambda$

$f_b' = 2533\ psi$ $F_b = 1607\ \frac{psi}{ft}$

$f_v' = 1295\ psi$ $F_v = 38\ \frac{psi}{ft}$

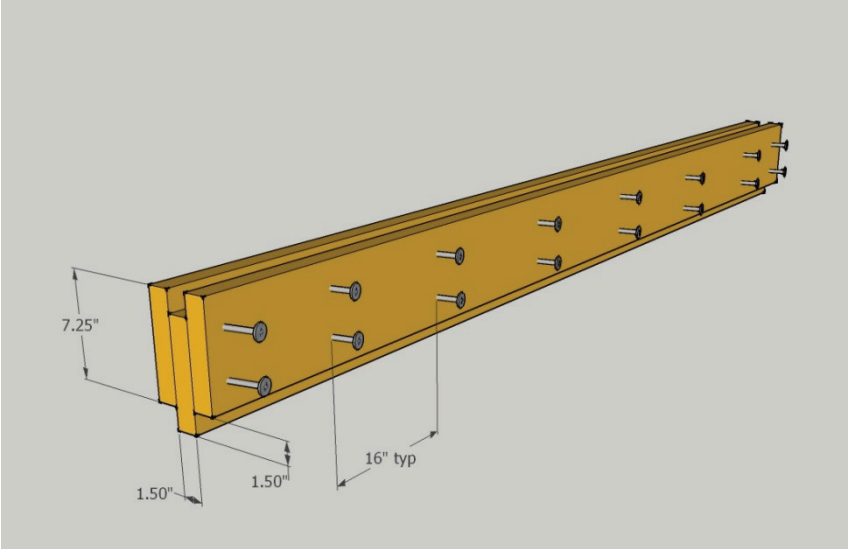
$f'_b \geq F_b$

Passes.

$f_v' \geq F_v$

Appendix B Wall Construction Details from FPL safe room project

Walls 1-3 and 5-8



Nailing scheme of single beam of wall section





Front and side views of assembled lumber portion of wall section. Sheathing added later for some sections.

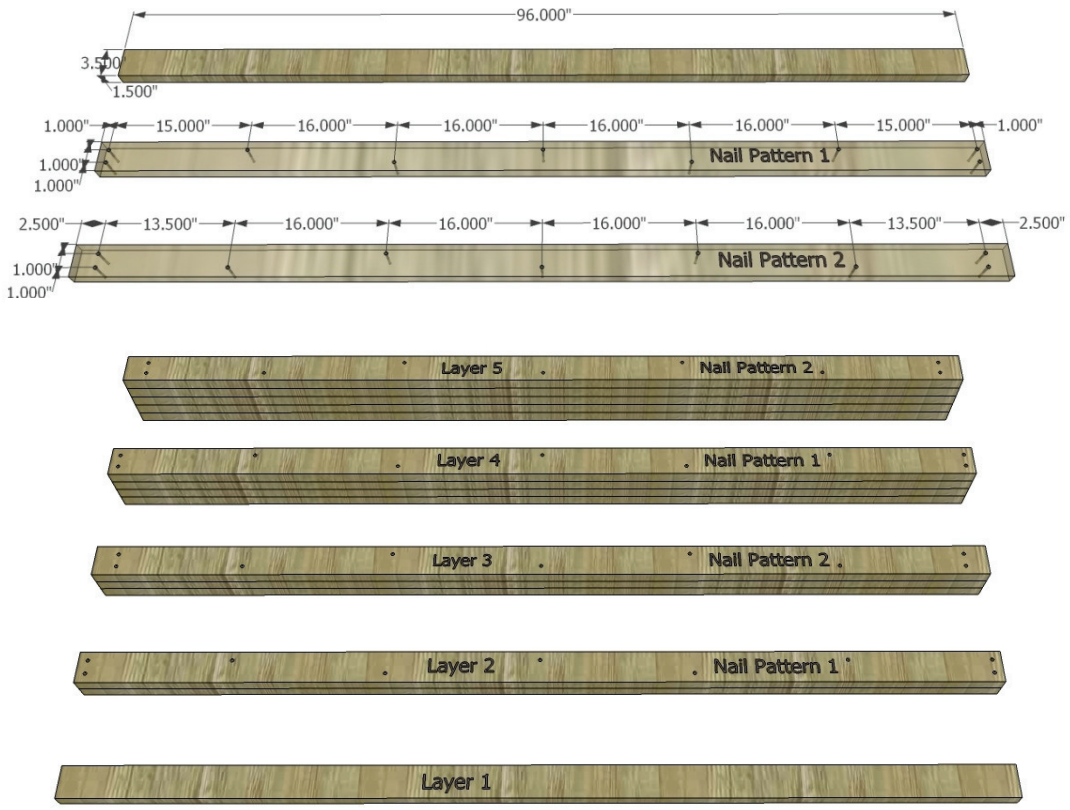


Nailing locations for attachment of sheathing.

Construction details of each wall.

Panel	Construction
1	Interlocking sections of 2x8's. Nailed
2	Interlocking sections of 2x8's. Nailed, with 1/2" OSB nailed to back.
3	Interlocking sections of 2x8's. Nailed, with 1/2" OSB nailed to back.
5	Interlocking sections of 2x8's. Nailed at an angle, with 3/4" CD grade Plywood nailed to back
6	Interlocking sections of 2x8's. Nailed with 3/4" CD grade Plywood nailed to both sides. Adhesive between 2x8's and Plywood, between adjacent 2x8's and between 2x8 layers.
7	Interlocking sections of 2x8's. Nailed with 3/4" CD grade Plywood nailed to both sides. Adhesive between 2x8's and Plywood and between adjacent 2x8's
8	Interlocking sections of 2x8's. Nailed with 3/4" CD grade Plywood nailed to both sides. Adhesive between 2x8's and Plywood.

Wall 4



Nailing pattern.

Construction details.

Panel	Construction
4	Stacked 2x4's oriented in strong direct. Nailed, with 1/2" OSB nailed to both faces



Front and side view of wall 4 prior to installation of sheathing.



Nailing locations for attachment of sheathing.

Appendix C Nonlinear Regression Code

Code:

```
##############################################################################################
# This file assumes that the working directory has been set to the directory containing this file by either
# RScript Session -> Set Working Directory -> To Source File Location, or with
# setwd("C:\Users\Eric\Documents\Safe Room Research\FPL Data")
#
# Wall2A_AllAdjusted.csv has the data prior to impact removed and the time values adjusted so
# that zero is the time of impact (displacement values are continuously increasing) and data
# after the oscillation has decayed removed before averaging the displacements.
#
# The impulse data is fitted to the standard damped sinusoid equation
# ---------------------------------------------------------------------------------------------
# y = A * e^(-Lamda*t) * sin(Omega*t + Phi) + Offset
# ---------------------------------------------------------------------------------------------
# then the coefficients for the impulse excitation equation are calculated from the resulting
# damped sinusoid coefficients
#
# Impulse excitation equation
# ---------------------------------------------------------------------------------------------
# y =   1/(M*Omega_d) * e^(-z*Omega_n*t) * sin(Omega_d * t)
# ---------------------------------------------------------------------------------------------
# Given A = 1/(M*Omega_d), Lamda = z*Omega_n, and Omega = Omega_d
#
# The formulas Omega_n = sqrt(k/m) and Omega_d = Omega_n * sqrt(1 - z^2) are then substituted
# into the 3 coefficient equations and M, k and z are solved for.
##############################################################################################
# m*v = Momentum of 2x4 missile
# m*v = mv
mv <- 0.068
# ---------------------------------------------------------------------------------------------
# Read the impact displacement vs time data into td
# ---------------------------------------------------------------------------------------------
td <- read.csv("Wall2A_AllAdjusted.csv", header=TRUE)
# ---------------------------------------------------------------------------------------------
# Plot the imported data as a reference to check the fitted coefficients
# ---------------------------------------------------------------------------------------------
plot(td, cex=0.2, main="Wall 2A Average Displacement vs. Time", sub="(Time(0) adjusted to impact)")
text(x=0.2, y=5, labels="Experimental Data (Black)", col="black")
# ---------------------------------------------------------------------------------------------
# Initial Values
#
# A is initial amplitude
# Lamda is log(2)/(time to 1/2 amplitude)
# Omega is 2*Pi/(period of oscillation)
```

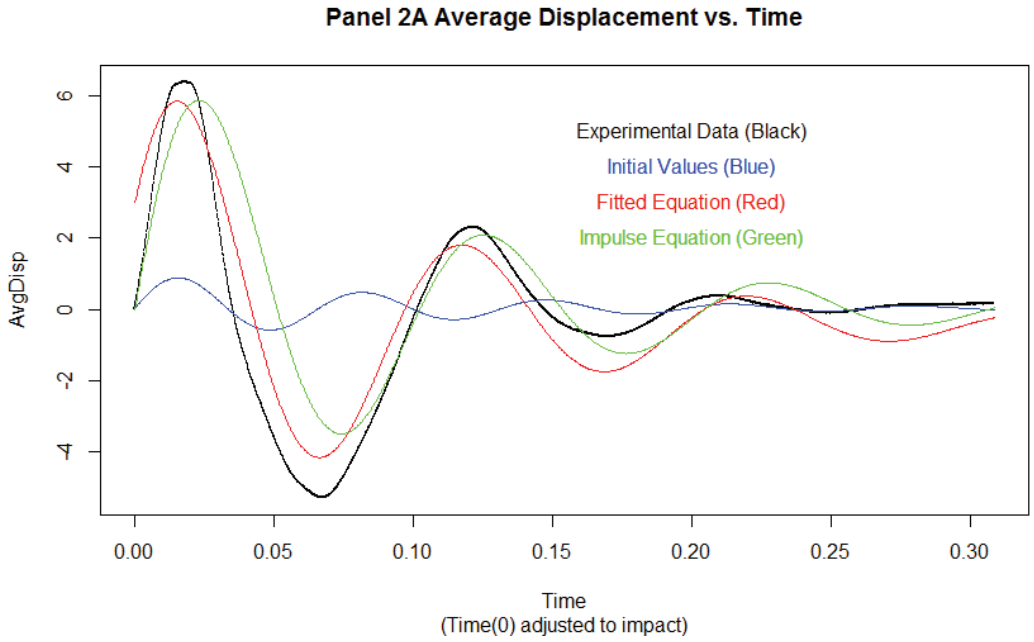
```
# Phi is angular offset (initially 0 due to time adjustment in raw data)
# Offset is the change in the average value of the measurement system after impact
#
# Lower case c is prepended to the coefficient names to avoid conflicts with R built in
# names
# ------------------------------------------------------------------------------------------
sv <- c(
  cA = 1,
  cLamda = log(2)/0.07,
  cOmega = (2 * 3.14)/0.066,
  cPhi = 0,
  cOffset = 0.03
)
# ------------------------------------------------------------------------------------------
# Add to plot using the initial values to the raw data plot
# ------------------------------------------------------------------------------------------
curve((sv["cA"]*exp(-sv["cLamda"]*x)*sin((sv["cOmega"]*x)+sv["cPhi"])+sv["cOffset"]),
     add=TRUE, col="blue", n=1000)
text(x=0.2, y=4, labels="Initial Values (Blue)", col="blue")
# ------------------------------------------------------------------------------------------
# Non-linear Least Squares Regression to find A, Lamda, Omega, Phi and Offset for the damped
# sinusoid
# ------------------------------------------------------------------------------------------
fit1 <- nls(td$AvgDisp ~ (cA*exp(-cLamda*td$Time)*sin((cOmega*td$Time)+cPhi)+cOffset),
          td,start=sv)
fit1c <- coef(fit1)
# ------------------------------------------------------------------------------------------
# Add to plot using the fitted coefficients
# ------------------------------------------------------------------------------------------
curve((fit1c["cA"]*exp(-fit1c["cLamda"]*x)*sin((fit1c["cOmega"]*x)+fit1c["cPhi"])+
       fit1c["cOffset"]), add=TRUE, col="red", n=1000)
text(x=0.2, y=3, labels="Fitted Equation (Red)", col="red")

# Display the fitted coefficients to the console
print(fit1c)
# ------------------------------------------------------------------------------------------
# Solve for M, k, and z
# ------------------------------------------------------------------------------------------
cz <- 1/sqrt(((fit1c["cOmega"]^2)/(fit1c["cLamda"]^2))+1)
cM <- sqrt(mv^2/((fit1c["cA"]^2)*(fit1c["cOmega"]^2)+(fit1c["cA"]^2)*(fit1c["cLamda"]^2)-1))
ck <- fit1c["cLamda"]^2 * cM / cz^2
cOmega_n <- sqrt(ck/cM)
cOmega_d <- cOmega_n * sqrt(1 - cz^2)
print(table(cz))
print(table(cM))
print(table(ck))

# Plot the Impulse equation using cz, cM and ck
```

```
# It differs from the damped sinusoid by cOffset
curve(mv * (exp(-cz*cOmega_n*x) * sin(cOmega_d*x))/(cM * cOmega_d),
    add=TRUE, col="green", n=1000)
text(x=0.2, y=2, labels="Impulse Equation (Green)", col="green")
```

Example Output



Example Design Procedure Calculations

Individual 2x8 Board Dimensions:

$h := 1.5\ in$ $b := 7.5\ in$ $l := 7.5\ ft$ $I := \frac{b \cdot h^3}{12}$ $I = 2.109\ in^4$

Material Properties: Douglas Fir

$E_L := 1500\ ksi$ $C_{LT} := 0.078$ $G_w := C_{LT} \cdot E_L$ $G_w = 117\ ksi$ $v := 0.372$

$C_L := 0.05$ $E_T := C_L \cdot E_L$ $E_T = 75\ ksi$ $SG := 0.5$

Locations of Interest and Unit Load:

$x_0 := 3.5\ ft$ $y_0 := 3.9\ ft$ Location of Impact

$x_{0.25} := 2.33\ ft$ $y_{0.25} := 2.6\ ft$ Quarter Point Locations

$P := 1\ kip$ Unit Load

Deflection of a Beam Subject to a Point Load at Midspan:

$$\Delta beam(x) := \frac{-P \cdot x}{48 \cdot E_L \cdot I} \cdot \left(3 \cdot l^2 - 4 \cdot x^2\right)$$

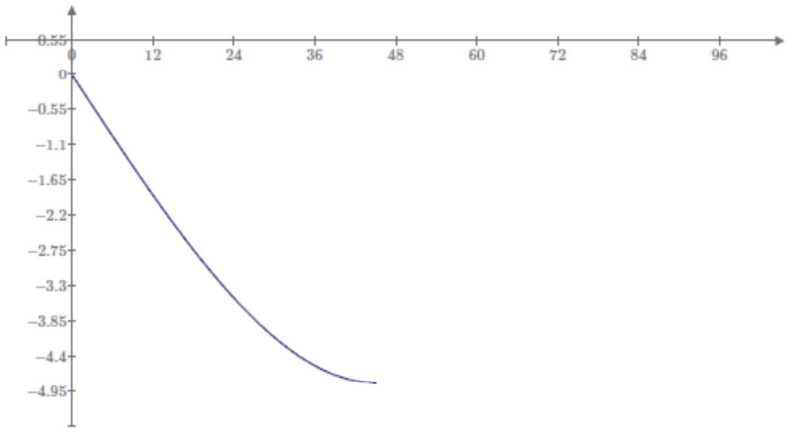
Stiffness Ratio (From Kratio vs. Eratio plot):

$K_{rat} := 0.405$

Midpoint Stiffness Estimate:

Three Beam Approximation (Lower Bound):

$x := 0\ in, 0.01\ in .. \frac{l}{2}$



$\Delta beam(x)\ \ (in)$

$x\ \ (in)$

Find % of wall fully engaged in bending:

$$per_{bending} := \frac{\int_0^{\frac{l}{2}} \Delta beam(x)\,dx}{\Delta beam\left(\frac{l}{2}\right) \cdot \frac{l}{2}} \qquad per_{bending} = 0.625$$

Determine effective beam properties:

$b_{wall} := 7.5\ ft \qquad h_{beam} := 1.5\ in$

$b_{eff} := per_{bending} \cdot b_{wall} \qquad b_{eff} = 56.25\ in$

Estimate the Stiffness of One Beam:

$$I_{beam} := \frac{b_{eff} \cdot h_{beam}^{\ 3}}{12} \qquad I_{beam} = 15.82\ in^4$$

$$\Delta beam(x) := \frac{P \cdot x}{48 \cdot E_L \cdot I_{beam}} \cdot \left(3 \cdot l^2 - 4 \cdot x^2\right)$$

$$k_{midbeam} := \frac{P}{\Delta beam(x_0)} \qquad k_{midbeam} = 1.6 \ \frac{kip}{in}$$

Non-Composite Wall Stiffness (Lower-Bound):

$$k_{midnoncomp} := 3 \cdot k_{midbeam} \qquad k_{midnoncomp} = 4.7 \ \frac{kip}{in}$$

Plate Approximation (Upper-Bound):

Approximate an Effective Depth, Normalized to Longitudinal Modulus:

$$h_{eff} := \frac{\frac{E_L \cdot 2 \cdot h + E_T \cdot h}{E_L} + \frac{E_L \cdot h + E_T \cdot 2 \cdot h}{E_L}}{2} = 2.363 \ in$$

"Section Modulus" of Plate:

$$D := \frac{E_L \cdot h_{eff}^{\ 3}}{12 \cdot \left(1 - v^2\right)}$$

Solving Plate Equation:

$a := 7 \ ft$ $b := 7.8 \ ft$ (Approximate Unsupported Wall Dimensions)

$$w(x,y) := \sum_{m=1}^{55} \sum_{n=1}^{55} \left(\frac{4}{a \cdot b} \cdot \sin\left(\frac{(2 \cdot m - 1) \cdot \pi \cdot x_0}{a}\right) \cdot \sin\left(\frac{(2 \cdot n - 1) \cdot \pi \cdot y_0}{b}\right) \cdot \sin\left(\frac{(2 \cdot m - 1) \cdot \pi \cdot x}{a}\right) \cdot \sin\left(\frac{(2 \cdot n - 1) \cdot \pi \cdot y}{b}\right) \right)$$
$$\Big/ \left(D \cdot \pi^4 \cdot \left(\frac{(2 \cdot m - 1)^2}{a^2} + \frac{(2 \cdot n - 1)^2}{b^2} \right)^2 \right)$$

Upper Bound Estimate:

$$k_{midcomp} := \frac{1}{w(x_0, y_0)} = 21.2 \ \frac{kip}{in}$$

Approximate % Composite:

$COMP := 0.158$ (See Partial Composite Action estimate in Appendix E)

Expected Quasi-Static Stiffness:

$k_{midstatic} := COMP \cdot \left(k_{midcomp} - k_{midnoncomp}\right) + k_{midnoncomp}$ $\quad k_{midstatic} = 7.3 \ \frac{kip}{in}$

$k_{quarstatic} := \frac{1}{K_{rat}} \cdot k_{midstatic}$ $\quad k_{quarstatic} = 18.1 \ \frac{kip}{in}$

Expected Dynamic Stiffness:

Dynamic to Static Stiffness Ratio:

$k_{dtos} := 0.45$ (Estimate from plot of dynamic to static stiffness ratios)

$k_{middynamic} := k_{dtos} \cdot k_{midstatic}$ $\quad k_{middynamic} = 3.29 \ \frac{kip}{in}$

Expected Mass:

2x8 Mass:

$n_b := 39$ $\quad b := 7.5 \ in$ $\quad h := 1.5 \ in$

Conservative Assumption that 1/2 Wall Engaged in Bending Used:

$n_b := \frac{1}{2} \cdot n_b$ $\quad n_b = 20$ $\quad n_b := 14$

$m := n_b \cdot b \cdot h \cdot l \cdot SG \cdot 1000 \ \frac{kg}{m^3}$ $\quad m = 7.958 \ slug$

Expected Damping:

Previous testing showed that damping ratio is >1.3 without adhesives:

$\zeta := 0.13$

Momentum of Missile:

$F_{imp} := 0.0684 \ kip \cdot s$

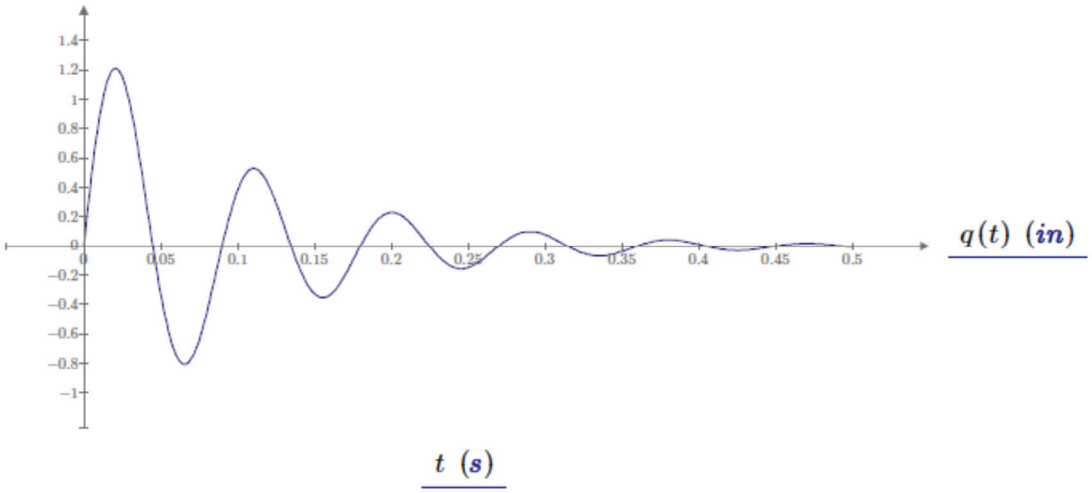
Vibrational Properties:

$$\omega_n := \sqrt{\frac{k_{middynamic}}{m}} \qquad \omega_n = 70.467\ \frac{rad}{s} \qquad \omega_d := \omega_n \cdot \sqrt{1-\zeta^2}$$

$$t := 0\ s, 0.001\ s .. 0.5\ s$$

Expected Midpoint Displacement:

$$q(t) := \frac{F_{imp}}{m \cdot \omega_d} \cdot \exp\left(-\zeta \cdot \omega_n \cdot (t)\right) \cdot \sin\left(\omega_d \cdot (t)\right)$$



$E := 1500\ ksi$ $L_{comp} := 7.8\ ft$ $L_{ten} := 7.5\ in$

Distance Between Centroidal Axes:

$h := 1.5\ in$ $s := 3.75\ in$

$k_{02} := 1 \cdot 10^{6}\ \frac{lbf}{in^{3}}$ $k_{01} := k_{02}$

Nail Dimensions:

$d_N := 0.148\ in$ $L_N := 3\ in$ $E_N := 29000\ ksi$ $I_N := \frac{1}{64} \cdot \pi \cdot d_N^{4}$ $I_N = (2.4 \cdot 10^{-5})\ in^{4}$

Nail, Load/Slip:

$$\lambda_1 := 2 \cdot \sqrt[4]{\frac{k_{01}}{\pi \cdot E_N \cdot d_N^{3}}} \qquad \lambda_1 = 2.713\ \frac{1}{in}$$

$$\lambda_2 := 2 \cdot \sqrt[4]{\frac{k_{02}}{\pi \cdot E_N \cdot d_N^{3}}} \qquad \lambda_2 = 2.713\ \frac{1}{in}$$

$a_1 := 1.5\ in$ $a_2 := 1.5\ in$

$\lambda_1 \cdot a_1 = 4.069$ $\lambda_2 \cdot a_2 = 4.069$

Case 1:

$r := \frac{k_{01}}{k_{02}}$ $r = 1$

$$\beta_1 := \frac{r \cdot \left(r + r^{0.75}\right)}{2 \cdot \left(r + r^{0.25}\right) \cdot \left(r + r^{0.75}\right) + \left(r - r^{0.75}\right)^{2}} \qquad \beta_1 = 0.25$$

$P\delta := \sqrt{2} \cdot E_N^{0.25} \cdot I_N^{0.25} \cdot k_{01}^{0.75} \cdot d_N^{0.75} \cdot \beta_1$ $P\delta = 13638.1\ \frac{lbf}{in}$

$S := \frac{P\delta}{s}$ $S = 3637\ psi$

Composite and Non-composite stiffness:

$E_1 := 0.05 \cdot E \qquad E_2 := E$

$A_1 := 7.5\ in \cdot 1.5\ in \qquad A_2 := A_1 \qquad A_1 = 11.25\ in^2$

$EI_{flangeu} := E_1 \cdot \frac{7.5\ in \cdot (1.5\ in)^3}{12} \qquad EI_{flangeu} = 158\ kip \cdot in^2$

$EI_{webu} := E_2 \cdot \frac{7.5\ in \cdot (1.5\ in)^3}{12} \qquad EI_{webu} = 3164\ kip \cdot in^2$

$EI_u := EI_{flangeu} + EI_{webu} \qquad EI_u = 3322\ kip \cdot in^2$

$EI_r := EI_u + \frac{E_1 \cdot A_1 \cdot E_2 \cdot A_2}{E_1 \cdot A_1 + E_2 \cdot A_2} \cdot h^2 \qquad EI_r = 5130\ kip \cdot in^2$

Deflection Amplification Factors:

$\alpha := \sqrt{\frac{h^2 \cdot S}{EI_r - EI_u} \cdot \frac{EI_r}{EI_u}} \qquad \alpha = 0.084\ \frac{1}{in}$

$f_{\Delta comp} := \frac{10}{(L_{comp} \cdot \alpha)^2 + 10} \qquad f_{\Delta comp} = 0.14$

$f_{\Delta ten} := \frac{10}{(L_{ten} \cdot \alpha)^2 + 10} \qquad f_{\Delta ten} = 0.962$

$DAF_{comp} := 1 + f_{\Delta comp} \cdot \left(\frac{EI_r}{EI_u} - 1\right) \qquad DAF_{comp} = 1.076$

$DAF_{ten} := 1 + f_{\Delta ten} \cdot \left(\frac{EI_r}{EI_u} - 1\right) \qquad DAF_{ten} = 1.524$

$R := \frac{EI_r}{EI_u} = 1.544 \qquad R = 1.544$

Tension and Compression Composite Action Estimates:

$$Composite_{comp} := \frac{R - DAF_{comp}}{R} = 0.303 \qquad Composite_{comp} = 0.303$$

$$Composite_{ten} := \frac{R - DAF_{ten}}{R} = 0.013 \qquad Composite_{ten} = 0.013$$

Global Composite Action Estimate:

$$Composite_{tot} := \frac{Composite_{comp} + Composite_{ten}}{2} \qquad Composite_{tot} = 0.158$$